

MARTENSITIC TRANSFORMATIONS IN HIGH MAGNETIC FIELDS

by

MICHAEL KARL KORENKO

B.S., Case Institute of Technology  
(1966)

M.S., Case Western Reserve University  
(1969)

Submitted in partial fulfillment of the requirements  
for the degree of  
DOCTOR OF SCIENCE

at the  
Massachusetts Institute of Technology

February, 1973

Signature of Author .....  
Department of Metallurgy and Materials Science  
January 17, 1973

Certified by .....  
Thesis Supervisor

Accepted by .....  
Chairman, Departmental Committee on Graduate Students



## ABSTRACT

## MARTENSITIC TRANSFORMATIONS IN HIGH MAGNETIC FIELDS

by

MICHAEL KARL KORENKO

Submitted to the Department of Metallurgy and Materials Science on January 17, 1973 in partial fulfillment of the requirements for the degree of Doctor of Science.

The influence of high magnetic fields on the nucleation, kinetics, and morphology of the martensitic transformation was investigated with fields up to 140 kOe, using electrical resistivity measurements and optical metallography. Four iron-nickel and iron-nickel-manganese alloys were chosen to cover the range of morphologies from lath (packet) to plate (lenticular) and the range of kinetics from isothermal C-curve behavior to bursting phenomena.

Magnetic fields accelerate the martensitic transformation in iron-nickel alloys both by increasing the Gibbs free-energy difference between the product and parent phases and by allowing the reaction to take place at higher temperatures. For example, the Fe<sub>22.5</sub>Ni<sub>4.0</sub>Mn alloy, which will not transform perceptibly at any temperature without a magnetic field, displays isothermal C-curve kinetics with fields in the range of 60 to 140 kOe. Thus, employing magnetic fields to induce the martensitic transformation is very different from lowering the temperature.

Lath and plate martensites in iron-nickel alloys are two extremes of a spectrum of morphologies each of which, in themselves, appear to be intermediate transition morphologies. The morphological transition from lath-to-plate is not a simple function of the temperature, Gibbs free-energy change, nickel content, activation energy, or the temperature difference between the Curie point and the martensitic-start temperature. The best kinetic correlation with the morphology in binary iron-nickel alloys is the rate of transformation which, in turn, can be approximated by the incubation time or the activation energy divided by the temperature. Lower temperatures, at constant driving force or at constant activation

energy, favors lath martensite which, up to the present use of magnetic fields, has always been overshadowed by the large increases in chemical driving force with decreasing temperature which favors plate martensite.

The average plate volume of the iron-nickel-manganese is insensitive to temperature or magnetic field strength; however, it is a strong function of the extent of transformation up to about 7 percent martensite, and becomes relatively insensitive thereafter. In addition, the orientation of the martensitic plates and their radius-to-semithickness ratios are not significantly dependent on the direction of the applied field.

The quantitative influence of magnetic fields on the martensitic kinetic behavior imposes a severe test on the current nucleation theories. The Cohen-Raghavan model can be fitted to much of the data, but there are important details that remain unexplained. In addition, high-temperature magnetic annealing and recrystallization experiments in the austenitic range do not support the hypothesis that the preexisting martensitic embryos are ferromagnetic in nature.

There is evidence that autocatalytic nucleation sites in the iron-nickel alloys may be an integral part of the moving austenite-martensite interface. Three important autocatalytic sites are identified: midrib impingement of a martensitic plate on another plate during thickening of the latter; the transition zone within a martensitic plate where the lattice-invariant mode switches from twinning to slip; and grain-boundary impingement by an advancing martensitic plate.

Magnetic fields are shown to be a valuable tool for studying the martensitic transformation in iron-base alloys. It permits a separation of the effects of driving force and temperature, and provides a critical test for the current nucleation theories.

Thesis Supervisor: Morris Cohen

Title: Ford Professor of Materials  
Science and Engineering

TABLE OF CONTENTS

	<u>Page Number</u>
TITLE PAGE .....	1
ABSTRACT .....	2
TABLE OF CONTENTS .....	4
LIST OF FIGURES .....	7
LIST OF TABLES .....	10
ACKNOWLEDGEMENTS .....	11
I INTRODUCTION .....	12
I-1 Classical Thermodynamics in Magnetic Fields .....	12
I-2 Thermodynamics of Martensite in Magnetic Fields .....	15
I-3 Advantages of Magnetic Fields for Research on Martensitic Transformations .....	23
II DISCUSSION OF LITERATURE .....	24
II-1 Martensitic Transformation Characteristics .....	24
II-1.1 Kinetics .....	24
II-1.2 Morphology .....	30
II-1.3 Nucleation .....	34
II-2 Magnetically-Induced Martensitic Transformations .....	41
II-2.1 General Magnetic Transformation Characteristics	41
II-2.2 Pulsed Versus Steady Fields .....	44
II-2.3 Isothermal Transformation Studies .....	47
II-2.4 Magnetic Effects on the Microstructure .....	48
II-2.5 Theoretical Treatment to Date .....	50
II-2.5.1 Thermodynamic Predictions .....	50



## TABLE OF CONTENTS (continued)

	<u>Page Number</u>
II-2.5.2 Kinetic Predictions .....	52
II-2.6 Potential Applications .....	53
III PURPOSE OF THESIS AND OUTLINE OF WORK .....	55
IV MATERIALS AND PROCEDURES .....	56
IV-1 Specimen Preparation and Composition .....	56
IV-2 Resistance Measurements .....	58
IV-3 Temperature and Magnetic-Field Control .....	60
IV-4 Magnetization Measurements .....	62
IV-5 Optical Microscopy .....	63
IV-6 Quantitative Metallography .....	64
IV-6.1 Grain-Size Measurements .....	64
IV-6.2 Volume-Fraction Measurements .....	64
IV-6.3 Measurement of Mean Volume per Plate and Radius- to-Semithickness Ratio .....	65
IV-7 Measurement of Nucleation Rate .....	66
IV-8 Averaging Techniques .....	66
V RESULTS AND DISCUSSION .....	67
V-1 Material Characteristics .....	67
V-1.1 Shear Modulus and Density .....	67
V-1.2 Magnetic Properties .....	69
V-1.3 Chemical Driving Force .....	72
V-2 Fe 28.7 Ni -- (Isothermal) .....	75
V-2.1 Kinetics .....	75

## TABLE OF CONTENTS (continued)

	<u>Page Number</u>
V-2.2 Morphology .....	78
V-3 Fe 29.6 Ni -- (Isothermal $\rightarrow$ Bursting) .....	81
V-3.1 Kinetics .....	81
V-3.2 Morphological Transition Behavior .....	85
V-3.3 Activation-Energy Correlations .....	93
V-3.4 Fit with the KCR Model .....	101
V-4 Fe 30.8 Ni -- (Bursting) .....	104
V-4.1 Kinetics .....	104
V-4.2 Morphology and Autocatalytic Nucleation .....	108
V-5 Fe 22.5 Ni 4.0 Mn -- (Isothermal C-curves) .....	115
V-5.1 Kinetics .....	115
V-5.2 Morphology and Quantitative Metallography .....	119
V-5.3 Fit with the KCR Model .....	130
V-6 Embryo Experiments .....	135
V-6.1 High-Temperature Magnetic Annealing .....	135
V-6.2 Low-Temperature Magnetic Annealing and Cycling Experiments .....	141
<b>VI CONCLUSIONS</b> .....	145
<b>VII SUGGESTIONS FOR FUTURE WORK</b> .....	148
<b>APPENDICES</b>	
I Magnetic Clausius -- Clapeyron Equation .....	149
II Quantitative Metallography of Thin Oblate Spheroids ....	151
<b>BIBLIOGRAPHY</b> .....	156
<b>BIOGRAPHICAL NOTE</b> .....	165

LIST OF FIGURES

<u>Figure Number</u>		<u>Page Number</u>
1	Schematic magnetization curve of an ellipsoidal single crystal of a paramagnetic material illustrating the energy changes involved .....	16
2	Schematic survey of past pulsed-field work .....	42
3	Schematic of cryogenic temperature controller used during transformation in applied fields .....	61
4	Room-temperature magnetization curves .....	71
5	Chemical free-energy change for the austenite-to-martensite transformation from Equation 27 .....	74
6	Transformation Kinetics of Fe 28.7 Ni under zero-field conditions .....	76
7	Field-induced transformation kinetics of Fe 28.7 Ni at 24.4°C .....	77
8	Lath-like morphology of Fe 28.7 Ni transformed in a field of 60 kOe at 24.4°C .....	79
9	Transformation kinetics of Fe 29.6 Ni under zero-field conditions .....	82
10	Field-induced transformation kinetics of Fe 29.6 Ni at - 2°C .....	83
11	Field-induced transformation kinetics of Fe 29.6 Ni at + 9°C .....	84
12	Morphological transition in Fe 29.6 Ni under zero-field conditions (a) Lath-like at - 13°C (b) Mixture of plate and lath-like martensite at - 196°C	86
13	Field-induced morphological transition in Fe 29.6 Ni at - 2°C (a) Lath-like at 40 kOe (b) Mixture of plate and lath-like martensite at 140 kOe	88

## LIST OF FIGURES (continued)

<u>Figure Number</u>		<u>Page Number</u>
14	An example of a twin-related loose-packet in Fe 29.6 Ni transformed in field of 60 kOe at - 2°C .....	90
15	An example of the transition plate morphology in Fe 29.6 Ni transformed in field of 140 kOe at - 2°C .....	91
16	Activation energy versus total Gibbs free-energy change for Fe 29.6 Ni .....	96
17	Activation energy divided by the temperature versus total Gibbs free-energy change for Fe 29.6 Ni .....	98
18	Logarithm of the rate of transformation versus experimental $\Delta W_a/T$ and calculated $\Delta U^*/T$ illustrating the morphological transition in Fe 29.6 Ni .....	99
19	Transformation kinetics of Fe 30.8 Ni under zero-field conditions .....	105
20	Field-induced transformation kinetics of Fe 30.8 Ni at - 20°C .....	107
21	Zero-field bursting morphology of Fe 30.8 Ni (a) - 46°C (b) - 196°C .....	109
22	Field-induced structure of Fe 30.8 Ni transformed in a 90 kOe field at - 20°C .....	110
23	An example of autocatalytic plates emitting from a midrib in Fe 30.8 Ni transformed under zero-field conditions at - 46°C .....	112
24	Field-induced transformation kinetics of Fe 22.5 Ni 4.0 Mn at - 81°C .....	116
25	Field-induced transformation kinetics of Fe 22.5 Ni 4.0 Mn at 140 kOe as function of various testing temperatures	117
26	Time to transform to 0.3% martensite as function of magnetic field and temperature .....	118
27	Morphology of the Fe 22.5 Ni 4.0 Mn alloy transformed in 140 kOe field at various temperatures .....	120

## LIST OF FIGURES (continued)

<u>Figure Number</u>		<u>Page Number</u>
28	Average plate volume for Fe 22.5 Ni 4.0 Mn as function of percent martensite, temperature, and magnetic-field intensity .....	123
29	Radius-to-semithickness ratio for Fe 22.5 Ni 4.0 Mn as function of percent martensite, temperature, and magnetic-field intensity .....	125
30	Orientation dependence of the morphology of Fe 22.5 Ni 4.0 Mn as function of direction of applied field (tested at - 81°C, 140 kOe) (a) Field perpendicular to specimen axis (b) Field parallel to specimen axis .....	127
31	Distribution of the number of plates aligned in a specific direction and their radius-to-semithickness ratios as a function of the direction of the applied magnetic field ..	128
32	Comparison of the KCR Model to the activation energy versus driving-force data .....	132
33	Comparison of the KCR Model to the $\Delta W_a/T$ versus driving-force data .....	133
34	Thermal-magnetic history of a typical embryo experiment ...	136
35	Equilibrium diagram illustrating the Curie temperatures and and martensitic-transformation range of FeNi alloys .....	138
36	Low-temperature transformation in Fe 29.6 Ni interrupted by upquenching, with and without a magnetic field .....	142

LIST OF TABLES

<u>Table Number</u>		<u>Page Number</u>
1	Relative Magnitudes of Various Magnetic Energies .....	22
2	Composition of Alloys in Weight Percentages .....	57
3	Material Characteristics of the Alloys Under Investigation	68
4	Incubation Times, Activation Energies, and Driving Forces for Fe 29.6 Ni .....	95
5	Incubation Times, Activation Energies, and Driving Forces for Fe 22.5 Ni 4.0 Mn .....	131

ACKNOWLEDGEMENTS

The author expresses his sincere appreciation to the following people for their assistance in conducting the work reported in this thesis:

Professor Morris Cohen for giving me a free hand to pursue independent research and providing continued guidance over the critical hurdles;

Miss Marguerite Meyer for her many special favors and general council;

Mrs. Miriam Rich, Mrs. Jane Operacz, and Mr. Robert Cava for their invaluable assistance with the optical and quantitative metallography;

Dr. Gilbert Speich for his measurements of the density and shear moduli of our alloys;

Mr. Larry Rubin, Miss Jean Morrison, and all the other helpful people at the Francis Bitter National Magnet Lab who made my work there a valuable and pleasant experience;

Ford Scientific Laboratory and the U. S. Steel Laboratory for Fundamental Research who supplied the alloys used in this investigation; and the National Science Foundation for supporting this work.

I am particularly indebted to my wife, Elaine, who by contributing to my financial support and by sharing the same interests has made my stay in the Cambridge/Boston area a truly memorable experience.

## I. INTRODUCTION

In typical steels, the martensitic phase is ferromagnetic while the austenite is paramagnetic. Under these conditions, the application of a magnetic field can induce an additional free-energy difference between the two phases. In this thesis, we have utilized this effect in order to study the nucleation and kinetics of the austenite-to-martensite transformation.

### I-1 Classical Thermodynamics in Magnetic Fields

The state of the material under investigation is annealed polycrystalline austenite which is textured to some extent because of the swaging and recrystallization steps necessary to obtain the specimen size. In addition, each grain contains several domains arranged in such a way as to give an overall value of magnetization near zero. It is impossible to rigorously describe the exact thermodynamic state of this system in a magnetic field. Fortunately, however, most of the complicating factors can be shown to be negligible, especially under high-field conditions.

The following general relationship among the three magnetic vectors will serve to define the important magnetic quantities:

$$\vec{B} = \mu_0 \vec{H} + \mu_0 4\pi \vec{M} \quad (1)$$

where  $\vec{B}$  is the magnetic induction (in gauss),  $\mu_0$  is the permeability of a vacuum ( $= 1$  gauss/oersted),  $\vec{H}$  is the magnetic field (in oersted), and  $\vec{M}$  is the magnetization or magnetic moment per unit volume (in ergs/gauss cm<sup>3</sup>).  $\vec{M}$  is the only material parameter in this equation and is the quantity to



be examined when predicting the effect of an applied magnetic field on an alloy.

The following discussion applies particularly well to diamagnetic or paramagnetic materials, but should be used with caution for ferromagnetic systems; in general, the latter exhibit hysteresis effects and many other complications which we will consider shortly.

Thermodynamically <sup>(1-4)</sup> the introduction of a field,  $\vec{H}$ , introduces another work term to the internal energy, much like the pressure introduces the PV term. When a specimen is placed in a solenoid, its dipoles align with the field, thereby increasing its magnetization. This increases the internal energy of the material. The battery driving the current in the solenoid supplies the extra energy by working against the back emf generated by the change in magnetization. The exact expression for the magnetic work that must be added to the internal energy can be broken into two terms:

$$dW_{\text{mag}} = \frac{1}{4\pi} \int (\vec{H} \cdot d\vec{B}) dV \quad (2)$$

$$= d\left(\frac{\mu_0}{8\pi} \int H^2 dV\right) + \mu_0 \int (\vec{H} \cdot d\vec{M}) dV \quad (3)$$

The first term on the right is just the energy contained in the field of the empty solenoid and has no material significance. The usual procedure is to redefine the zero of energy as including the energy of the field in a vacuum. Since we will be dealing with energy differences, this is of little consequence. To put this equation into a useable form, it is necessary to assume that the magnetization is independent of position within the domain. This assumption applies quite well to a completely

homogeneous specimen which is ellipsoidal in shape; however, it may be violated by material inhomogeneities or demagnetization effects at the boundaries. With these assumptions:

$$dW'_{\text{mag}} = \mu_0 \vec{H} \cdot d\vec{I} \quad (4)$$

where  $I$  is the total magnetic dipole moment of the system ( $= \int M dV = MV$ ).

The definition of the internal energy is now:

$$dU' = TdS - PdV + \sum \mu_j dN_j + \mu_0 \vec{H} \cdot d\vec{I} \quad (5)$$

The extensive parameter descriptive of the magnetic system is the component of the total magnetic moment parallel to the external field, while the intensive parameter in the energy representation is  $\mu_0 H$ . (2)

The internal energy of a material is raised by a magnetic field, yet we know that paramagnetic or ferromagnetic materials are attracted to a magnet. Why would it seem to go to a higher energy state? The answer to this dilemma is that the potential energy of the material is lowered or, alternatively, the overall energy change of the specimen plus the constant field solenoid is negative.

Physically, we would like to consider the specimen as the system and to treat the solenoid as a magnetic-field reservoir. We are transforming austenite under constant temperature, pressure, and external magnetic field. The correct thermodynamic potential for these conditions is the partial Legendre transform of the internal energy with respect to  $T$ ,  $P$ , and  $H$ :

$$U[T,P,H] = U - TS + PV - \mu_0 \vec{I} \cdot \vec{H} \quad (6)^{15}$$

$$dU[T,P,H] = -SdT + VdP + \sum \mu_j dN_j - \mu_0 \vec{I} \cdot d\vec{H} \quad (7)$$

$$dU[T,P,H] = dG_o + dG_{\text{magnetic}} \quad (8)$$

These equations show that we can add the magnetic contribution directly onto the Gibbs free-energy change.

Figure 1 (1) illustrates how the magnetic term may be calculated and offers some physical insight into the relevant thermodynamics. The shaded area above the magnetization curve is equal to the increase of internal energy of the specimen ( $= \mu_0 \int \vec{H} \cdot d\vec{I}$ ).  $\mu_0 HI$  is the total area of the dashed rectangle and is equal to the decrease in energy of the magnetic-field reservoir. Finally,  $\mu_0 \int \vec{I} \cdot d\vec{H}$  is the area under the magnetization curve and is equal to the energy change of the system plus the reservoir. When measured under constant temperature and pressure conditions, this is the magnetic contribution to the Gibbs free energy.

## I-2 Thermodynamics of Martensite in Magnetic Fields

The above analysis can be applied to ferromagnetic materials within a single ellipsoidal domain. However, even in this idealized situation, demagnetization and anisotropy effects must be taken into account. The best way to sort out the additional energy contributions in ferromagnetic system is to consider each energy term individually<sup>(5-11)</sup>.

1. The exchange energy arises from the quantum-mechanical interaction of the spins of unpaired electrons. The "molecular field" is essentially defined such that the energy of interaction of the magnetic moment of the atom with the molecular field is equal to the exchange energy. This energy does not enter the thermodynamic picture except as a

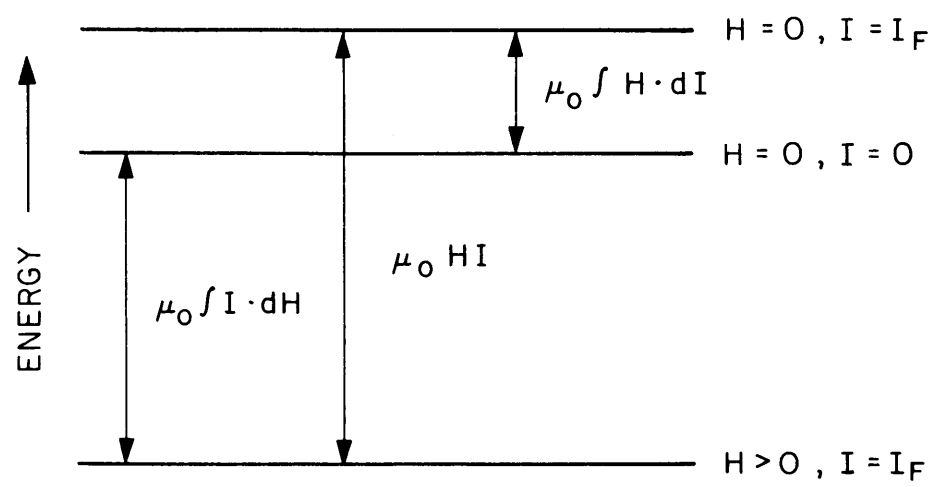
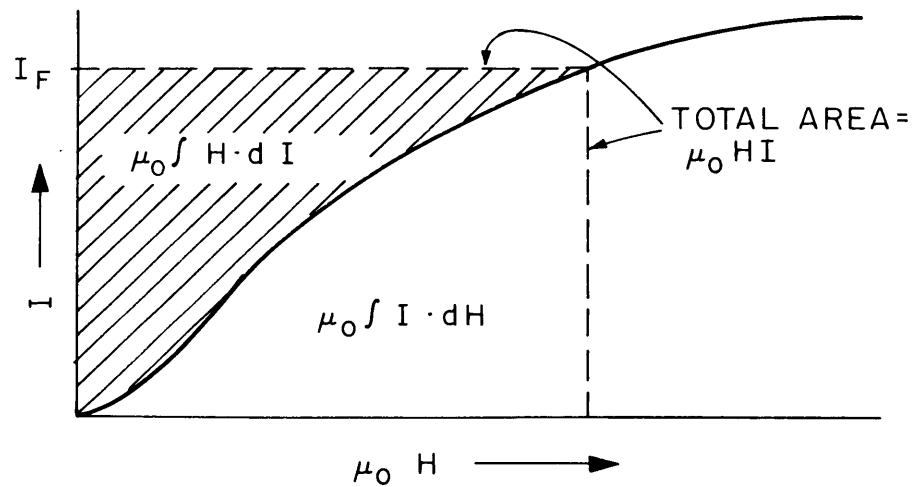


FIG. 1 SCHEMATIC MAGNETIZATION CURVE OF AN ELLIPSOIDAL SINGLE CRYSTAL OF A PARAMAGNETIC MATERIAL ILLUSTRATING THE ENERGY CHANGES INVOLVED.

contribution to domain wall energy because we have considered the domained, ferromagnetic crystal as the standard state, i.e. this energy has already been included in the standard Gibbs free-energy change.

The size of the molecular field is estimated to be about  $10^7$  gauss. This is important because it shows that even our "high" applied fields of  $10^5$  gauss will have little effect on the saturation magnetization,  $I_s$ , which already exists in the domains. Since  $I_s$  does not change significantly with the applied field,  $dI = 0$  and equation (5) shows that the internal energy due to magnetization will not change with the field. The mutual energy between the specimen and the field,  $dG_{\text{mag}}$  of equation (8), is now equal to  $-\mu_0 \vec{I}_s \cdot d\vec{H}$  and is the overriding factor, especially under high-field conditions.

2. The anisotropy energy or the magnetocrystalline energy arises because the magnetic dipoles tend to align along certain easy directions of magnetization. The orbital magnetic moment of the electrons is strongly coupled to certain lattice directions due to electrostatic interactions. The spin magnetic moment of the electrons, which accounts for more than 90% of the observed magnetization, is weakly coupled to the orbital moment. Under the influence of an external field, the spin dipoles rotate out of this coupling "easy" direction in order to reduce the Gibbs magnetic energy. The order of magnitude of this effect for complete rotation into the hard direction is less than  $5 \times 10^5$  ergs/cm<sup>3</sup> for Fe-Ni alloys. The free-energy change of the austenite-to-martensite transformation is of the order of  $10^9$  to  $10^{10}$

ergs/cm<sup>3</sup> which completely overshadows the magnetocrystalline effect.

3. The magnetoelastic energy arises from the interaction between the magnetization and the mechanical strain of the lattice. Kittel and Galt <sup>(8)</sup> have shown that this energy can be thought of as the change in magnetocrystalline energy with strain. A crystal will deform spontaneously in order to lower the anisotropy energy and we observe this effect as magnetostriction. The strains involved are  $10^{-6}$  to  $10^{-4}$ , and they exist with or without the applied field. The field, however, can alter the value of the magnetostriction by changing the magnitude and orientation of the magnetization.

The lowest energy state of the crystal occurs when these strains are allowed to take place. When the domains are confined by other domains or other crystals, the energy of the crystal is not allowed to decrease and a certain amount of elastic energy is stored at the boundaries. The normal Gibbs free energy is measured for a crystal that has a domain structure in which the net magnetization is near zero. This means that it already contains many domains of closure and, therefore, a certain amount of magnetoelastic energy. When a field is applied to the polycrystalline specimen, the domains of closure disappear in favor of domains with dipoles aligned with the field. This eliminates the magnetoelastic energy of the domains of closure, but we now have different grain-boundary constraints which could increase the magnetoelastic energy. Fortunately, the strains are small and the energies involved are negligible, i.e. of the order of  $10^3$  ergs/cm<sup>3</sup> in iron.

4. The magnetostatic energy, the self energy, the demagnetization energy, and the free-pole energy are all one and the same thing. In one line, it is the energy of the magnetic field generated by the dipoles of the specimen, and the interaction of its magnetization with that field. Even though an isolated magnetic pole does not exist, mathematically and conceptually, it is sometimes convenient to consider the magnetization of the material in terms of free poles of magnetism at opposite ends of the specimen. These surface poles produce a field within the material of value,  $H_d$ , which is antiparallel to the magnetization. The energy of interaction of the magnetization with this demagnetizing field,  $-\frac{1}{2} \int \vec{H}_d \cdot \vec{M} dV$ , is only readily calculable for one general shape, the ellipsoid. Other more complex shapes are very difficult to treat because of nonuniform demagnetizing fields and internal free poles. This leads to serious complications, such as nonuniform magnetization within the specimen. (It is necessary to assume uniform magnetization in order to derive equation (4).) For the ellipsoid,  $H_d = -NM$  where  $N$  is the demagnetizing factor varying from zero (along needles) to  $4\pi$  (normal to discs). The magnetostatic energy per unit volume is then:

$$E_{ms} = 1/2NM^2 \quad (9)$$

This energy is sizeable and cannot be ignored until the applied field,  $H_a$ , is much larger than  $1/2NM$  (i.e.  $1/2H_d$ ). Taking  $M_s = 1700$  ergs/gauss  $\text{cm}^3$  and  $N = 4\pi$ , we see  $1/2NM \approx 20$  kOe. Therefore, at lowest applied field of 20 kOe in the present research, the demagnetization effect can be the same order of magnitude as the magnetic contribution

to the Gibbs free energy.  $N$ , however, is usually much lower than the maximum value of  $4\pi$ .

Since the bulk austenite in the alloys under study here is paramagnetic or weakly ferromagnetic, its value of the magnetization is small enough to make  $H_d$  insignificant compared to the level of our applied fields. In addition,  $N$  is much smaller than the maximum value of  $4\pi$ , inasmuch as the adopted specimen is rod-shaped. Although, there are free poles at grain boundaries, these are usually considerably fewer in number than the free surface poles, especially when the domains are aligned with the external field. A ferromagnetic austenite spontaneously lowers its energy by creating domains of closure and by aligning the domains from grain to grain. When the field is applied, the domains of closure are consumed by domains oriented nearly parallel to the field. This causes an increase in the magnetostatic energy at grain boundaries and other surfaces. The exact energy changes are too complex to calculate. Fortunately, this energy is small compared to the Gibbs magnetic-energy change of the transformation.

The magnetostatic energy of the strongly ferromagnetic martensite phase is also complex. If we approximate the martensite morphology by oblate spheroids with large radius-to-semithickness,  $r/c$ , ratios, and if they are magnetized parallel to their major axis,  $r$ , the demagnetization factor,  $N_r$ , approaches zero. If, however, they are magnetized parallel to the semi-thickness axis,  $c$ ,  $N_c$  can approach  $4\pi$ . For an oblate spheroid, the energy difference between a plate oriented parallel with, versus perpendicular to, the field is (11)



$$\Delta E_{ms} = 1/2(\Delta M_s)^2(N_c - N_r) \quad (10)$$

Substituting  $N_c = 0.926$ ,  $N_r = 0.037$  (for  $r/c = 20$ ) (12) and  $\Delta M = 1400$  erg/gauss  $\text{cm}^3$ , (the difference in magnetization between austenite and martensite), yields a value of  $1.1 \times 10^7$  ergs/ $\text{cm}^3$  for  $\Delta E_{ms}$ . This energy is two or three orders of magnitude smaller than the free-energy change of the transformation; however, it is no less than 10% of the contribution of the magnetic Gibbs term for applied fields of 20 to 140 kOe.

The martensite morphology should, therefore, have the following tendencies:  $r$  will tend to align parallel to  $H$  and the  $r/c$  ratio of plates parallel to the field should be greater than that perpendicular to the field. However, as the volume fraction of the martensite increases, the free poles of the individual plates interact and the orientation dependence should become less significant.

5. The Block or domain-wall energy arises from the exchange energy and magnetostatic effects at the boundary. When a high field is applied to a domained structure, the favorably oriented growing domains eventually eliminate the domain walls. This lowers the internal energy of the material. Block-wall energies are of the order of 1 to 3 ergs/ $\text{cm}^2$  and are negligible for present purposes. In iron, the wall is about 120 atoms thick and has an energy of 2.9 ergs/ $\text{cm}^2$ . This is equivalent to an energy density of  $\sim 10^6$  ergs/ $\text{cm}^3$  (7) ( $\sim 10^5$  ergs/ $\text{cm}^3$  for nickel), and could be a factor during nucleation. However, small particles ( $\sim <200\text{\AA}$  in diameter) are probably composed of single domains;

therefore, the domain-wall energy does not enter the nucleation calculations, except perhaps as a small contribution to the surface energy of the martensitic interface.

We have now shown that equation (7) is adequate to describe the free energy of each phase. The total free-energy change per unit volume of the martensitic transformation is then given by:

$$\Delta g_T = \Delta g_o - \mu_o \vec{H} \cdot \Delta \vec{M} \quad (11)$$

where  $\Delta g_o$  is the usual Gibbs free-energy change and  $\Delta \vec{M} = \vec{M}_\alpha - \vec{M}_\gamma$  i.e. the difference between the magnetization of the two phases. Thermodynamically, the other energy contributions, except possibly the magnetostatic energy, are negligible with respect to  $\Delta g_T$ . (This is summarized in Table 1.) On the other hand, we cannot say that the kinetics of the reaction are not altered by these complications.

TABLE 1

Relative Magnitudes of Various Magnetic Energies

<u>Type of Energy</u>	<u>Energy Range, ergs/cm<sup>3</sup></u>
$\Delta g_o^{\alpha \rightarrow \gamma}$	$10^9 - 10^{10}$
$\Delta g_{\text{magnetic}}$	$10^7 - 10^8$
magnetostatic (shape anisotropy)	$0 - 10^7$
magnetocrystalline	$0 - 10^5$
magnetoelastic	$0 - 10^4$
domain wall	$10^5 - 10^6$ (1 - 3 ergs/cm <sup>2</sup> )

### I-3. Advantages of Magnetic Fields for Research on Martensitic Transformations

Magnet fields, like hydrostatic pressure, offer another thermodynamic variable to study martensitic transformations. For a strong influence by a magnetic field, there must be a large difference in magnetization between the parent and product phases. Martensitic transformation in steels more than satisfy that criterion.

Pressure can be used to suppress the martensitic transformation because the molar volume of the martensite is greater than that of the austenite. Although the experimentally attainable effect of pressure is greater than that of magnetic fields (1 kbar  $\approx$  21 kOe for  $\gamma$  to  $\alpha$  at 300°K in pure iron), obscuring side-effects can enter when pressure is applied to influence a reaction that takes place by a shear mechanism. It is also experimentally easier to measure the physical properties of a crystal in an applied field than one confined in a pressure chamber.

In order to calculate the free energy of a phase at high pressures, it is necessary to know the molar volume of both phases as a function of pressure. This is difficult to measure, and it is usually assumed that the compressibilities of both phases remain unchanged under pressure. To interpret magnetic experiments, we need to know the magnetization as a function of field strength. This is readily measurable; in fact, we have already shown that, for most cases, the saturation magnetization leads to accurate values of the Gibbs magnetic energy. Magnet fields, therefore, offer a unique opportunity to study the kinetics of a thermally activated shear transformation without changing the temperature, pressure, or stress state of the material.

## II. DISCUSSION OF LITERATURE

### II-1 Martensitic Transformation Characteristics

The characteristics of the martensitic transformation have been repeatedly documented in the literature. (e.g.13-14) The following discussion is merely designed to introduce the terminology, to bring up the pertinent equations, and to pinpoint the critical issues.

#### II-1.1 Kinetics

A martensitic transformation is best defined as a diffusionless transformation that exhibits a macroscopic shape-change. Attempts<sup>(15-17)</sup> have been made to further classify the reaction according to the observed kinetic behavior, i.e. how the reaction proceeds with time and temperature. Much of the disagreement between these schemes has just been a matter of semantics; however, there are some fundamental differences and misconceptions. Raghavan and Entwisle (R-E)<sup>(15)</sup> separate the kinetic classification into three categories: athermal (defined as transformations in which the progress of the reaction depends mainly on falling temperatures), burst, and completely isothermal. Magee and Paxton (M-P)<sup>(16)</sup> define athermal transformations as those in which time at temperature is not important, i.e. the total fraction transformed should not be a function of prior thermal history. Stabilization effects which occur in the "R-E athermal" alloys eliminate these from the M-P definition of athermal. They view the kinetics of ferrous martensitic transformations as basically isothermal with the reaction rate having a maximum with respect to temperature. The difference in observed kinetics are interpreted as stemming from the "parasitic" influences of

stabilization and autocatalysis (e.g. bursting phenomena).

Raghavan and Cohen<sup>(17)</sup> used the term anisothermal<sup>(18)</sup> to describe thermally activated transformation during cooling to the test temperature in which the activation energies for nucleation are so low that the initial transformation cannot be measured or suppressed (due to the limitations of our measuring equipment and the experimentally attainable quench rates). They also define the athermal mode as transformation without thermal activation corresponding to the situation in which the activation energy for nucleation,  $\Delta W_a$ , goes to zero or to the level of thermal energy available at the test temperature.

Although the R-E definition of athermal is convenient for practical purposes, the question of whether all martensitic transformations are thermally-activated isothermal reactions or whether there exists true athermal modes at higher driving forces is fundamental to the transformation theories. From the Kaufman-Cohen-Raghavan model<sup>(19-20)</sup> one would expect a true athermal behavior at temperatures below that which  $\Delta W_a$  approaches  $kT$ . Magee and Paxton<sup>(16)</sup> performed a critical experiment to determine whether a distinguishable athermal nucleation mode is operative. They found that a temperature exists ( $\approx 135^\circ\text{K}$  in Fe 31.5Ni) below which the transformation rate decreases and there is no evidence for athermal nucleation. They, therefore, concluded that the alloy exhibits thermally activated isothermal C-curve kinetics and it is the elastic coupling between plates, i.e. bursting, that is largely responsible for the accentuation of the transformation during cooling.

However, these experiments were not quite that clear-cut because the investigators did not find a C-curve by straight quench-and-hold experiments, but by first quenching to 77°K and then upquenching to the test temperature, using the method of Machlin and Cohen.<sup>(21)</sup> (They also went through a 77°K → room temperature → testing temperature cycle in order to avoid the complication of anisothermal martensite formed on upquenching.)

Magee<sup>(22)</sup>, in his small particle experiments, was able to observe isothermal kinetics in a normally bursting Fe 22 Ni 0.49C alloy over the temperature range of 163° to 223°K. Unfortunately, he did not perform the critical experiment of transforming these particles at 77°K in order to look for the C-curve kinetics. He would have answered these questions once and for all.

The actual quantitative kinetic analysis has recently been reviewed in detail by Ragahavan and Cohen.<sup>(17)</sup>  $n_t$ , the number of most potent embryos existing at any time per unit volume of alloy, can be expressed as:

$$\begin{aligned} n_t &= (n_i + p f - N_v) (1 - f) \\ &= (n_i + f [ p - \frac{1}{\bar{V}} ] ) (1 - f) \end{aligned}$$

- where
- $n_i$  = number of preexisting nucleation sites or embryos in the parent austenite.
  - $p$  = number of autocatalytic embryos produced per unit volume of martensite.
  - $f$  = volume fraction of martensite formed.
  - $N_v$  = number of martensite plates per unit volume of alloy.
  - $\bar{V}$  = mean volume per martensitic plate.

The  $(1 - f)$  factor on the right hand side of Eq. 12 takes into account the potential nuclei that are swept up by the transformed martensite before they can nucleate. The pf autocatalytic term<sup>(15)</sup> assumes that the number of autocatalytic embryos created are proportional to the volume fraction of transformed martensite, suggesting that elastic and plastic strains set up in the austenite by the martensite might be involved in the autocatalytic mechanism. pf works as well as or better than other attempted<sup>(23)</sup> functional relations, using the fit between the experimental transformation curves and those calculated from these kinetic equations as the criterion. The best up-to-date equation<sup>(17)</sup> to describe the kinetics from measurements amenable to quantitative metallography is the following:

$$\frac{df}{dt} = n_t \nu \exp(-\Delta W_a/RT) (\bar{V} + N_v \frac{d\bar{V}}{dN_v}) \quad (13)$$

where  $t$  is the time in seconds,  $\nu$  is the lattice vibrational frequency, and  $\Delta W_a$  is the activation energy for nucleation at temperature  $T$ . This equation contains many inherent assumptions, such as a single activation energy for all nucleation sites and random nucleation events. A detailed critical analysis of Eq. 13 will be given in a later section of this thesis.

If the mean plate volume is not a function of the amount of transformation, then  $\frac{d\bar{V}}{dN_v}$  equals zero in Eq. 13. The Fisher partitioning formula<sup>(24)</sup> predicts that as  $f$  increases, the transformed plates divide the austenite grains into smaller and smaller untransformed pockets giving rise to smaller and smaller plates. Pati and Cohen<sup>(25)</sup> have

shown that this overestimates the number of martensite plates required to give a certain fraction of transformation. If martensite were to nucleate uniformly throughout the specimen, as Eq. 13 implicitly assumes, then one might expect a Fisher type of partitioning to take place. In fact, however, plate clustering is commonly observed during the early stages of transformation. The average plate volume within a cluster might not be a strong function of  $f$ , if the cluster is simultaneously spreading into new austenite grains. Obviously, the average plate size must eventually decrease during the final stages of transformation when the clustering is complete and new plates are forced to nucleate within the small pockets of retained austenite.

Ragahavan<sup>(26)</sup> did just such an analysis. Following the Johnson-Mehl-Avrami treatment and assuming that the autocatalytic effect is of the same magnitude on both sides of the grain boundary, he considered the transformation as a two-stage process: (i) the increase with time of the number of austenite grains in which first-plate nucleation takes place, and (ii) the progress of further transformation within such grains. Using this treatment, he was able to extend the fit between the calculated and experimental transformation curves to higher percentages of martensite. To be able to fit the whole transformation curve for a variety of testing conditions with a minimal number of floating parameters-still remains as the unfulfilled goal of the martensite kineticists.

Experimentally, McMurtrie and Magee<sup>(27)</sup> found that the average volume of martensite plates was constant ( $\approx 7 \times 10^{-9} \text{ cm}^3$  for a grain size of 0.02 cm in an Fe<sub>24</sub>Ni 0.4C alloy) over a range of volume fractions from



0.07 to 0.55. By assuming that the number of new plates per unit volume of austenite per degree temperature change equals  $\phi \frac{d(\Delta G_o^{\gamma \rightarrow \alpha})}{dT}$ , where  $\phi$  is a proportionality constant and  $\frac{d(\Delta G_o^{\gamma \rightarrow \alpha})}{dT}$  is the entropy change on transformation, Magee<sup>(28)</sup> derived:

$$\ln(1 - f) = \bar{V} \phi \left( \frac{\partial \Delta G_V^{\gamma \rightarrow \alpha}}{\partial T} \right) (M_s - T_q) \quad (14)$$

where  $T_q$  is the quench temperature below  $M_s$ . A plot of  $\ln(1 - f)$  versus  $(M_s - T_q)$  was linear up to  $(1 - f) = 0.05$ , implying  $\bar{V}$  is effectively constant over this range if Eq. 14 is valid. Contrary to the other workers, Pati and Cohen<sup>(25)</sup> found that, in an Fe24Ni3Mn isothermally-transformed alloy, the initial plate volume ( $f \sim 0.01$ ) was largest near the nose of the C - curve, and varied from 1 to  $4 \times 10^{-10} \text{ cm}^3$  over the  $60^\circ\text{C}$  range on either side of the nose. At about 30% martensite,  $\bar{V}$  at all the reaction temperatures approached a constant value of  $1 \times 10^{-10}$ . The apparent discrepancy with other investigators may be due to differences in alloy composition, however, it is more likely attributable to the fact that Pati measured plate volumes very early in the transformation before the steady-state cluster-spreading mode set in. Unfortunately, in the sensitive temperature range near the nose, Pati has no  $\bar{V}$  measurements between 1 and 33% martensite; therefore, any rapid drop off of  $\bar{V}$  with  $f$  is only speculation at this stage. An additional point related to this topic is that one might not expect much variation in "plate" volume if the martensite morphology is lathlike and grows in packets, as described in the next section.

## II-1.2 Morphology

Ferrous martensites are often divided into two major types - lath (or packet) and plate (or lenticular) - which vary with respect to alloy composition, temperature range of formation, crystallography, and fine structure.

Lath (or packet) martensite, as the name implied, grows as thin narrow strips, usually with the long direction parallel to with  $6^\circ$  of  $[110]_\gamma$  (29-30). Adjacent laths having parallel widths may be twin related. In these cases, the common interface is a  $(112)_\gamma$  plane which is closely parallel to the  $[110]_\gamma$  but  $\sim 5\ 1/2$  degrees from the long axis of the lath. The laths are typically aligned along a  $\{111\}_\gamma$  plane with their widths and lengths approximately parallel to each other. These planes of laths, in turn, are stacked parallel to one another, forming what is usually referred to as the packet structure when observed by optical microscopy. The habit plane of these packet planes is  $\{111\}_\gamma$ , but this may be considered as a pseudo-habit since the laths themselves are nearly parallel to a  $\{112\}_\gamma$ , or  $\{hh1\}_\gamma$  type.

Lath martensite forms by slip and contains a high density of dislocations. Speich<sup>(31)</sup> estimated the dislocation density inside the laths to be between  $0.3$  and  $0.9 \times 10^{12}$  cm/cm<sup>3</sup> from electrical resistivity measurements. Because of the close proximity of the planes of laths in a packet, the austenite can transform to 100% martensite. In contrast to the plate (or lenticular) martensites, which can grow at one-third the speed of sound in the metal, there is evidence<sup>(32-33)</sup> that lath martensite grow more slowly at speeds that can be filmed.

Plate martensite, which is often idealized as double-convex lens in shape, can have  $\{3,10,15\}_\gamma$ ,  $\{259\}_\gamma$  or  $\{225\}_\gamma$  habit planes. The considerable scatter around these habits has been attributed by Bell and Bryans<sup>(34)</sup> (for the  $\{3,10,15\}_\gamma$  habit) to the effect of prior transformation and prestrain causing accommodation distortion during growth. However, this is a matter of considerable controversy. The  $\{3,10,15\}$  type of plates are well characterized by the phenomenological crystallographic theories, but the  $\{225\}$  type requires either a dilatation in the habit plane or a deformation of the parent austenite<sup>(35)</sup> to fit the theories. The plates themselves often contain a midrib composed of a regular array of  $\{112\}_\gamma$  transformation twins spaced 60 to 100Å apart. Shearing action appears to start on the plane of the midrib and is propagated in parallel but opposite directions on both sides of this plane.

Bokros and Parker<sup>(32)</sup> have demonstrated that the bursting phenomenon commonly associated with the  $\{259\}_\gamma$  habit can be related to mechanical coupling between plates, implying that autocatalysis is strongly influenced by the surrounding stress and plastic strain fields caused by the existing plates. These plates are commonly observed to have an inner twinned region and an outer slipped region. Various investigators<sup>(37-39)</sup> have suggested that the change in the lattice-invariant mode from twinning to slip is associated with a local temperature rise due to the enthalpy of transformation. Recent observations by Krauss and Marder<sup>(33)</sup> in which  $\{259\}$  martensite was tempered at 157°C and then requenched demonstrated that certain plates widen on the second quench by a simple extension of the outer slipped region with no apparent twinning. Since the enthalpy heat of the first formed section had long been dissipated,

this shows that temperature is not the overriding factor, otherwise the new sections would have formed by twinning. Huizing and Klostermann<sup>(40)</sup> have pointed out that surface martensite, lath martensite, and the untwinned part of a martensitic plate formed after a burst are all morphologically different, but may be formed by a common mechanism.

Several alternate explanations have been offered to explain the transition from lath to plate martensite. Owen, Wilson, and Bell<sup>(41)</sup> suggested that if  $M_s$  is greater than  $T_z$ , the Zener ordering temperature, lath martensite should form. However, low-carbon alloys having  $T_z$  near 0°K should always form in the packet mode, but Fe 31 to 33 Ni alloys transform to plates.<sup>(42)</sup> The proposal<sup>(e.g.43)</sup> that low stacking-fault energy favors the formation of lath martensite has also been rejected<sup>(33)</sup> because both Ni and Mn favor plate formation, whereas Ni raises the stacking-fault energy and Mn lowers it. The situation is not clear-cut, however, in as much as the Fe Ni Mn alloys have a {225} habit which is not well understood. Increasing carbon or nickel favors the formation of plates, but both of these alloying elements also lower the  $M_s$  temperature. The temperature of transformation has been shown<sup>(e.g.33)</sup> to offer the best correlation for the lath-to-plate transition. Lower temperature favors a twinning mode of transformation which presumably favors plate martensite. Recently, however, Davies and Magee<sup>(42)</sup> were able to produce plate morphologies at temperatures as high as 210°C in low-carbon Fe Ni Co alloys. They demonstrated that packet martensite always formed from paramagnetic austenite and that austenite ferromagnetism is a necessary but not sufficient condition for the formation of plate morphologies in invar-type alloys. This effect was attributed to

increased flow resistance of the austenite due to ferromagnetic strengthening.

The strength or plastic behavior of the martensite and austenite is emerging as a viable explanation for the transition in modes of transformation and is gathering a growing body of support. Related to this line of reasoning, some investigators<sup>(33,44)</sup> suggest that an important criterion is the relative magnitudes of the critical resolved shear stress for slip and twinning at a given temperature and composition. On the other hand, Owen, Schoen, and Srinivasan<sup>(45)</sup> feel that the different morphologies are the result of differences in the growth rate of the two martensitic types, whereas Christian<sup>(46)</sup> feels that the growth mechanism is determined by the nature of the interface. Both views can be self-consistent if the growth rate determines the nature of the interface or vice versa. An additional idea by Bell and Owen<sup>(47)</sup> is that it is necessary to exceed a critical driving force ( ~ 315 cal per mole) to change from dislocated to twinned martensite. Pascover and Radcliffe<sup>(48)</sup> applied this concept to other FeNi and FeCr alloys and found agreement, except for Fe5Cr which should have been twinned but was not. Olson,<sup>(49)</sup> in considering strain-induced nucleation, pointed out that we might expect the lath morphology when the ratio of the nucleation-to-growth rate is high and plates when the ratio is low. This suggestion could have some merit, but it may be that the actual event of changing modes in the lattice-invariant strain plays an important role in the generation of new autocatalytic nucleation sites.

### II.1.3 Nucleation

At present, there are two schools of thought concerning the crucial mechanism involved in the nucleation of martensite: The older Kaufman-Cohen<sup>(19)</sup> model views the creation of new interface dislocations as the rate-controlling step, while other investigators, e.g. Magee<sup>(28)</sup>, believe that the motion of the austenite-martensite interface is rate-determining.

At this time, the Kaufman-Cohen-Raghavan<sup>(20,50)</sup> (KCR) model (which is an improvement and an extension of the Kaufman-Cohen model) is the only quantitative treatment of martensite nucleation, and for this reason it is the only model used for quantitative comparisons in this thesis. In order to have a starting point, they assumed that embryos greater than that needed for classical nucleation preexist. They envision that the embryos could have formed at high temperatures (at which the austenite is actually the stable phase) by the incorporation of existing dislocations. These embryos are then frozen-in on cooling at temperatures near 300°C and are ready to trigger-off when brought into the  $M_s$  range.

This is very speculative, but just how the embryos originate is not critical to the model. They then assume that the embryo is in the form of a Knapp-Dehlinger<sup>(51)</sup> mini-plate having a  $(225)_\gamma$  Frank<sup>(52)</sup> interface. Christian<sup>(53)</sup> has criticized the use of Frank's model of the interface because of the experimental evidence that the close-packed directions of the two phases are not exactly parallel and do not lie in the habit plane. These observations are contrary to Frank's assumptions.

Christian<sup>(54)</sup> also pointed out that the Frank interface is essentially two dimensional and predicts a large dilatational strain which is energetically unfavorable and not observed experimentally in the fully grown plates. Finally, Owen et al.<sup>(41)</sup> point out that Frank's model of the interface produces the lattice invariant deformation by slip, whereas electron microscopy studies have always revealed a finely twinned structure for this habit, although not completely out to the final interface.

These criticisms seem damaging, and no one, including the authors, expects that the embryos are really well-formed particles of martensite. Someone had to be bold enough to make this kind of assumption in order to get the job underway. The KCR model is really a prototype model which to-date has worked remarkably well to fit a wide range of data despite all its shortcomings. It has also evolved from a model of the initial nucleation site to a kinetic model describing the growth of a plate. The Raghavan-Cohen grow-path paper<sup>(50)</sup> expanded Magee's<sup>(16)</sup> analysis and considered the growth path of the embryo in terms of its radial-growth and thickening kinetics. The predicted behavior of rapid radial-growth until impingement followed by a slower thickening process is reminiscent of the micrographs of plates showing a fast midribbed section and an outer slower-growing slipped region. This is one of the encouraging results of their model. A simple extension of the model to include twinning and heat effects would be enlightening.

The critical step for nucleation in the above model is the creation of a critical interfacial dislocation loop of radius  $\rho^*$  at the tip of the plate. This newly created loop is parallel to the already existing loops which are perpendicular to the "flat" austenite-martensite interface. The normal of the loop is in the  $[554]_{\gamma}$  direction for a  $(225)_{\gamma}$  habit. The

critical step of loop nucleation corresponds to growth in the radial direction. Plate thickening is envisioned to occur by the motion of the screw components of the dislocation loop which are parallel to the  $(225)_{\gamma}$  habit plane and lie along the  $[110]_{\gamma}$  direction.

There is no driving force for thickening during the first few radial-growth steps near the saddle point, but as the system moves sufficiently along the free-energy surface, the free-energy change per unit growth step in a given direction depend only on the partial derivative of the free-energy change in that direction. It is envisioned that the embryo is not at the saddle point but somewhat beyond in the super-critical regime. The actual growth path is then determined by kinetic factors, i.e. by the relative velocities of motion in the radial and thickening directions. These, in turn, will depend on the transformational forces in these directions, as well as on the prevailing kinetic barriers. The growth in the radial direction of the edge component of the existing loops is easier than thickening, yet it was assumed that the embryo maintains its oblate-spheroidal geometry during the growth process. One might expect the Knapp-Dehlinger plate to be unstable and that the edge components of the loops would run off in the  $[1\bar{1}0]_{\gamma}$  direction. If this can happen, the Magee suggestion that dislocation motion is the critical step would be substantiated.

The specific equations of the KCR model which were used in this thesis to check the correlation with the data are the following:

$$\Delta G = \frac{4}{3}\pi r^2 c \Delta g_T + \frac{4}{3}\pi r c^2 A + 2\pi r^2 \sigma \quad (15)$$

$$\frac{\partial \Delta G}{\partial r} = -\frac{5}{4}\mu b^2 \frac{rc'}{\rho^*(\delta r)} [\ln(\rho^*/b) + 0.4 + z] \quad (16)$$



$$\Delta U^* = \frac{5}{16} \mu b^2 \rho^* [\ln(\rho^*/b) - 1.6 + z] \quad (17)$$

- where
- $\Delta G$  = free-energy change attending the formation of a martensitic particle oblate-spheroidal in shape of radius  $r$  and semithickness  $c$ ,
  - $\Delta g_T$  = total (chemical plus magnetic) free energy per unit volume given by Eq. 11,
  - $\Delta c/r$  = strain energy per unit volume of the particle,
  - $\sigma$  = interfacial energy per unit area which is considered coherent in the loop nucleation step but semi-coherent for the bulk interface,
  - $\mu$  = shear modulus of the austenite,
  - $b$  = Burgers vector,
  - $\rho$  = critical-loop radius,
  - $c'$  = semithickness of the embryo at a distance  $\delta r$  from the tip,
  - $\delta r$  = incremental growth step of the plate in the  $r$  direction,
  - $z$  = core-energy parameter  $\sim 1$ .

Experimentally, the small-particle and the high-pressure experiments have given us the greatest insight into the nature of the embryo. Electron microscopy observations are also valuable because they give us a feel for the types of dislocation structures, stacking faults, and interfaces that are associated with the martensitic product. Much effort has been directed to observing the embryo directly, but as Pati and Cohen<sup>(23)</sup> pointed out, it is improbable that one exists in the small volume of an electron-microscopy specimen under actual observation. In one instance, Venables<sup>(56)</sup> found a strain-induced embryo at the intersection of two

plates, and Olson and Cohen<sup>(57)</sup> used a double shear model to describe the mechanism of its formation. Detailed treatments such as these throw a great deal of light on the nucleation mechanism.

The classical small-particle experiments of Cech and Turnbull<sup>(58)</sup> contain a number of simple yet revealing results. By demonstrating that some particles would not transform at the lowest cooling temperature, they proved that the nucleation site for martensite has a heterogeneous character, thereby eliminating all homogeneous nucleation theories as viable explanations. From the particle size at which about 1/2 of the particles transform on quenching, we can obtain a rough estimate of the numbers of initial embryos per unit volume ( $\sim 10^7 \text{ cm}^{-3}$ ). About 3/4 of their powders were single crystals. By comparing the number of particles containing grain boundaries in the transformed versus the untransformed specimens, they were able to conclude that grain boundaries are not important nucleation sites for the martensitic transformation. Pati and Cohen<sup>(23)</sup> came to this same conclusion using a much more indirect approach on bulk specimens. Cech and Turnbull also reported that the particles that transformed did so by bursting. This is strong evidence that autocatalytic embryos are newly created and not the triggering of prior existing embryos.

Cech and Turnbull treated the martensitic transformation as an athermal reaction, whereas Magee<sup>(22)</sup> studied the isothermal aspects using polycrystalline atomized powders in the "as received" condition. As mentioned previously, he was able to observe isothermal kinetics even in his bursting alloy. He also showed that, when autocatalytic effects are

suppressed, there is no nucleation incubation time. Mechanistically, this means that no detectably slow precursor steps occur in the nucleation process. In other words, at least some of the sites are initially capable of immediately nucleating a martensite plate.

The concept of a single activation energy for initial embryos did not fit the Magee<sup>(22)</sup> data; rather the embryos were found to have a distribution of effectiveness. By assuming that the exponential law for thermally activated processes is valid and that there is a constant attempt frequency, Magee calculated a distribution of activation energies,  $\Delta W_a$ , to fit his data. The derived distribution was quite unexpected in that it showed a negligible number of embryos with activation energies below a certain  $\Delta W_{\min}$  and then an equal number for each additional energy increment thereafter. By using this  $\Delta W_a$  distribution, Magee derived the following:

$$\begin{aligned} \frac{dN_v}{dt} &= \int_0^{\infty} v \exp\left(-\frac{\Delta W_a}{RT}\right) n^*(\Delta W_a) d\Delta W_a \\ &= n^*(\Delta W_a) v RT \end{aligned} \quad (18)$$

where  $n^*(\Delta W_a) d\Delta W_a$  is the number of sites per unit volume having activation energies between  $\Delta W_a$  and  $\Delta W_a + d\Delta W_a$ . Comparison with Eqs. 12 and 13 in Section II-1.1 indicates that  $n_i = n^*(\Delta W_a) v RT$ . The experimental values of  $n^*(\Delta W_a) v RT$  range from  $3 \times 10^4$  to  $2 \times 10^5 \text{ cm}^{-3}$  for FeNiMn, whereas the most widely used previous estimate is  $10^7 \text{ cm}^{-3}$ . He also noted that  $n^*(\Delta W_a) v$  increased with decreasing temperature and suggested that larger driving forces could increase the density of effective embryos. When Magee's tabulated data are plotted, however, (either  $n^*(\Delta W_a)$

or  $n^*(\Delta W_a)$  RT versus T), it is apparent that even the magnitude of the embryo-distribution function varies in a C-curve fashion with temperature. This may be intrinsic, but it would just as easily stem from the assumptions made in the analysis.

The classical high-pressure experiments of Kaufman, et al.<sup>(58)</sup> were interpreted as definite proof that martensitic embryos exist and that they have a higher specific volume than the austenite. An Fe<sub>32.4</sub>Ni austenite had been annealed at high pressures and then quenched under pressure to room temperature. The resulting  $M_s$  temperature at 1 atm pressure was found to be greatly reduced, as the Kaufman-Cohen embryo theory would predict. In addition, it was found that this effect could be reversed, i.e. upon reheating above a certain freeze-in-temperature, Kaufman, et al. were able to raise the  $M_s$  temperature of the alloy back to nearly its normal value. These experiments seem to contradict the results of Radcliffe and Schatz<sup>(59)</sup> who cooled Fe(0.3 - 1.2)C austenites under pressure all the way from 927°C to the  $M_s$  temperature. They concluded that the  $M_s$  depression was that expected from the change in thermodynamic driving force with pressure, and that there was no additional effect of a change in embryo potency. The discrepancies between the two sets of experiments could be related to the large differences in carbon content; however, interstitials should be mobile at the higher temperatures of these experiments. Additional work is needed to clarify this issue using gas-pressure rigs with low-carbon bursting alloys.

## II-2 Magnetically-Induced Martensitic Transformations

The application of a magnetic field to influence a metallurgical process is not a new concept; it has already been used to alter texture<sup>(60-67)</sup>, order-disorder<sup>(e.g. 68-69)</sup>, precipitation<sup>(9,60,70-72)</sup>, and spinodal transformations.<sup>(73)</sup>

### II-2.1 General Magnetic Transformation Characteristics

In 1929, E. Herbert<sup>(74)</sup> demonstrated that magnetizing a quenched steel caused an increase in hardness. This effect was not linked to the martensitic transformation until 1960, when Sadovskii, et al.<sup>(75)</sup> reported that they induced "intensive" martensite transformation in fine-grained Fe 1.5 Cr 23 Ni 0.5 C at 77°K with a pulsed field of 350 kOe. Since that time, work in this area has flourished<sup>(76-97)</sup>. The bulk of this effort has been by Russian scientists using up to 500 kOe pulsed magnetic fields on athermal chromium-nickel alloys. (A pulsed field of  $10^{-4}$  to  $10^{-3}$  second duration is generated by discharging a capacitor bank through a solenoid. Most of the transformation occurs with the first pulse<sup>(77,88)</sup>; the third and subsequent pulses give no noticeable change in the amount of martensite.) These results are summarized schematically in Fig. 2. Typically, the effect of the field is to raise  $M_S$  in a linear fashion by some 0.1 to 0.3°C/kOe, as shown in Fig. 2a. At any given temperature, above the normal  $M_S$ , it is necessary to raise the field to a certain critical value,  $H_K$ , before any effect can be detected.  $H_K$  increases the  $M_S$  temperature to that of the testing temperature. Fields greater than  $H_K$  induce greater and greater amounts of martensite, as depicted in Fig. 2b.

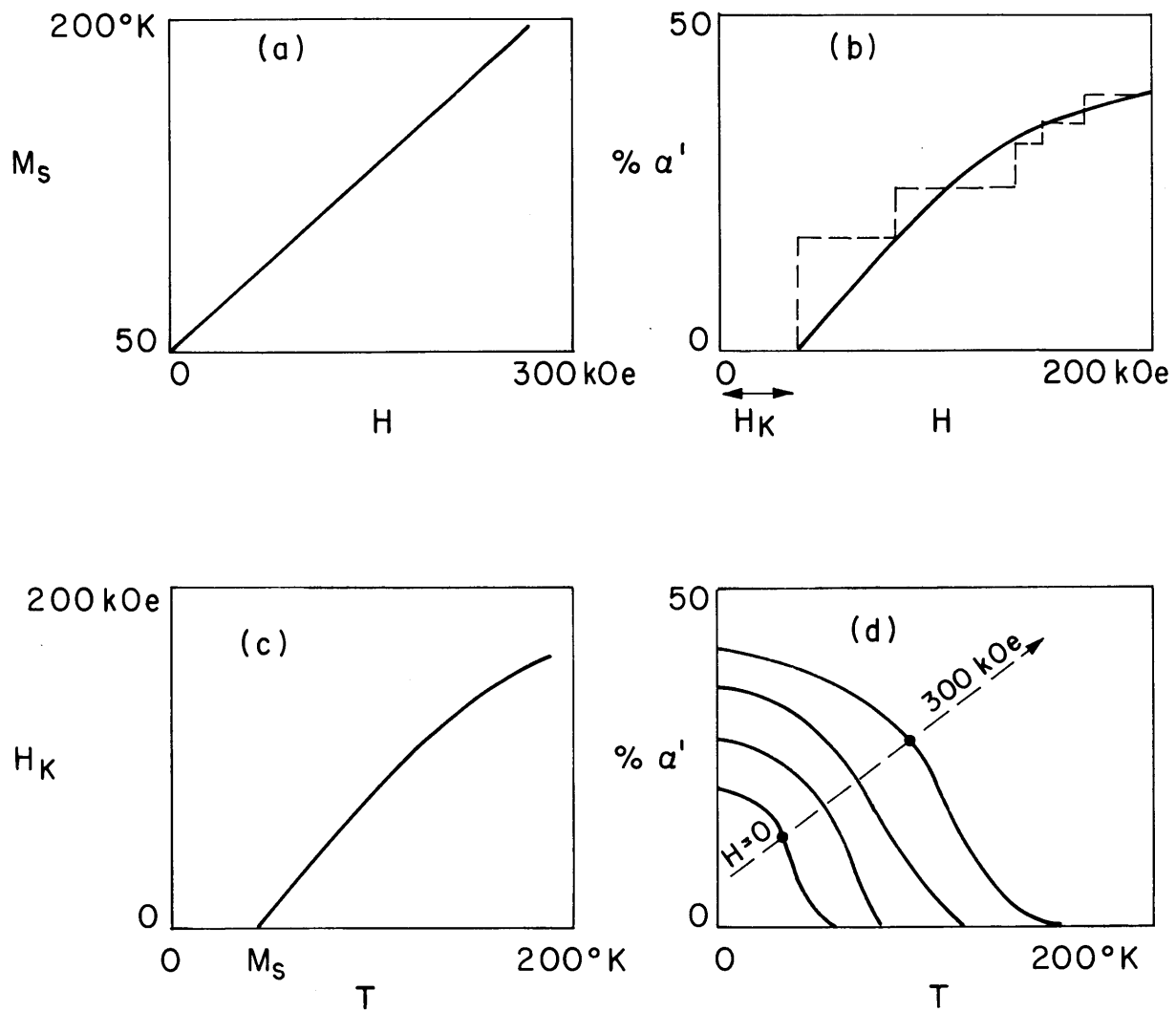


FIG. 2 SCHEMATIC SURVEY OF PAST PULSED FIELD WORK

The solid line is measured from a series of different specimens; however, if larger and larger pulses are applied to the same specimen, we see a stepped behavior in which the first jump at  $H_K$  is the largest. As might be expected, Fig. 2c indicates that higher and higher values of  $H_K$  are necessary to initiate an observable field effect as the temperature is raised. Finally, Fig. 2d illustrates the overall athermal transformation characteristics for applied fields from 0 to 300 kOe. The whole transformation curve is shifted to higher temperatures. Turning on a field during the course of a transformation effectively shifts the system to one of the higher transformation curves.

Early workers<sup>(75)</sup> in studying the effect of H on the  $\alpha'$  transformation varied the grain size of their alloy in such a way that the finest grained specimen had an  $M_S$  just below liquid nitrogen temperatures. When the field was applied, they saw the largest increase in the amount of  $\alpha'$  with the finest grained specimen, i.e. in which there was no significant prior transformation. Unfortunately, the interpretation of this effect was that "the martensite had been 'artificially stabilized' by the small grain size giving a sort of 'supermetastable' state which undergoes supercooling below the normal position of the transformation point." This reasoning led researchers astray for a number of years. They were interpreting the pulse as "destabilizing"<sup>(81)</sup> the austenite or as "removing obstacles to the development of the potentially possible transformation under magnetostriction stresses."<sup>(79)</sup> On the other hand, this viewpoint led to the investigation of other forms of "austenite stabilization", i.e. that due to deformation and prior transformation.

The only study of the effect of elastic deformation was by Fokina and Zavadskiy<sup>(77)</sup> who showed that the combined effect of elastic stresses and magnetic field were additive. Plastic deformation of the austenite was considered to suppress the  $\alpha'$  transformation; thereby, requiring larger values of  $H_K$  in order to initiate the reaction. If we have prior  $\alpha'$ , it is usually much more difficult for the field (or any other driving force) to increase the percent martensite; therefore, fields are not very effective in eliminating retained austenite.

Malinen and Sadvoskii<sup>(85)</sup> have shown that the  $A_S$  temperature for the reverse ( $\alpha'$  to  $\gamma$ ) transformation in Fe (26-31) Ni alloys is raised by a steady field of 22 kOe. This is consistent with the increased stability of the ferromagnetic phase in high fields (as long as  $A_S < \theta_C$ , the Curie temperature).

## II-2.2 Pulsed Versus Steady Fields

The application of a pulsed rather than a steady field could introduce complications. In fact, early investigators believed that the induced stresses were triggering the reaction. Since then, much Russian effort has been devoted to proving that pulsed fields give the same results as steady fields and that it is only the Gibbs magnetic term that is important. As a rough approximation, they are correct. Fokina et al.<sup>(83)</sup> showed that an Fe 23 Ni 0.5 C steel in liquid helium transformed from 8-9% martensite to 20-21% in either a 40 kOe pulsed or steady field. In addition, predictions based on the thermodynamic effect of field alone give reasonable agreement with the observations.



The troublesome complications are all related to the pulse-induced eddy currents. Faraday's law predicts that an emf proportional to  $\frac{dB}{dt}$  will be generated, opposing the applied field. Pulsed fields, unfortunately, have high values of the rate-of-change of field with time. Evidence for the existence of eddy currents in these experiments has been given by Voronchikhin and Fakidov<sup>(84)</sup>; the temperature of their specimens increased with the square of the applied field. (A 200 kOe pulsed field of 5 kHz gave a 5°C temperature increase.) Eddy-current power losses are typically proportional to  $B^2 F^2$  where F is the frequency of the pulse and B is the magnetic induction.

Aside from the heating effects, eddy currents lead to two other more serious complications. The first of these has been called the "ponderomotive force". In short<sup>(80)</sup>, the induced eddy currents interact with the surrounding magnetic fields leading to a stress proportional to  $H^2$ . On pulsing in a solenoid, a cylindrical specimen is known to be subjected to compressive forces normal to its cylindrical surface and tensile forces along the axis<sup>(88)</sup>. In strong fields, these forces can be quite high; in fact, it has already been demonstrated<sup>(98-99)</sup> that copper can be plastically deformed with a 350 kOe pulse. Although no plastic deformation of the higher strength steels has been detected, the stresses are still there. Investigators were not able to alter the  $\gamma$  to  $\epsilon$  (both paramagnetic) martensitic transformation in  $Fe(14-21)M_n$ <sup>(87-94)</sup> or the  $\gamma'$  to  $\beta$  thermoelastic martensite in  $Cu 14 Al 4 Ni$ <sup>(89)</sup> by pulsing with high fields. They concluded that the overriding effect is not the induced stress, but rather the magnetic contribution to the Gibbs free energy.

Another complication of the eddy currents, known as the skin effect,

stems from the opposition of the applied field by the eddy current field. The net effect is that the internal field varies within the specimen, being maximum at the surface ( $= H_{\text{applied}} + 4\pi M - H_d$ ) and minimum in the interior ( $= H_{\text{applied}} + 4\pi M - H_d - H_{\text{eddy}}$ ). This, in turn, introduces second-order complications, such as nonuniform magnetization and demagnetizing fields. Malinen, et al.<sup>(87)</sup> plated the surface with a thin layer of high conductivity copper. The enhanced eddy currents in this layer reduced the effectiveness of the applied pulse for inducing martensite by a factor of two! Finally, Fakidov,<sup>(80)</sup> et al. found that the critical field to induce martensite,  $H_K$ , was a function of the applied pulse frequency. The effect was sizeable;  $H_K$  varied from an extrapolated value of 50 kOe at  $F = 0$  to 100 kOe at  $F = 2 \times 10^4$  Hz. The exact functional relationship,  $H_K = H_0 + 5F^{0.25}$ , is critical because ponderomotive stresses should reduce  $H_K$  with increasing  $F$ , whereas if the skin effect were dominating it should reduce the effective field and, therefore,  $H_K$  should increase with  $F$  (as observed). Thus, skin effects have been shown to be more important than stress effects; however, both exist and the relative contribution of each is a complex function of the specimen shape, conductivity, elastic and plastic properties, and the reaction being studied.

Even though pulsed fields are complicated by eddy-current effects, they do offer some advantages over steady fields. They are more economical to generate and may lend themselves well to certain commercial applications. Also, by using a single pulse, we can interrupt the martensite transformation at an early stage never before possible.

### II-2.3 Isothermal Transformation Studies

There has been relatively little magnetic work on FeNiMn alloys which will isothermally transform.<sup>(81-82,86)</sup> The first study by Estrin<sup>(82)</sup> showed that the application of a steady field of 18.6 kOe did not cause a sudden increase in the overall amount of martensite, rather there was an increase in the rate of transformation. He intuitively interpreted this as a shift of the transformation C-curve to shorter times and to higher temperatures, but he gave no evidence to back up this reasoning.

There has never been a study of an isothermal transformation by applying a large number of pulses and observing the transformation as a function of accumulative time. Presumably, with a pulse length of  $10^{-4}$  seconds and allowing time for the capacitors to charge up, the experiment would take an inordinate length of time. This technique could still be a valuable tool for interrupting reactions with very high initial nucleation rates. Malinen, et al.<sup>(86)</sup> applied a pulsed field of 360 and 400 kOe to Fe 23.6 Ni (3.3 and 3.6) Mn alloys which had normal isothermal nose temperatures of - 100 and - 140°C respectively. The field accelerated the reaction, but the extent of transformation in both alloys rose monotonically with decreasing temperature (as depicted in Figs. 2b and d) with no evidence of any kind of maximum at the nose temperature. They unsuccessfully tried to apply nucleation kinetics to their results and finally interpreted the effect as a shifting of the transformation kinetics from the isothermal to the athermal mode. This line of reasoning is contrary to Magee and Paxton's<sup>(16)</sup> interpretation that all martensite transformations are basically isothermal.

The most recent isothermal work has been by Peters, Bolton, and Miodownik<sup>(96)</sup> on Fe 26 Ni 2 Mn with a steady field up to 20 kOe over a temperature range of - 60 to - 80°C. They varied the fields during the course of the reaction, and used the Kaufman-Cohen<sup>(19)</sup> model to calculate values of surface energy and critical embryo radius as a function of temperature. They did not dope the surface of their alloys to suppress the surface complications, and therefore could not study the initial nucleation rates. They circumvented this difficulty by extrapolating a plot of  $\log t$  versus  $f$ , the volume fraction of martensite, to  $f = 0$ , and using the slope and intercept of this plot to calculate the initial nucleation rate (assuming the average plate volume  $\bar{V}$  to be constant). Since autocatalysis from the surface undoubtedly wiped out their initial transformation regions, the  $\log t$  vs.  $f$  plot looks somewhat linear over the small range they tested; in contrast, if this plot is made for a doped specimen, it is sigmoidal in nature. (Replotting their data shows the expected curvature.) Ignoring these complications, the K-C model was found to fit the data well and the major effect of the field was to vary the thermodynamic driving force.

#### II-2.4 Magnetic Effects on the Microstructure

Visual inspection of the microstructures shown in the literature<sup>(75, 87-88,92-93)</sup> does not reveal any directional alignment of plates or changes of morphology with the applied field. (The  $\epsilon$  to  $\alpha'$  transformation looks<sup>(94)</sup> somewhat directional, but no indication was given of the direction of the applied field.) Malinen et al.<sup>(87)</sup> noted that new plates appeared in previously untransformed austenite rather than around prior martensite. This

was used to counter the arguments that induced magnetostresses around prior plates might be significant.

Bernshteyn et al.<sup>(10)</sup> examined the isothermal  $\gamma$  to  $\alpha'$  transformation while tempering Fe (5-16) Ni (0.03-1.1) C alloys under a steady field of 16 kOe. They reported (without micrographs) that in almost every case there was an increase in the etchability of the boundaries of the martensitic crystals. Undefined "statistical" treatment of the results revealed that the crystals themselves were thinner, longer and showed less random orientation (as we might expect from magnetostatic considerations discussed in Section I-2). These structural differences were greater for the higher nickel concentrations. It is possible that at the higher temperatures of this study, transformation stresses were less dominant; however, Fokina et al.<sup>(13)</sup> transformed normal carbon steels in this same temperature range with no observable orientation effects. Since Bernshteyn had to use a "statistical" analysis and since no micrographs were shown, the morphological changes are probably difficult to detect with the naked eye.

Anisotropy in transformed specimens has been indirectly detected by Yermolayev et al.<sup>(11)</sup> with magnetic torque measurements. The specimens which were cooled without a field remained magnetically isotropic, while those cooled in the magnetic field acquired uniaxial anisotropy. Assuming that this resulted from magnetostatic-energy shape effects (as discussed in Chapter I), they found that, as the total amount of martensite increased from 4 to 20% (by using higher and higher fields), the total amount of oriented martensite varied from 2 to 4%. (These calculations are valid to about a factor of two.) These experiments show that anisotropies do

exist, and the best way to detect them is during small amounts of transformation before strain energies and other constraints begin to override. It is interesting to note that the authors were not able to detect these anisotropies metallographically.

## II-2.5 Theoretical Treatment to Date

The martensitic transformation is not governed entirely by bulk thermodynamics as evidenced from the strong effects of specimen history; however, most investigators have concentrated on the effect of magnetic fields on the thermodynamics of the transformation and have neglected or misinterpreted the kinetic aspects.

### II-2.5.1 Thermodynamic Predictions

Meyer and Taglang<sup>(100)</sup> were the first to derive a "Clausius-Clapeyron" type of equation for magnetic fields:

$$\Delta T_0 = \frac{H\Delta I}{\Delta S} = \frac{T_0 H\Delta I}{L} \quad (19)$$

where  $T_0$  is the equilibrium temperature,  $\Delta S$  is the entropy change on transformation, and  $L$  is the latent heat or the enthalpy difference between the two phases. (A more rigorous derivation of this equation is given in Appendix I.) This equation only applies for reversible equilibrium of phases with heat capacities and magnetizations that are not strong functions of temperature and field. Satyanarayan et al.<sup>(92)</sup> derived the same equation using similar triangles on a linear  $\Delta g$  versus temperature curve, assuming

that the other contributions to the thermodynamics such as the strain energies,  $\Delta g_\epsilon$ , are not dependent on the field. This linear  $\Delta g$  (or constant heat capacity) assumption is crude since most free-energy curves show some curvature. ( $\Delta T_0 = \frac{H\Delta I(T_0 - M_S)}{\Delta g_\epsilon}$  gives a better approximation<sup>(95)</sup> for non-linear free-energy curves, but  $\Delta g_\epsilon$  is a hard number to pin down.) If we neglect these complications, Eq. 19 predicts that the greatest effect of field will be on alloys with a large  $\Delta I$  and  $T_0$  and a small latent heat. Unfortunately,  $T_0/L$  does not seem to be a strong function of anything; therefore,  $\Delta I$  is still the most important material parameter.

Equation 19 does not strictly apply to the  $M_S$  change of the irreversible martensitic transformation, yet it successfully predicts the linear dependence of  $M_S$  on the field depicted in Fig. 2a. Investigators<sup>(82,84,92)</sup> have become so confident in this equation that they have employed it to obtain quick and easy estimates of the enthalpy and entropy changes: Voronchikhin and Fakidov<sup>(84)</sup> vacuum insulated a specimen and pulsed a field through it while monitoring the temperature. After subtracting out the eddy-current effects, this simple form of calorimetry (which does not involve the usual cooling technique) gave values of the latent heat ( $\Delta H$ ) within 5 to 9% of those calculated from the  $M_S$  temperature shift using Eq. 19. Eq. A-1 in Appendix I shows that the measured  $\Delta S$ , the entropy change of the transformation, approaches the correct value as the induced temperature-shift becomes smaller; i.e. as  $\frac{\Delta T}{\Delta H}$  approaches  $\frac{dT}{dH}$ .

To conclude, the magnetic Clausius-Clapeyron equation reflects the behavior of the athermal martensitic reaction, but it must be used with caution. Unfortunately, these thermodynamic equations have been repeatedly

invoked to interpret kinetic effects.

### II-2.5.2 Kinetic Predictions

Malinen et al.<sup>(86)</sup> gave the first quantitative treatment of nucleation kinetics under a magnetic field while unsuccessfully trying to describe the pulsed transformation of an isothermal alloy. He assumed the martensitic reaction was governed by an equation of the form:

$$\dot{N} = k \exp \left[ - \frac{\Delta W + U}{RT} \right] \quad (20)$$

where  $\Delta W$  and  $U$  are the activation energies for nucleation and growth respectively. The ratio of the nucleation rate with the applied field,  $\dot{N}_H$ , to that without,  $\dot{N}$ , is (assuming  $U$  is small or, at least, insensitive to the field):

$$\frac{\dot{N}_H}{\dot{N}} = \exp \left[ - \frac{(\Delta W_H - \Delta W)}{RT} \right] \quad (21)$$

where  $\Delta W_H$  is the activation energy for nucleation in the presence of a field. Malinen used the classical value for the nucleation energy,  $W$ , which is inversely proportional to  $(\Delta g)^4$ , yielding:

$$\frac{\dot{N}_H}{\dot{N}} = \exp \left[ \frac{\Delta W}{RT} \left( 1 - \frac{(\Delta g_0)^4}{(\Delta g_0 + \mu_0 HM)^4} \right) \right] \quad (22)$$

Peters, Bolton, and Miodownik followed the identical treatment as Malinen but plugged in the Kaufman-Cohen value for  $\Delta W = K_1 + K_2 \Delta g$  in which  $K_1$  and



$K_2$  are functions of the surface energy, elastic constants, and the embryo potency. This yielded:

$$\frac{\dot{N}_H}{N} = K_2 \left[ \frac{MH}{RT} \right] \quad (23)$$

which accurately described their isothermal transformation kinetics under a changing field.

## II-2.6 Potential Applications

Magnet fields can be used to alter the physical and mechanical properties of a steel through the martensitic reaction. Under most circumstances, magnetic fields will have no significant effect. It is necessary to be close enough to the  $M_S$  temperature so that the value of the critical field,  $H_K$ , required to initiate the transformation is not too large. In many cases, if we were this close to  $M_S$ , it would be cheaper to quench the part to a lower temperature. Also, if we have greater than about 60% martensite, further reduction in retained austenite becomes increasingly difficult (both by increasing  $H$  or by lowering  $T$ ). Most experiments have shown that the application of a field to reduce the retained austenite is not worth the effort (e.g. 75); and, in particular, if the martensite is generated by quenching to subzero temperatures, the application of a field at room temperature appears to have little effect.

Magnet fields, however, do offer certain advantages. It is much better suited to mass production techniques than are low-temperature quenching methods. One can envision miles of continuous cast rod whipping

through the core of a high-field magnet. There has been recent interest in magnetic-pulse fabrication of sheet-body parts for cars. With the right choice of alloys, one could simultaneously deform and transform. Fields also have other advantages, such as minimizing quenching-stress gradients and the ability to transform only a local section<sup>(75,88)</sup> of a large part by applying a field only to that area. If an FeNiC alloy<sup>(10,89)</sup> is quenched through a field to produce martensite and then tempered (or if it is given a normal quench and then tempered in a field), the martensite decomposition during the first stage tempering is suppressed. If the tempering temperature is raised to a point where the retained austenite decomposition begins, the field accelerates the reaction more than one would predict from the thermodynamics. Obviously, tempering in a magnetic field is an area that still requires attention.

### III. PURPOSE OF THESIS AND OUTLINE OF WORK

The objectives of this thesis are to use magnetic fields as a tool in order to investigate the nucleation and kinetics of the martensitic transformation as well as to examine the intrinsic effects of the field itself. The alloys chosen for this study were designed to cover the range of morphologies from lath (packet) to plate (lenticular) and the range of kinetics from isothermal C-curve behavior to bursting. Particular emphasis is placed on the underlying causes for these transitions in morphology and kinetics. Since temperature and magnetic field can be varied independently, the effects of chemical driving force and temperature can then be studied separately. Furthermore, using the magnet field as an additional thermodynamic variable places a further test in the evaluation of current theories of martensitic nucleation.

The research itself is divided into two broad categories: (i) Comparisons of the kinetics and morphology between zero-field and field-accelerated transformations, and (ii) High- and low-temperature magnetic annealing and cycling experiments designed to influence the prior martensitic nucleation sites.

#### IV. Materials and Procedure

##### IV-1 Specimen Preparation and Composition

The compositions and designations of all alloys used in this investigation are listed in Table 2. The first alloys were cast at the U.S. Steel Laboratory for Fundamental Research in the form of 17-pound cylindrical ingots and hot rolled to one-inch slabs with intermediate anneals at 1200°C. (Microprobe analysis revealed a periodic variation of composition with a wavelength of about 150 microns. Chemical fluctuations were typically  $\pm 0.4\%$  at 72% Fe,  $\pm 2\%$  at 28% Ni, and  $\pm 0.6\%$  at 3% Mn\*. On a relative basis, the manganese composition fluctuations were the most severe). The second set of alloys was cast at the Ford Scientific Laboratory in the form of 15 to 20-pound tapered cylindrical ingots. These pieces were hot forged to 1/2-inch diameter rods at the AMMRC Laboratory in Watertown introducing intermediate 900°C soaking treatments when necessary.

Rods 0.75-inch and 0.38-inch in diameter respectively were machined from the above two sets of alloys. These rods were swaged approximately 30% and then vacuum ( $10^{-5}$  atm) encapsulated in quartz for a 3-day homogenization treatment at 1300°C. After this anneal, 0.1 inch was removed from the diameter in order to circumvent any surface-composition complications. The stock was then swaged down to 0.070-inch wire, with 30 minute 800°C softening anneals after about every 70% reduction in area. The resulting wire was cut into 1.2-inch long specimens and the ends

---

\*All composition and alloy descriptions are given in weight percent, unless otherwise indicated.

TABLE 2

Composition\* of Alloys in Weight Percentages

<u>Designation</u>	<u>Ni</u>	<u>Mn</u>	<u>C</u>	<u>H</u>	<u>N</u>	<u>O</u>	<u>S</u>
USS 1439	28.7	--	0.0058	0.00029	--	--	0.003
FORD V925	29.6	--	0.0090	--	--	--	0.005
FORD V927	30.8	--	0.0054	--	--	--	0.003
USS 1345	22.5	4.0	0.0055	--	0.0006	0.0089	--

---

\* Balance iron

ground flat to a smoothness of 320 grit with a slight bevel on the edges.

At this point in the processing, the grain size was established using a 1-hour 900°C anneal in evacuated vycor capsules. Eight-inch nickel (>100 ppmC) electrical resistivity leads were batch homogenized in 0.2 atm CO for 2 hours at 1000°C to insure reproducible carbon contents. These leads were spot welded near the ends of the specimen which was then electropolished for 2 minutes, with 30-second intervals, in a 4% perchloric - 96% glacial acetic acid solution at 90 to 120 volts. The surface was carbon doped by vacuum encapsulating the polished specimens (together with the nickel lead wires), and annealing for 14 minutes at 800°C. The assumed doping mechanism is the transport of carbon from the nickel leads to the specimen via CO gas. (CO gas by itself (0.3 to 1.0 atm) was also found to be an effective dopant, but was usually not used in this study.) The specimens were air cooled after this anneal and were usually subjected to transformation runs within 12 hours.

#### IV-2 Electrical Resistance Measurements

Relative resistance changes measured with a Kelvin double bridge were adopted to follow the course of the isothermal reactions. It was necessary to measure [a] the initial ( $R_{25I}$ ) and final ( $R_{25F}$ ) resistances at 25°C, [b] the initial untransformed ( $R_I$ ) and final ( $R_F$ ) resistances at the testing temperature, and [c] the time-varying resistance ( $R$ ) during the course of the reaction at the test temperature. If the incubation time happened to be less than the first measured time for transformations occurring at subzero temperatures under no field conditions,  $R_I$  could still

be accurately estimated from the measured temperature coefficient of resistivity. From these observations, the percent martensite as a function of time was calculated from:

$$\% \alpha' = \frac{(R_{25F} - R_{25I}) (R_F - R)}{A R_{25I} (R_F - R_I)} \quad (24)$$

where A is the conversion factor equal to the  $\Delta R_{25}/R_{25I}$  change corresponding to a 1% transformation from austenite to martensite (determined by comparing the 25°C resistivity change with the amount of martensite measured by pointcounting). A was found to be  $6.96 \times 10^{-3}$ ,  $7.78 \times 10^{-3}$ , and  $3.10 \times 10^{-3}$  for Fe 28.8 Ni, Fe 30.8 Ni, and Fe 22.6 Ni 3.9 Mn respectively.

The Kelvin bridge was capable of detecting at  $5 \times 10^{-6}$  ohm change or less. For a typical specimen resistance of 0.01 ohm, this corresponded to about 0.1% martensite. Unfortunately, a  $1/2^\circ\text{C}$  temperature variation could also cause this order of change in resistance. In addition, a small ( $\frac{\Delta R}{R} \approx + 2 \times 10^{-4}$ ) increase in resistance was observed due to magneto-resistance effects of the field. This does not complicate matters since Eq. 24 shows that we were always dealing with resistivity differences at the test temperature. If, however, there were some transformation during the interval before the first resistivity point was taken, it was necessary to add the small magneto-resistance-increase to the resistance measured at the test temperature just before the field was applied for an accurate estimate of  $R_I$ .

In order to avoid undue ambiguities, 0.3% martensite was used to mark the "beginning of the reaction". The reaction time was started when the field reached about 95% of its final value and the first

resistivity point was taken within about 0.3 of a minute. This put a practical lower limit on the measurable incubation times. Any reported times less than this are linear extrapolations from longer times.

#### IV-3 Temperature and Magnetic-Field Control

Initially, subzero temperatures were obtained using the standard baths of water and ice, methanol or acetone and dry ice, or 75% petroleum ether - 25% methylcyclohexane and liquid nitrogen. Unfortunately, there was only about one inch of working space inside the dewar in the magnet, and inadequate stirring led to temperature fluctuations of up to  $\pm 2^{\circ}\text{C}$ . It was necessary to build a low-temperature controller shown diagrammatically in Fig. 3 consisting of a copper pipe closed at one end and wound with a bifilar brass-wire heater. In operation, the insulated tube was filled with one of the previously mentioned solvents and stirred with a stream of cooled helium or nitrogen gas. The whole assembly was immersed in a cooling bath of liquid nitrogen or dry ice - methanol which was also used to pre-cool the stirring gas. Two thermocouples were positioned within 1/8 inch of the specimen to monitor the temperature and for input into a temperature controller. The temperature controller itself was converted to a low-temperature controller by using a liquid-nitrogen cold junction. With this setup, a  $20^{\circ}\text{C}$  subzero-temperature change could be completely equilibrated within three minutes, and the temperature could be controlled to  $\pm 0.2^{\circ}\text{C}$  over the temperature range of  $+ 10^{\circ}$  to  $-140^{\circ}\text{C}$ .

High temperatures ( $300^{\circ}$  to  $900^{\circ}\text{C}$ ) were obtained by means of a spiral



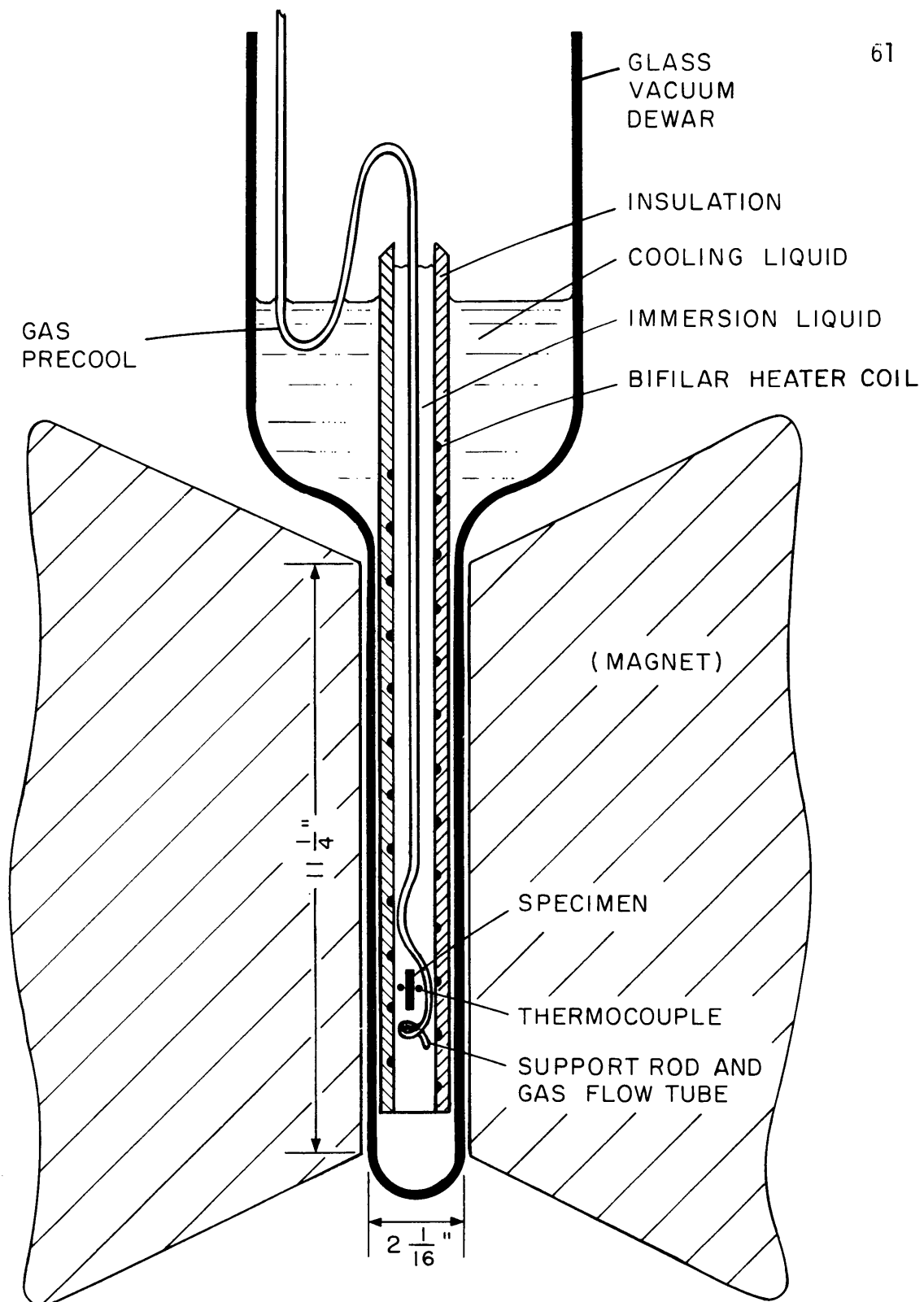


FIG.3 SCHEMATIC OF CRYOGENIC TEMPERATURE CONTROLLER USED DURING TRANSFORMATION IN APPLIED FIELDS.

silicon carbide globar inserted from the bottom of the magnet and surrounded by a water-cooled copper jacket. A 14mm, vycor tube was placed in the center of the globar, which served both as a support for an encapsulated specimen and as a channel for an air-blast quench. The temperature was maintained constant over a 2-inch distance to within  $\pm 5^\circ\text{C}$  and the specimen could be air-blast cooled to  $200^\circ\text{C}$  in about 20 seconds.

The magnetic fields for this study were generated at the Francis Bitter National Magnet Laboratory by passing up to 25 kamps through special axial-flow helical solenoids. The fields varied from 20 to 140 kOe for times up to 3.5 hours in a 2.1-inch bore magnet. It took approximately 15 seconds to turn up the field to 140 kOe because of control-room restrictions, however, even if we could have turned the field up faster, it would have taken about that long for eddy-current effects to die down.

#### IV-4 Magnetization Measurements

The magnetization of the austenite and martensite of each alloy was measured at the temperatures of interest as a function of field strength, using a vibrating-sample magnetometer in a Janis Super-Vari-Temp dewar. The magnetometer was calibrated before each run with a pure nickel sample having a known ( $M = 54.4 \text{ erg/gauss gm}$ ) magnetization. 4.5 mm long sections cut from the center of the 0.070-inch diameter wire specimens were vibrated parallel to the wire axis in a transversely applied field up to 10 kOe. For the martensitic samples, it was necessary to subtract out the magnetization of the retained austenite assuming

the contributions from the two phases to be additive. The martensitic phase comes very close to its saturation magnetization at 10 kOe; no attempt was made to extrapolate these values to higher field strengths.

#### IV-5 Optical Microscopy Examination

The specimens to be studied were mounted longitudinally in Clear Cast cold-setting compound. After mechanical polishing to Linde A grit, they were immersed in methylene chloride for a few hours in order to disintegrate the mounting material. The specimens were then electro-polished for 1.5 minutes, in 30 second intervals, in a 4% solution of perchloric acid in glacial acetic acid at 90 to 120 volts and 0.6 amps/cm<sup>2</sup>; the temperature range was 12° to 18°C.

The optimum polishing condition was obtained when a bubble-free brown polishing layer was formed, which tended to "drip off" the surface. The specimen was immediately rinsed in water and etched in a solution of 250 grams/liter of sodium bisulphite in water. This solution, 100 times more concentrated than usually used, brought out the structure in 10 to 200 seconds depending on the alloy composition. (Intermediate exposures to air during the course of the etch or an acetic acid dip will accelerate the reaction.) Careful control of the etching conditions was found to result in orientation-dependent color contrast varying from blue-reds to tan-browns.

## IV-6 Quantitative Metallography

### IV-6.1 Grain-Size Measurements

Grain-size measurements were carried out on specimens heavily etched to reveal the austenetic grain and twin boundaries. The mean linear intercept,  $L$ , was determined by counting at least 800 intersections of grain and twin boundaries while making four longitudinal passes along the specimen length and recording the total distance traversed.

The grain size was converted to equivalent spherical diameter using (101)

$$\bar{d} = 1.65 L \quad (25)$$

$\bar{d}$  for Fe 29.6Ni, Fe 30.8Ni, and Fe 22.6Ni3.9Mn were 0.0407, 0.0590, and 0.0220mm respectively. The FeNiMn ternary alloy had a factor of two smaller grain size, which must be kept in mind when comparing its reaction kinetics to that of the binary FeNi alloys.

### IV-6.2 Volume-Fraction Measurements

The mean volume fraction of martensite,  $f$ , was determined by superimposing a grid on a 500X or 1000X photomicrograph and counting the number of point-intersections (out of a possible 1200) that landed on martensite. (Boundary hits were counted as 1/2). This procedure was repeated for 3 to 5 random photomicrographs and the results averaged.  $f$  was used either to determine the conversion factor for the resistivity change to percent martensite or as an input parameter in the average volume-per-martensitic-plate calculations.

#### IV-6.3 Measurement of Mean Volume per Plate and Radius-to-Semithickness Ratio

The number, length, and maximum thickness of all plates within an 18 by 20 cm square area were measured on 3 to 5 random longitudinal photomicrographs blown up to 2000X. This usually meant measuring from 300 to 600 plates for each specimen. For specimens with larger volume fractions of martensite, smaller representative areas (approximately 10 by 11 cm square) were picked out and all the plates within this area were counted. Special care had to be taken to count even the smallest plates. The measurements were recorded to the nearest 0.005 inch on a 2000X photomicrograph, which works out to be about 0.06 microns. Many times, the "plates" themselves were ill-defined, especially in the Fe 29.6Ni alloy.

From these measured numbers and from the point-counted values of the volume fraction of martensite, we computer-calculated  $\bar{E}$ ,  $\bar{F}$ ,  $\overline{\left(\frac{r}{c}\right)}$ ,  $N_A$ ,  $N_V$ , and  $\bar{V}$ , assuming the plate shape to be approximated by thin oblate spheroids. The definitions of these quantities and the derivation of the the relevant equations are described in Appendix II. Conservatively, the absolute values of these calculated parameters are probably valid to within a factor of 5; however, the relative values with respect to each other should be good to  $\pm 10\%$ .

#### IV-7 Measurement of Nucleation Rate

The initial nucleation rate was estimated from the relation proposed by Shih et al:<sup>(102)</sup>

$$0.003 = \dot{N}\bar{V}\tau_i \quad (26)$$

where  $\dot{N}$  is the initial nucleation rate,  $\bar{V}$  is the mean plate volume, and  $\tau_i$  is the time to reach 0.3% martensite. This equation is only an approximation, since it incorrectly assumes that the rate of nucleation and the average plate volume are constant during the incubation period. The ramifications of these assumptions will be analyzed in a later chapter.

#### IV-8 Averaging Techniques

A very time-consuming problem encountered in this investigation was the experimental scatter in the isothermal-transformation studies. This seems characteristic of martensitic research of this nature. The problem was resolved by repeating the experiments under identical conditions from 3 to 15 times and picking the "most representative" curve which had the median value of incubation time. Rather than use this median incubation time in Eq. 26 to calculate  $\Delta W_a$ , we felt it was more accurate to obtain  $\Delta W_a$  for each full curve and then take the median  $\Delta W_a$  in this way.

## V. RESULTS AND DISCUSSION

### V-1 Material Characteristics

Before proceeding into the main body of the results, it may be helpful to examine the material characteristics of the alloys under investigation. These are summarized in Table 3.

#### V-1.1 Shear Modulus and Density

The values of the shear modulus and density of these alloys in the austenitic condition were measured by Speich at the U. S. Steel Fundamental Laboratory. These data are presented in the form of computer-fit least-square equations as a function of temperature in °C. The FeNiMn modulus data were determined over the whole temperature range of interest down to - 196°C; however, the binary FeNi moduli were not measured below - 20°C because of the ensuing martensitic transformation. The actual values are not as precise as shown in the table; these were the equations used to accurately reflect changes with temperature in our model-fitting exercises.

Note that the shear modulus of the FeNiMn alloy is greater than that of the binary FeNi alloys. The Mn alloy will, therefore, require more energy to nucleate and grow since both dislocation core energies and strain energies<sup>(51,103)</sup> are proportional to the shear modulus. In the KCR model, a large shear modulus can prevent the athermal-transformation mode from ever occurring, thereby yielding isothermal C-curves (as observed in FeNiMn alloys near the composition being studied in this thesis). Also, by making the assumption that the moduli of the austenite and martensite

TABLE 3  
Material Characteristics of the Alloys Under Investigation

<u>Alloy</u> (wt. %)	<u>Grain Size</u> (mm)	<u>~ Density (<math>\alpha'+\gamma</math>)<sup>*</sup></u> (gm/cm <sup>3</sup> )	<u>Shear Modulus (<math>\gamma</math>)</u> (dyne/cm <sup>2</sup> )	<u><math>\theta_{C\gamma}</math><sup>**</sup></u> (°C)	<u><math>\Delta M^{\gamma \rightarrow \alpha'}</math></u> (ergs/gauss gm)
Fe 28.7 Ni	--	--	--	-10	--
Fe 29.6 Ni	0.041	8.183 $-3.2 \times 10^{-4} T$	$6.840 \times 10^{11}$ $-1.11 \times 10^8 T$ $-3.75 \times 10^5 T^2$	30	148.1 at - 2°C 150.8 at + 9°C
Fe 30.8 Ni	0.059	8.173 $-3.2 \times 10^{-4} T$	$6.678 \times 10^{11}$ $+1.53 \times 10^8 T$ $-1.09 \times 10^6 T^2$	73	123.3 at - 20°C
Fe 22.5 Ni 4.0 Mn	0.022	8.148 $-1.96 \times 10^{-4} T$	$7.469 \times 10^{11}$ $-3.68 \times 10^8 T$ $-7.75 \times 10^5 T^2$	<-196	162.3 at -196°C 165.3 at -120°C 163.9 at - 81°C 162.6 at - 20°C

\* T is temperature in °C for this table only.

\*\* From reference (42).



are additive in a duplex structure, Speich's data show that the martensite modulus is at least 20% smaller than that of the austenite. This is in agreement with the findings of Goldman and Robertson<sup>(104)</sup>. These lower values suggest that the martensite may be the phase to elastically and plastically accommodate the strains. This, in turn, could alter the kinetics and morphology of the transformation, e.g. self-accommodating strains in the martensite could force the growing plate to change from the twinning to the slip mode.

The densities of the  $\alpha' + \gamma$  listed in Table 3 were determined from transformed specimens containing from 50 to 90% martensite. These least-square fit equations were used as a rough approximation to the temperature variation of density in the conversion of cal/mole to ergs/cm<sup>3</sup>.

#### V-1.2 Magnetic Properties

All three binary FeNi alloys are ferromagnetic at lower temperatures; however, the Fe 28.7 Ni alloy can transform at temperatures above  $\theta_{C\gamma}$  in the paramagnetic austenite region. The FeNiMn alloy remains paramagnetic down to liquid nitrogen temperatures in the austenitic condition. Mossbauer studies on a similar alloy (Fe 24.2 Ni 2.98 Mn) at the U.S.S. Laboratory revealed a broad split austenite peak at 12°K. This type of pattern has been interpreted<sup>(105)</sup> (in an FeNiCu system) as an indication of the occurrence of a mixture of antiferromagnetic and ferromagnetic phases. This interpretation supports the two  $\gamma$ -state ideas of Miodownik<sup>(106)</sup>, which were employed by Kaufman<sup>(107)</sup> in his calculation of the chemical driving-force equations used in this thesis.

As discussed in Section II-1.2, Davies and Magee<sup>(42)</sup> have correlated  $(\theta_C - M_S)$  with morphology. We will show later that our zero field structures fit very well into their classification scheme; however, the field-induced morphologies reveal that their correlation does not give the complete story.

The values of the magnetization at 10 kOe, shown in Table 3, have an estimated accuracy of about 5% on an absolute scale. In the Fe 29.6 Ni alloy,  $\Delta M$  is larger at + 9°C than at - 2°C because the former is just below  $\theta_{C\gamma}$ ; consequently, the magnetization of the austenite is a strong function of temperature in this region. Since the Gibbs magnetic energy is proportional to  $H\Delta M$ , the field is more effective at higher temperatures in this alloy. The value of  $\Delta M$  is lower in the Fe 30.8 Ni alloy because the austenite is more strongly ferromagnetic.

The magnetization curves shown in Fig. 4 can yield additional information pertinent to the martensitic transformation. The binary FeNi magnetization curves reach a plateau of saturation after a relatively sharp transition region, whereas the ternary FeNiMn alloy saturates over a much wider range of fields. This behavior is reminiscent of the differences in the shape of the kinetic curves in these alloys as they approach the final stages of the martensitic transformation. This comparison could be significant since the motion of Block walls and the rotation of domains may be somewhat similar to the motion of the martensite interfaces and the atomic shuffles of the transformation. It has been suggested<sup>(e.g. 33)</sup> that deformation studies would be valuable in correlating the plastic properties of a material with its martensitic-transformation behavior. The variation

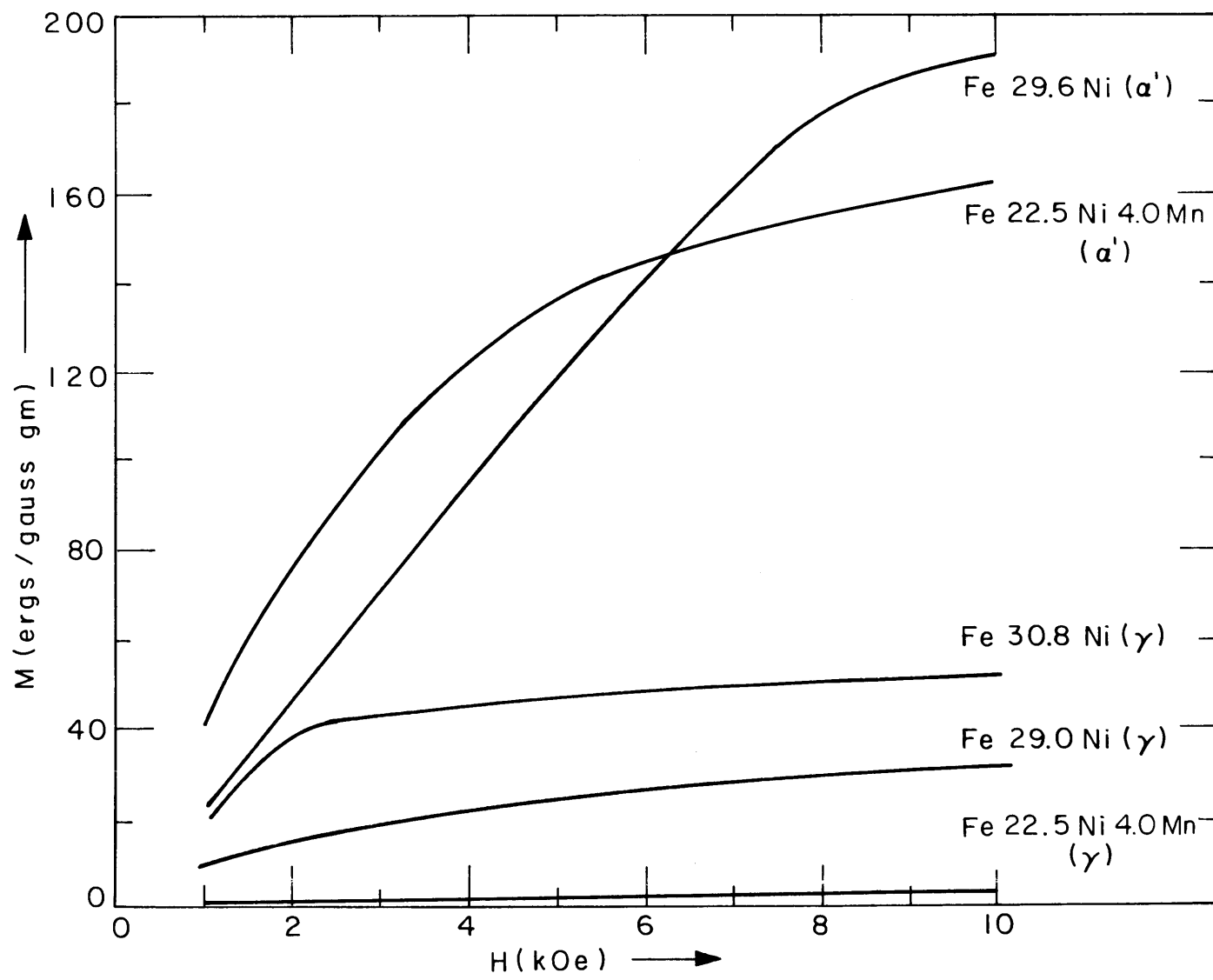


FIG. 4 ROOM TEMPERATURE MAGNETIZATION CURVES

of the shape and hysteresis of these magnetization curves as a function of the rate of applied field could yield similar data but with a simple nondestructive test. The FeNiMn magnetization curves have a smaller hysteresis area than the binary alloys implying that they were more reversible in nature. Temperature has little effect on the hysteresis of these curves; however, varying the sweep rate from 0.02 to 0.2 kOe/sec increased the hysteresis by an order of magnitude for all three alloys tested.

### V-1.3 Chemical Driving Force

The chemical driving force,  $\Delta G_0$ , (in cal/mole) was calculated from the chemical compositions, using Kaufman's<sup>(107)</sup> latest equations:

$$\begin{aligned} \Delta G_0 = & (1-X-Y)G_{Fe} + XG_{Ni} + YG_{Mn} + X(1-X-Y)G_{FeNi} + 1000 XY \\ & + (1-X-Y)Y(-5950 + (6.17 \times 10^{-3})T^2) \end{aligned} \quad (27)$$

where T is the absolute temperature in °K, X and Y are the atomic fractions of nickel and manganese respectively, and:

$$G_{Fe} = 1303 + (1.78 \times 10^{-3})T^2 - (2.87 \times 10^{-5})T^3 + 4.91 \times 10^{-8})T^4$$

$$G_{Ni} = -940 - (9.82 \times 10^{-4})T^2 + (1.16 \times 10^{-6})T^3 - (3.37 \times 10^{-10})T^4$$

$$G_{Mn} = 260 + (1.18 \times 10^{-4})T^2 - (7.64 \times 10^{-7})T^3$$

$$G_{FeNi} = -1350 + (1.48 \times 10^{-4})T^2 + (2.02 \times 10^{-7})T^3.$$

The results of these calculations are plotted in Fig. 5. The curves flatten out at lower temperatures as expected from the third law of thermodynamics; consequently, lowering the temperature below 100°K does not give much of an additional driving force. It is also to be noted that the driving force versus temperature behavior of the FeNiMn alloy is very similar to that of the Fe 29.6 Ni alloy, suggesting that the large differences in their transformation kinetics is not due to driving-force considerations.

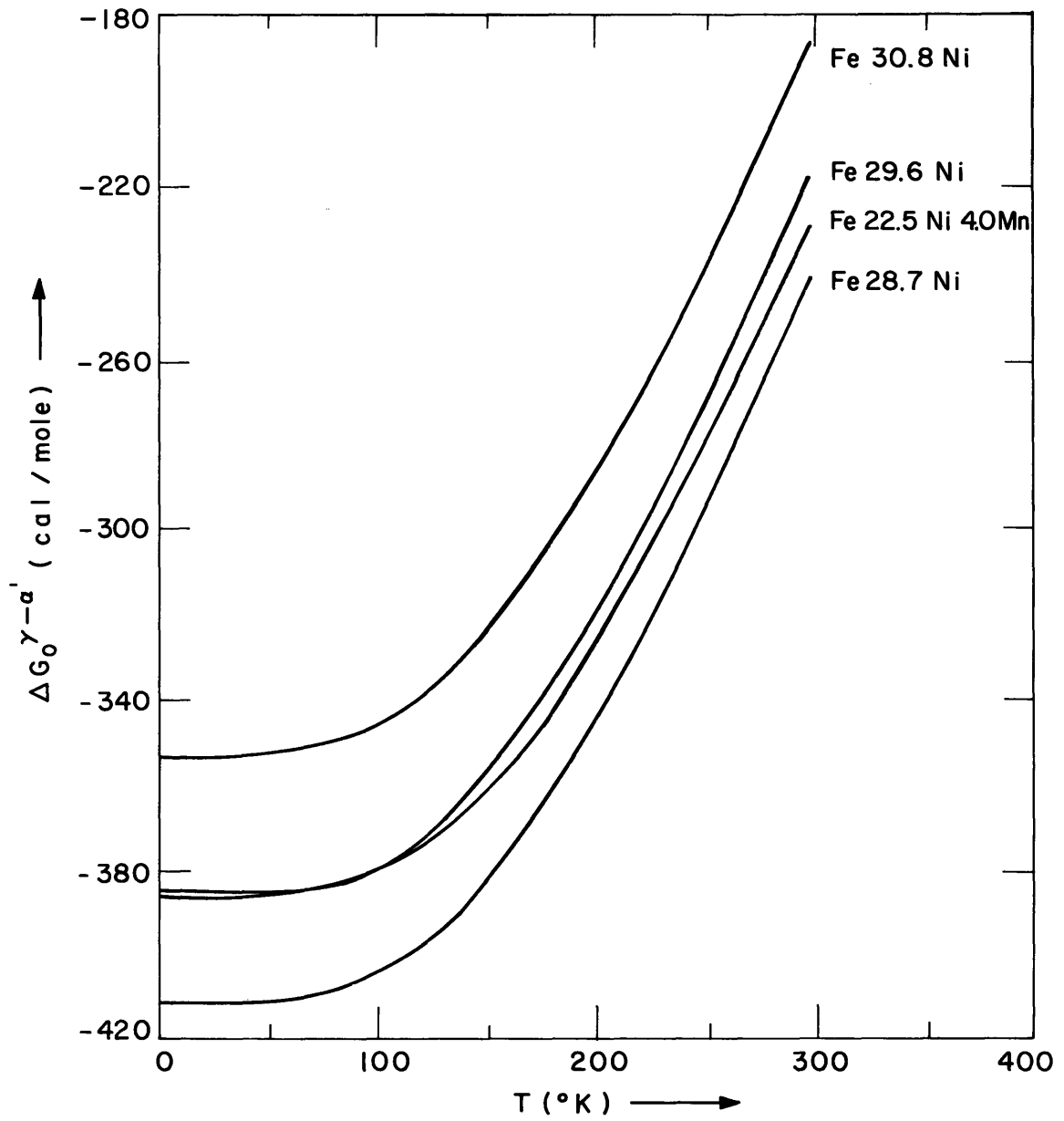


FIG. 5 CHEMICAL FREE-ENERGY CHANGE FOR THE AUSTENITE-TO-MARTENSITE TRANSFORMATION FROM EQUATION 27

## V-2 Fe 28.7 Ni -- (Isothermal)

### V-2.1 Kinetics

The three FeNi alloys investigated in this thesis cover the range of kinetics from isothermal to burst transformations and the range of morphologies from lath to plate. Fig. 6 shows the transformation behavior of the Fe 28.7 Ni alloy under zero-field conditions. (The earth's magnetic field is only about 0.4 gauss at the Magnet Laboratory.) The reaction becomes easily detectable at temperatures near 13°C and, as the temperature is lowered, this alloy transforms at a continuously increasing rate to higher and higher final percentages of martensite. Over the temperature range studied, isothermal kinetic behavior is unquestionably observed. As is characteristic for FeNi alloys, the transformation reaches a relatively abrupt slow-down at the final stages. The reasons for this plateau behavior is not well understood.

Fig. 7 illustrates the accelerated kinetics under the influence of magnetic fields at + 24.4°C, 12°C above the temperature of the first detectable transformation without a field. Increasing field and decreasing temperature behave similarly in that both raise the driving force and accelerate the kinetics. A closer comparison of the two figures reveals that there are some differences. In particular, the field-accelerated curves reach their plateau faster than the zero-field curves at lower temperatures. This suggests that the plateau behavior is thermally activated and is enhanced at the higher temperatures of the field-induced transformation. Later discussions will show that this approach is too

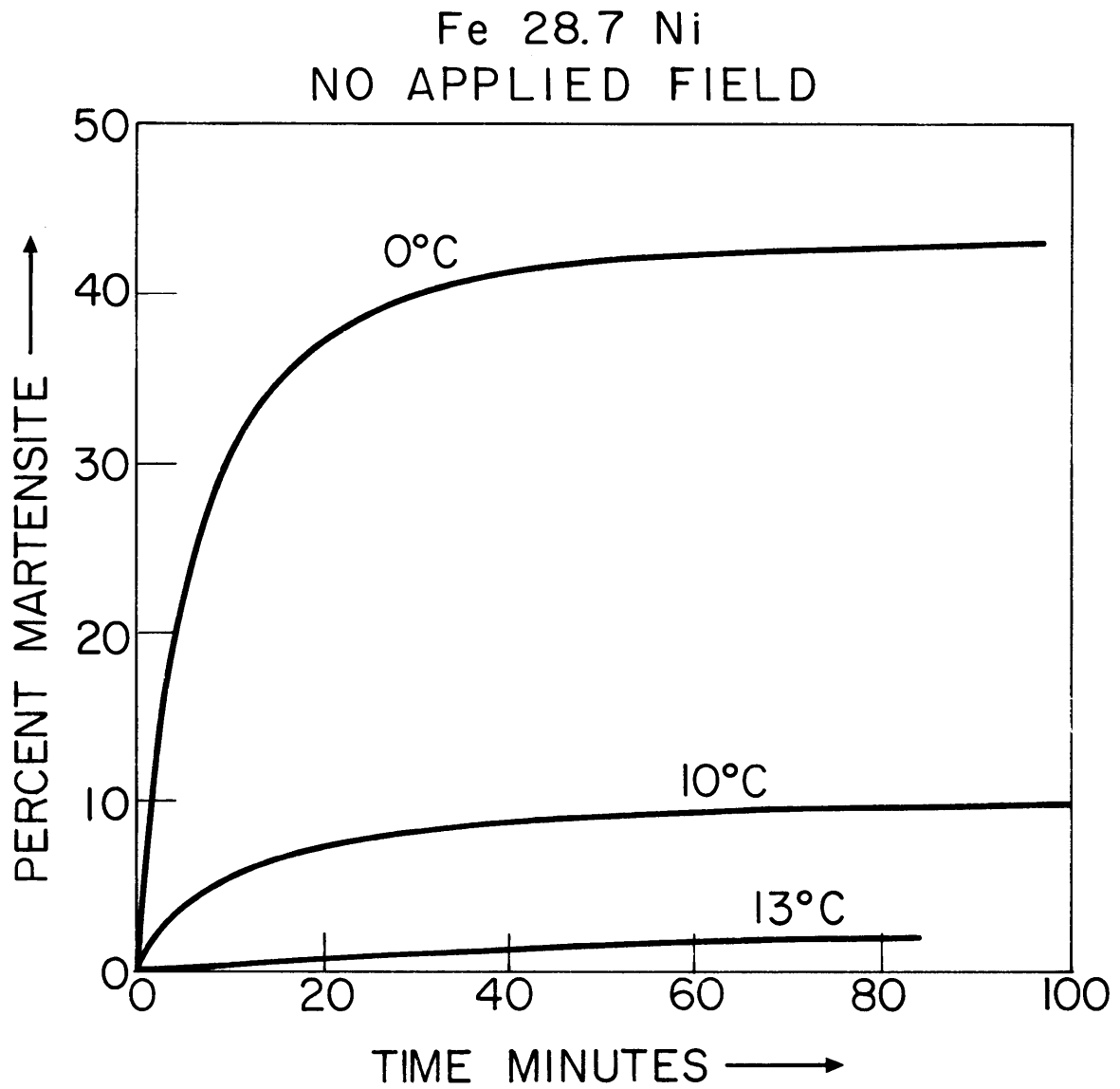


FIG. 6 TRANSFORMATION KINETICS OF Fe 28.7 Ni  
UNDER ZERO-FIELD CONDITIONS



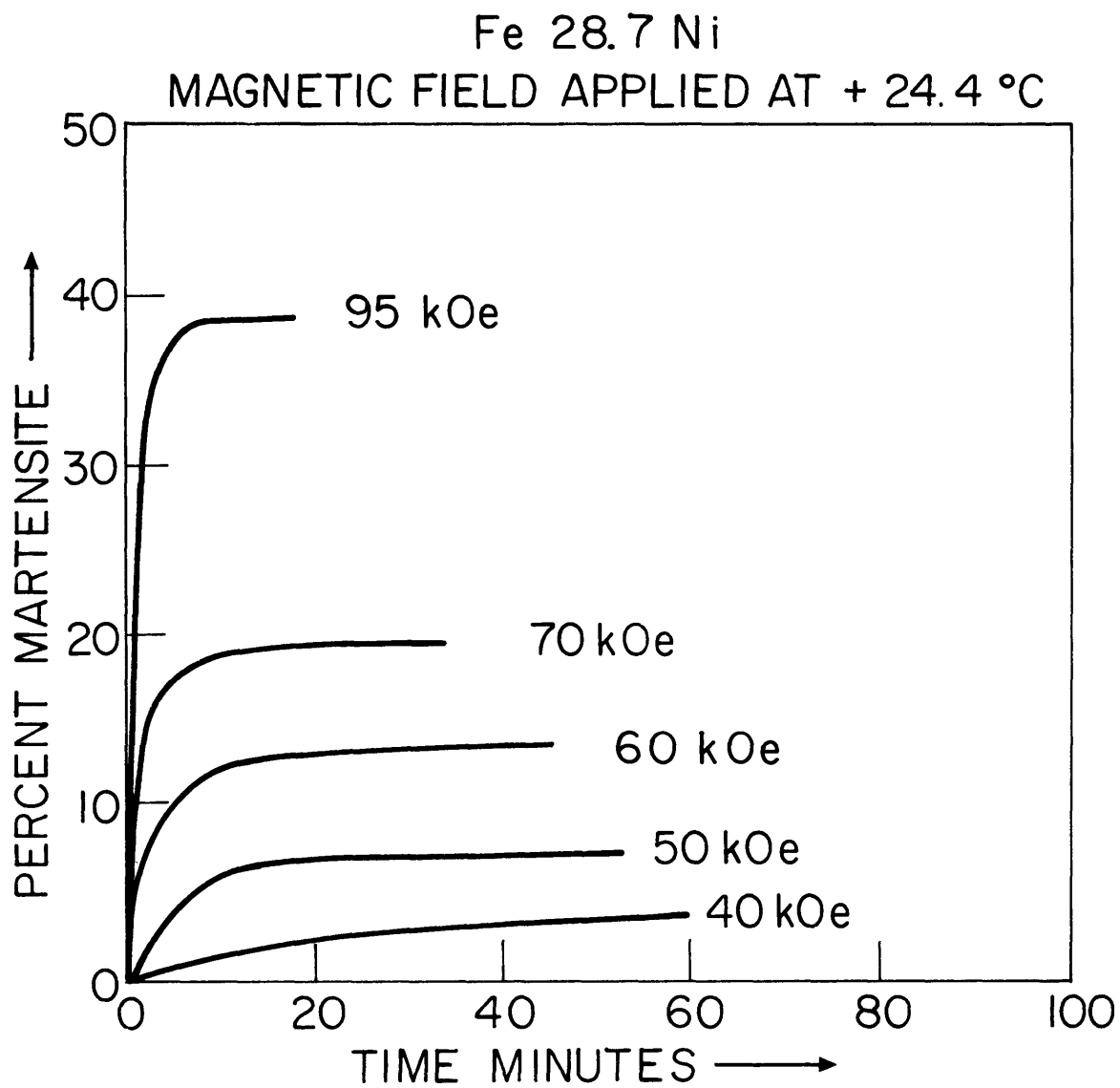


FIG. 7 FIELD-INDUCED TRANSFORMATION KINETICS  
OF Fe 28.7 Ni AT 24.4 °C

simplified.

Could we have predicted the effect of magnetic field on the transformation curves from the thermodynamic driving forces and a knowledge of the zero-field characteristics of Fig. 6? It might seem reasonable to assume that the kinetic reaction rate would be a simple function of the thermodynamic driving force which we can increase by lowering the temperature or raising the field. At zero field, a transformation at + 13°C has a chemical driving force of 256.8 cal/mole. Comparison of Figs. 6 and 7 shows that 40 kOe at 24.4°C gives roughly comparable transformation kinetics. The chemical driving force at + 24.4°C is 244.5 cal/mole and the magnetic  $\mu_0MH$  contribution is about 9.1 cal/mole yielding a total driving force of 253.6 cal/mole. Thus, we see that the field-induced transformation occurs with a smaller driving force. At higher fields, the difference is even more marked. Obviously, the thermodynamic driving force is not the only parameter dictating the kinetics of the reaction.

#### V-2.2 Morphology

Iron-nickel alloys with nickel less than 28.5 wt. % have lath morphologies, while those containing greater than 30.5% exhibit plate characteristics. The alloys in the narrow band of composition in-between exhibit what has been described<sup>(42)</sup> as mixed (not intermediate) morphologies. The morphology of the Fe 28.7 Ni alloy, shown in Fig. 8, is just within this transition range. The structure is extremely hard to characterize, to say the least. It is definitely not plate-like, but it

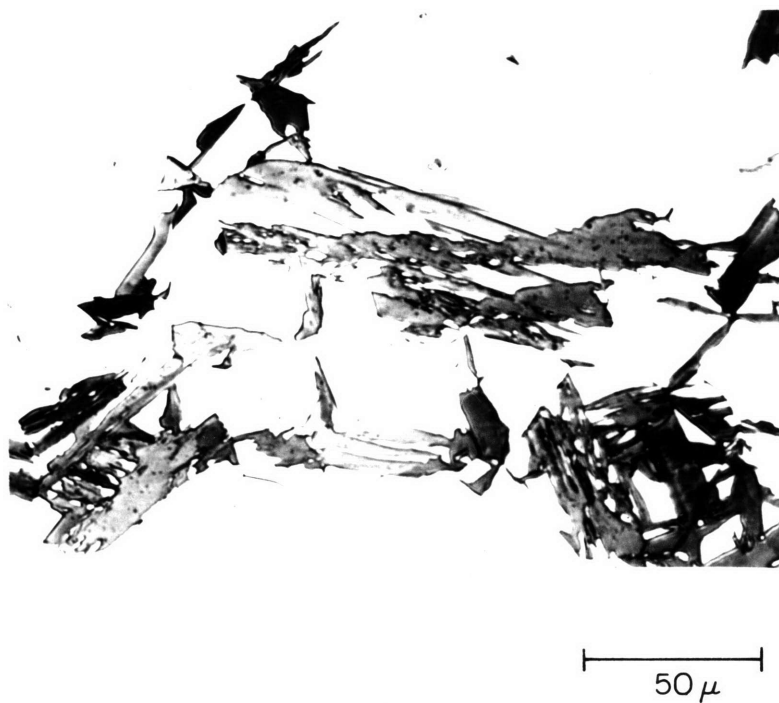


FIG. 8 LATH-LIKE MORPHOLOGY OF  $\text{Fe}_{28.7}\text{Ni}$   
TRANSFORMED WITH A 60 kOe  
FIELD AT 24.4 °C.

does not exhibit the packet blocks of lath martensite, either. For future designation, this will be referred to as lath-like martensite exhibiting a loose-packet structure. Because the transformation temperature was so close to room temperature, surface artifacts due to mechanical polishing and even surface-induced martensite during electropolishing hampered the morphological investigation. In addition, this alloy exhibited severe clustering of the martensite in streaks parallel to the specimen axis. Within these limitations, the field had no apparent effect on the morphology.

### V-3 Fe 29.6 Ni - (Isothermal → Bursting)

#### V-3.1 Kinetics

The zero-field kinetics of the Fe 29.6 Ni alloy are shown in Fig. 9. The transformation can be observed within a reasonable length of time at temperatures of about - 8 or - 9°C. As the temperature is lowered, the kinetics are accelerated, but remain definitely isothermal, until a "transition" temperature near - 20°C is reached at which the transformation can be described as a very fast initial reaction followed by a slower isothermal reaction. One specimen at - 20°C took about 30 seconds before it was possible to detect any transformation, and then it abruptly transformed with a fast "burst" and audible clicking. This illustrates that even the fast bursting region is thermally activated. At liquid-nitrogen temperatures, there is a much more dramatic burst and a smaller "isothermal" tail.

The effect of large magnetic fields on the transformation kinetics at constant temperature is illustrated in Figs. 10 and 11. Again, the field-accelerated reaction yields a series of curves very similar to those generated by lowering the temperature. It is necessary to go to higher fields at + 9°C than at - 2°C because of the smaller chemical driving force available at the higher temperature. The final plateau stage is reached at earlier times in the field-induced curves than in the no-field curves generated by lowering the temperature. The effect, however, is not nearly as noticeable as in the Fe 28.7 Ni alloy tested at + 24.4°C. The fact that this effect is less noticeable at + 9°C than

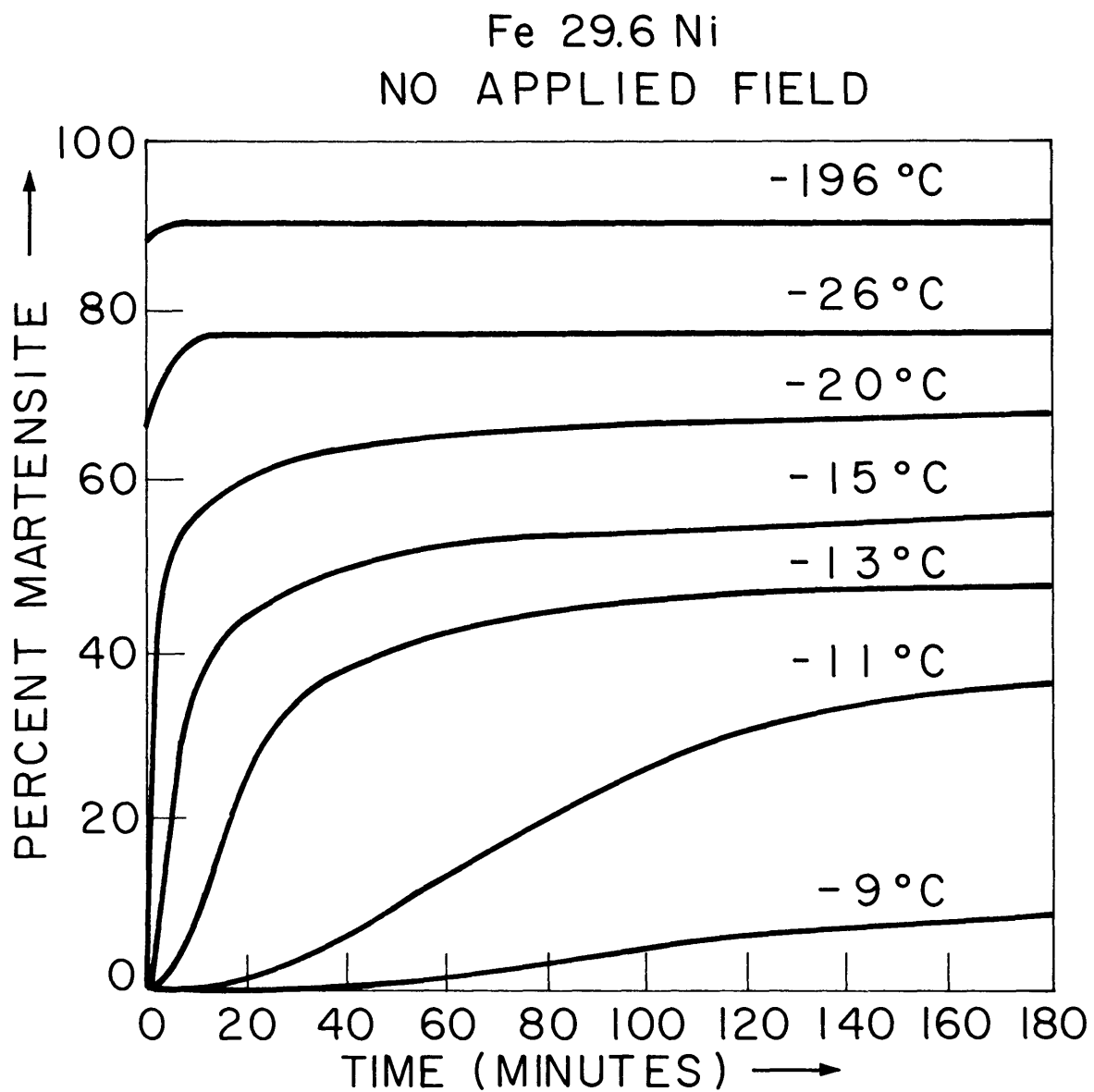


FIG. 9 TRANSFORMATION KINETICS OF Fe 29.6 Ni  
UNDER ZERO-FIELD CONDITIONS

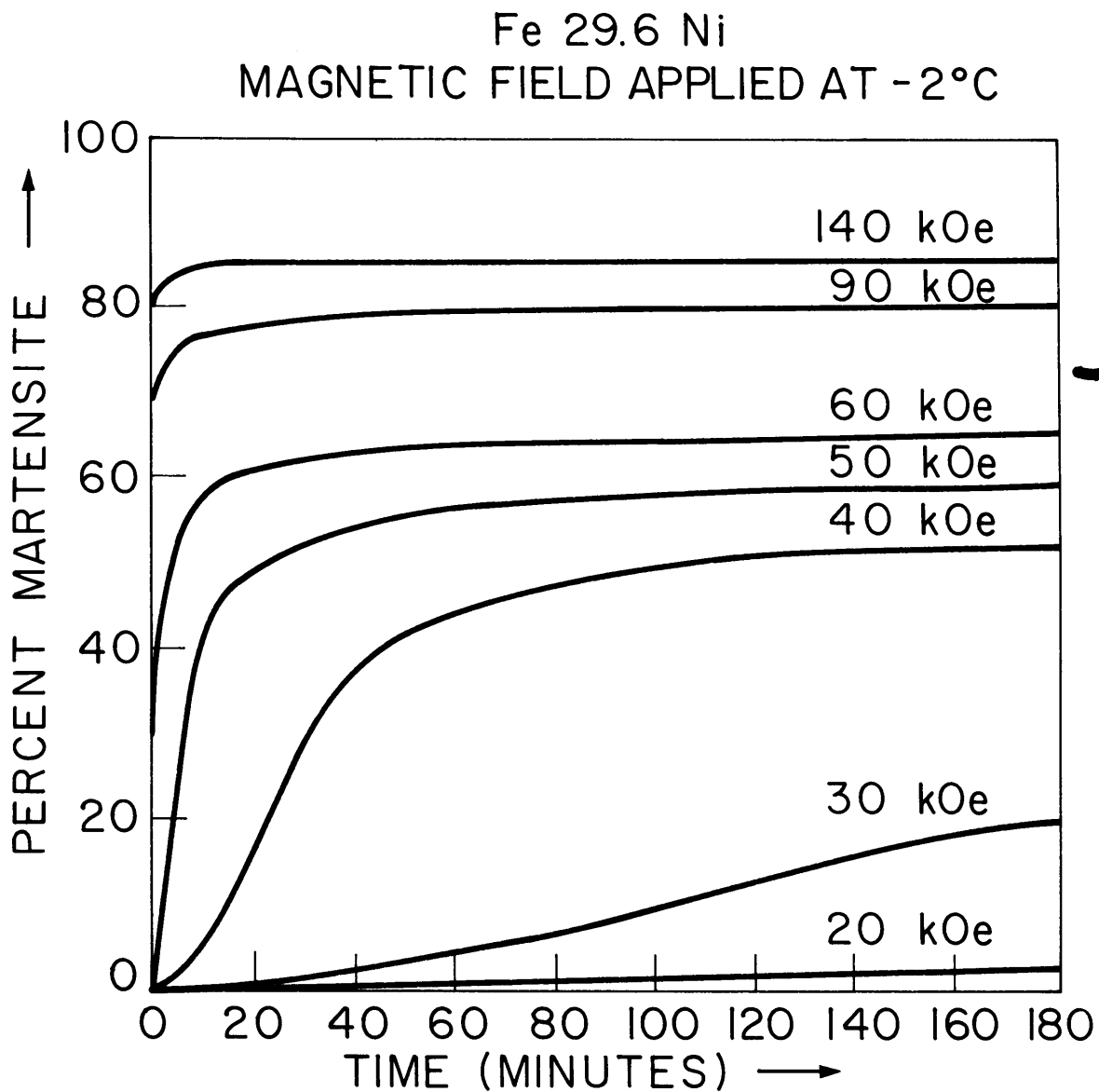


FIG. 10 FIELD-INDUCED TRANSFORMATION KINETICS  
OF Fe 29.6 Ni AT  $-2^{\circ}\text{C}$

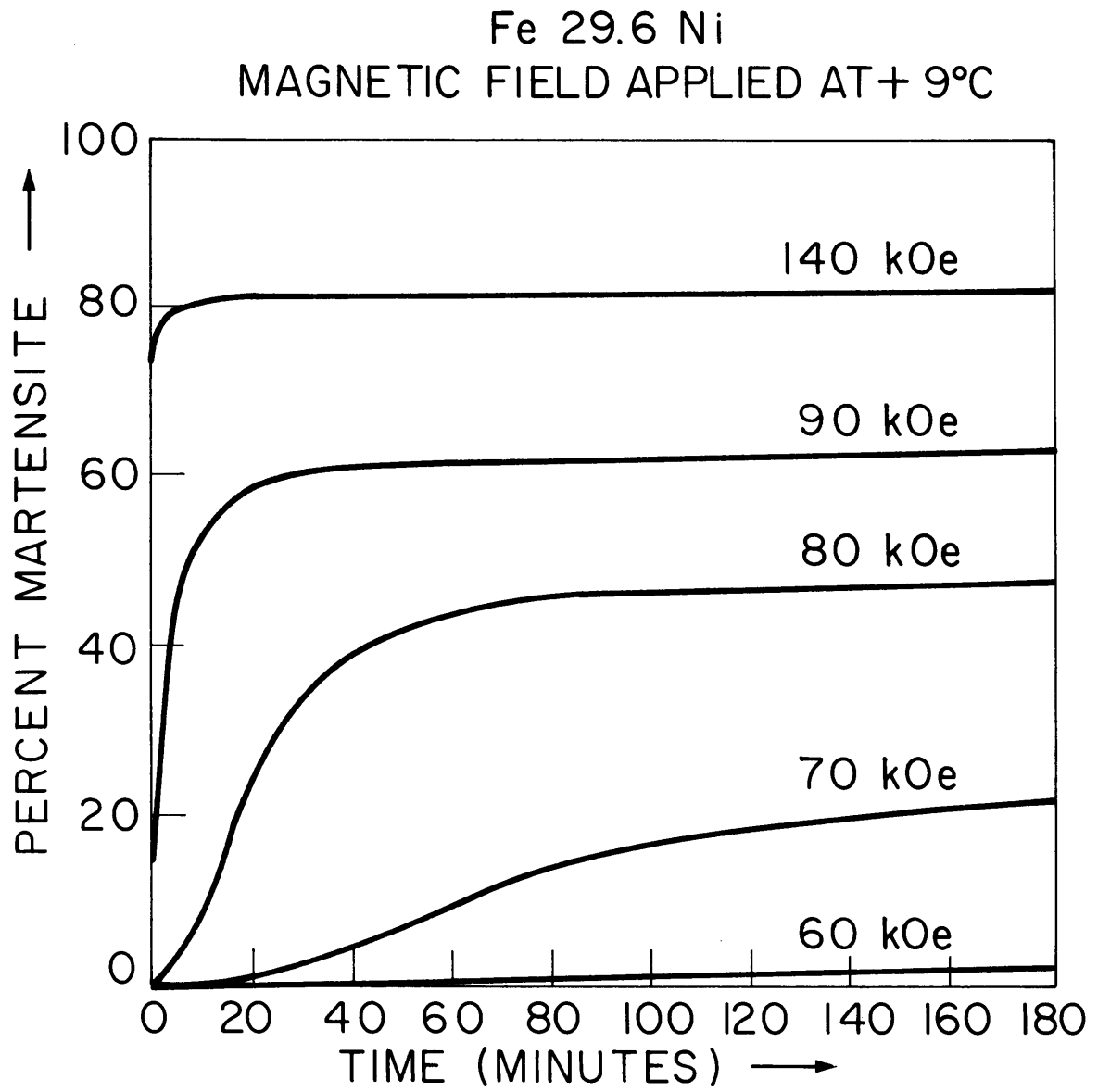


FIG. II FIELD-INDUCED TRANSFORMATION KINETICS  
OF Fe 29.6 Ni AT + 9°C



at +24.4°C might be taken as further evidence to support the hypothesis that the plateau behavior is related to a thermally activated phenomenon; however, discussions in Section V-3.3 will show that this is too simplified an approach.

### V-3.2 Morphological Transition Behavior

Optical microscopy reveals some interesting correlations and some new clues as to the intrinsic differences between lath and plate martensites. As mentioned previously, the Fe 29.6Ni alloy falls about midway within the lath-to-plate transition composition range. Under zero-field conditions at temperatures from - 9°C to - 15°C, the structure is lath-like, reminiscent of the Fe 28.7Ni structure. As the temperature is lowered, however, the structure changes to a mixture of plates (with a definite midrib) surrounded by the higher temperature lath-like structure, as in Fig. 12. The morphological transition temperature of the Fe 29.6Ni alloy is near - 20°C, the same temperature at which we saw the transition in the kinetic mode in Fig. 9. As the temperature is lowered even further, the plate morphology begins to predominate. This is strong evidence to support the hypothesis (e.g. 16) that all martensitic transformation kinetics are isothermal and the only difference between bursting and isothermal alloys is the cooperative nature of the bursting morphology. This also proves that the temperature of transformation is more correlative with the lath-to-plate transition than alloy composition. However, it should be emphasized that these relationships in Fe Ni alloys do not necessarily apply to Fe Ni Mn alloys.

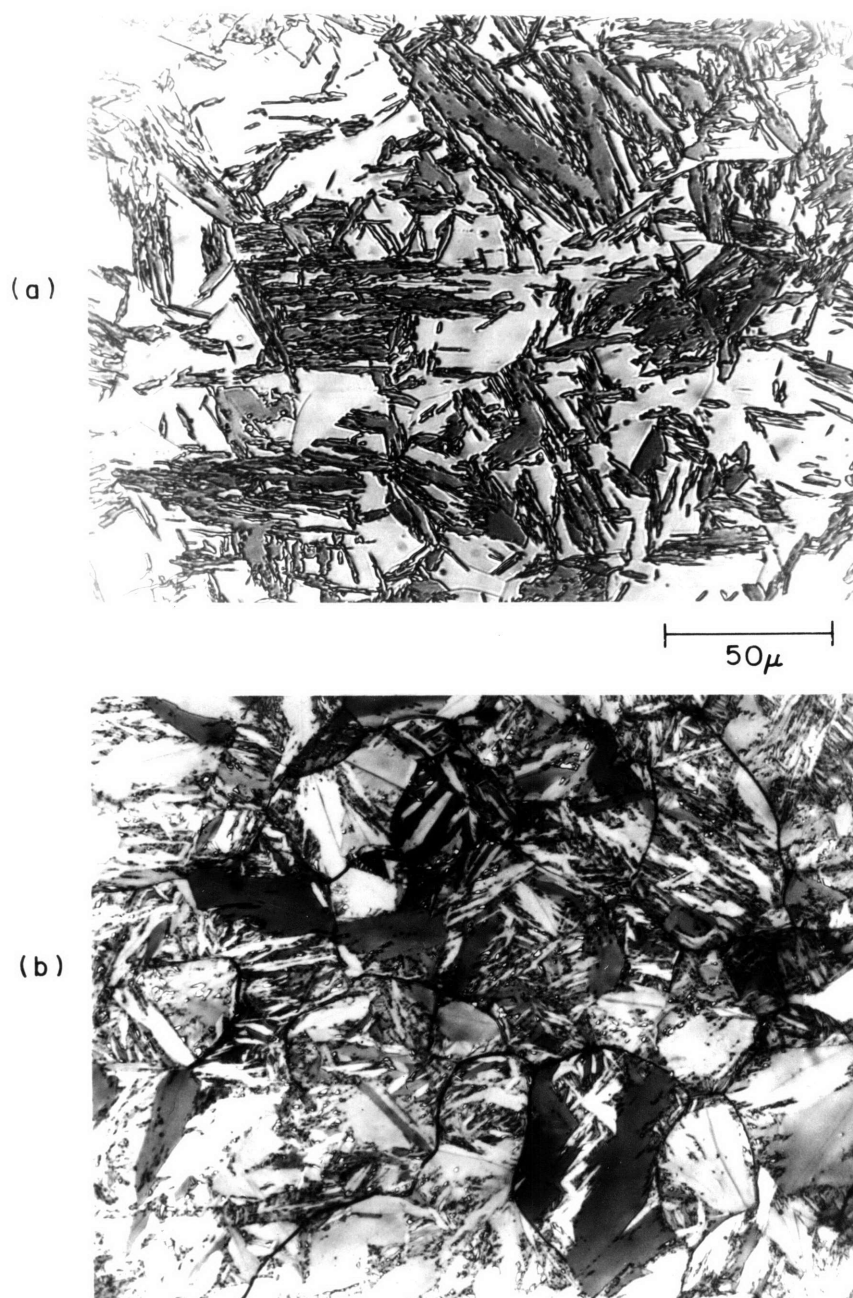


FIG. 12 MORPHOLOGICAL TRANSITION IN Fe 29.6 Ni  
UNDER ZERO-FIELD CONDITIONS  
(a) LATH-LIKE AT -13°C  
(b) MIXTURE OF PLATE AND LATH-LIKE  
AT -196°C

An examination of the morphology of the higher temperature field-induced transformations, shown in Fig. 13, reveals that they also go through the same structural transition as the zero-field transformations. This transition in the Fe 29.6 Ni alloy occurs roughly with a field of 50 kOe at  $-2^{\circ}\text{C}$  and with 90 kOe at  $+9^{\circ}\text{C}$ . These findings demonstrate clearly that temperature is not the only important factor in correlating the lath-to-plate transition. The  $+9^{\circ}\text{C}/140$  kOe specimens have fewer plates than do the  $-26^{\circ}\text{C}$  zero-field specimens with a comparable amount of transformation. However, this could be related to the fact that it takes more time to raise the field to 140 kOe than to quench to  $-26^{\circ}\text{C}$ .

The hypothesis that the total Gibbs free-energy change is a proper correlation parameter for the morphological transition seems appealing at first. Comparison of Figs. 9 and 11 show that the zero-field/ $-9^{\circ}\text{C}$  and the 60 kOe/ $+9^{\circ}\text{C}$  curves display nearly the same kinetic (and morphological) behavior. Their total (chemical plus magnetic) driving forces are 257.2 and 249.7 cal/mole respectively. Thus, just as in the Fe 28.7 Ni case, the magnetically-induced transformations occur with smaller driving forces.

So far, we have shown that the chemical composition, temperature, and free-energy change do not correlate well with the kinetics or morphology of the martensitic transformation. This situation should come as no surprise, however, since it is rare that a complex kinetic reaction can be described by a single thermodynamic parameter. More satisfactory correlations with kinetic parameters will be made in the next section.

Because of the loose-packet nature of the lath-like martensite, it

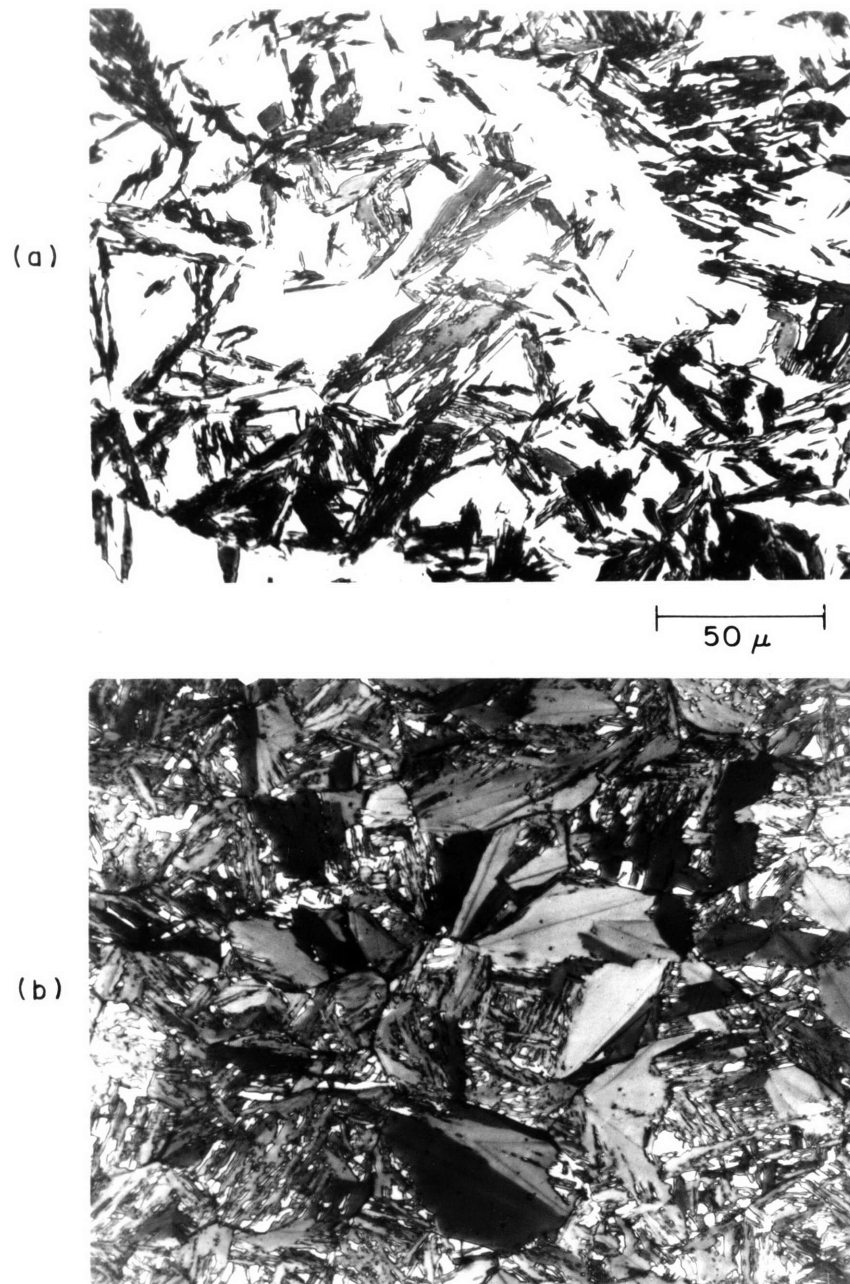


FIG. 13 FIELD-INDUCED MORPHOLOGICAL TRANSITION  
IN Fe 29.6 Ni AT -2°C  
(a) LATH-LIKE AT 40 kOe  
(b) MIXTURE OF PLATE AND LATH-LIKE  
AT 140 kOe

was practically impossible to analyze quantitatively, as has been done for plate structures.<sup>(25)</sup> Visual comparisons between the structures of several specimens revealed that the lath-like structure was insensitive to changes in temperature, field, percent martensite, and the simultaneous existence of plates. (The mean volume per plate was somewhat larger when the martensite content was <5%). In addition, although austenitic twin boundaries usually behaved like grain boundaries and stopped the growing martensite, there were examples of twin-related loose-packets as shown in Fig. 14.

These transition structures have been referred to as a mixture of plate and lath martensite, but they are more than that. We have already seen that the lath martensite in the mixture is only lath-like; moreover, closer inspection discloses that the plates themselves also have an intermediate structure. When a plate is cut nearly perpendicular to the thickness axis, the cross-section is very irregular in shape and contains pockets of untransformed austenite. Fig. 15 is a higher magnification photomicrograph of a typical "plate". Note the irregular lath-like interface which grows off at an angle of 25 to 30° from the midrib. Many times, this lath-like interface of the plates is indistinguishable from the surrounding lath-like morphology. The twin-related loose-packets in Fig. 14 probably do not emanate from a midrib because the former usually occur with a much broader range of angles relative to the twin plane, and because inspection of Fig. 15 reveals that the "laths" are parallel to each other on opposite sides of the midrib and are not mirror-imaged as in Fig. 14. The linear



50  $\mu$

FIG.14 AN EXAMPLE OF A TWIN-RELATED  
LOOSE-PACKET IN  $\text{Fe}_{29.6}\text{Ni}$   
TRANSFORMED WITH 60 kOe AT  $-2^\circ\text{C}$ .

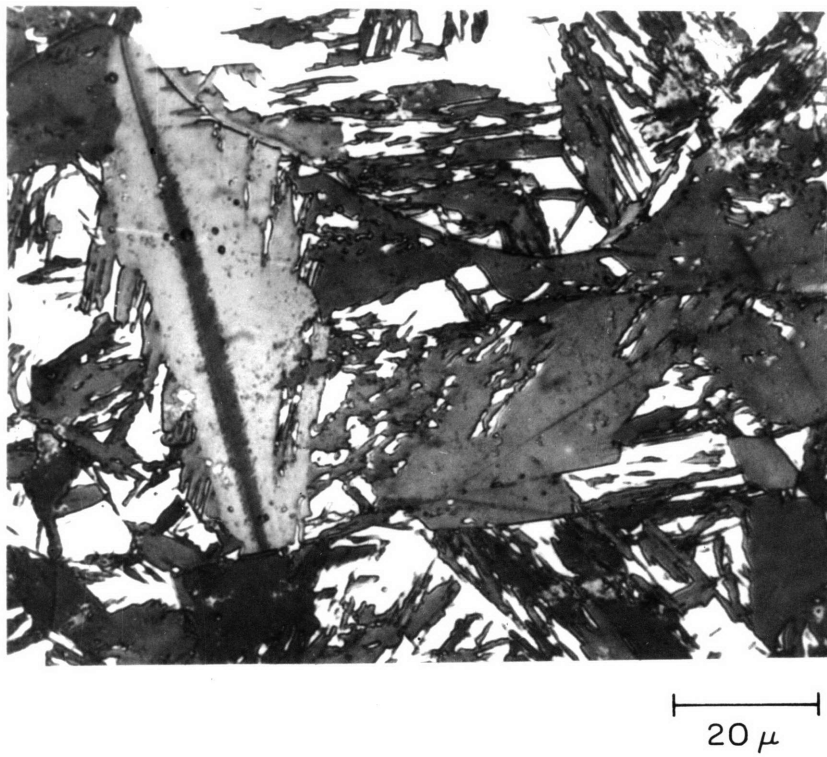


FIG. 15 AN EXAMPLE OF THE TRANSITION PLATE MORPHOLOGY IN Fe<sub>29.6</sub>Ni TRANSFORMED WITH A 90 kOe FIELD AT -2 °C.

nature of the pockets of retained austenite and the straight  $\alpha'$ - $\gamma$  interfaces on some of the plates indicate that the slower growing outer regions of the plates grow unidirectionally and in antiparallel directions on either side of the midrib. These observations suggest that plate-thickening and lath-like martensite are both slow-growing slip martensites.

In light of the jagged nature of some plate interfaces and of lath-like martensites, we must be careful to distinguish between the jagged continued growth of existing martensite and the "true" autocatalytic nucleation of a martensite unit having a different growth direction than its precursor. According to the discussions in Section V-4.2, it is highly improbable that the autocatalytic nuclei preexist as distinct entities in the parent austenite. Thus, there is a fine line between continued growth of a given martensitic unit and autocatalytic nucleation. Most of the martensite we see in this Fe Ni alloy is best thought of as martensite cluster-spreading rather than the individual nucleation events of separate embryos.

Davies and Magee<sup>(42)</sup> mapped out the observed structure of a series of Fe Ni and Fe Ni Co alloys on a plot of  $\theta_{c\gamma} - M_S$  versus  $M_S$ . They found that, for these alloys, austenite ferromagnetism above  $M_S$  is a necessary, but not sufficient, condition for the formation of lenticular rather than packet martensite. The structures of the present zero-field transformations in all three binary Fe Ni alloys fit into their classification scheme. However, as the magnetic field is applied,  $M_S$  increases while  $\theta_c$  increases much less; consequently  $\theta_c - M_S$  decreases with



increasing field. According to the correlation plot, this should shift the structures to more lath-like martensite when, in fact, the observed structures are more plate-like in nature. Davies and Magee interpreted their results in terms of austenite strength, i.e. above some critical austenite flow stress, lenticular martensite would require less energy to form than packet martensite because the latter includes slip in austenite as an intrinsic part of its formation. The inconsistencies of our field-induced structures with their plot would have to be interpreted as a decrease in austenite strength with increasing fields. There is some evidence for this as will be discussed in Section V-3.4; however, we will show in the next section that the lath-to-plate transition is best correlated with other kinetic parameters.

### V-3.3 Activation-Energy Correlations

Eq. 26 was used to calculate the activation energy,  $\Delta W_a$ , from  $\tau_{0.3}$ , the time to transform to 0.3% martensite,  $\bar{V}_i$  the average initial plate volume,  $n_i$ , the concentration of initial embryos, and  $\nu$ , the attempt frequency. (This is only an approximate calculation, as will be discussed in a later section). The value of  $\tau_{0.3}$  adopted for these calculations was the median of several runs under identical testing conditions.  $\bar{V}_i$  was measured using the procedure outlined in Section IV-6.3. Because of the lath-like nature of this morphology, the measurements were extremely difficult and time-consuming. In addition, the thin-disk or oblate-spheroid approximations does not work well for lath-like structures. For these reasons, the value of  $\bar{V}_i$  ( $= 7 \times 10^{-9} \text{ cm}^3$ ) is only an order of magnitude value. Any inaccuracies in  $\bar{V}_i$  will just change all the  $\Delta W_a$

values by a constant factor. Magee's experiments <sup>(22)</sup> suggest that  $n_i$  should be  $\sim 10^5$  embryos/cc for small particles; however we felt a value of  $10^7$  was more appropriate since we are testing the bulk kinetics of a material that has been subjected to a complex thermal and mechanical history. The attempt frequency was taken as  $10^{14} \text{ sec}^{-1}$  to be consistent with the Raghavan-Cohen growth path paper<sup>(50)</sup>; however, using a value of  $10^{11} \text{ sec}^{-1}$  as suggested by Magee<sup>(28)</sup> does not change the overall shape of the curves. The choice of these numbers is not very critical since  $\Delta W_a$  (from Eq. 26) is not a sensitive function of the product  $n_i v$ .

The results of these calculations and the values of the chemical and magnetic driving forces calculated from Eqs. 11 and 27 are listed in Table 4 and plotted in Fig. 16. The use of magnetic fields has allowed us to extend the range of  $\Delta W_a$  values over that which was possible by varying temperature alone. Note that the  $\Delta W_a$  values decrease somewhat with increasing driving force or decreasing incubation time. This would be due to a factor of 2 increase in initial plate volume with higher driving forces, but it is more likely caused by autocatalytic effects which are not taken into account in Eq. 26.

Since we have two independent variables - temperature and magnetic field - which can change the driving force, we are in a position to evaluate the relative effects of driving force and temperature. When the morphology and kinetics of two specimens with nearly the same  $\Delta W_a$  or  $\Delta g_T$  are compared, the field-induced specimen is found to have greatly accelerated kinetics compared to the lower-temperature specimens.

TABLE 4

Incubation Times, Activation Energies, and Driving Forces for Fe 29.6 Ni

Temperature (°C)	Magnetic Field (kOe)	Chemical $\Delta G_0$ (cal/mole)	Magnetic $\Delta G_m$ (cal/mole)	Total $\Delta g_T$ ( $10^9$ erg/cm <sup>3</sup> )	$\tau_{0.3\%}$ (min)	$\frac{\Delta W_a}{(10^{-12} \text{ ergs/event } ^\circ\text{K})}$
- 9	0	257.2	0	- 1.56	23.5	1.55
- 11	0	259.4	0	- 1.57	12.1	1.54
- 13	0	261.5	0	- 1.58	4.0	1.46
- 15	0	263.7	0	- 1.60	1.0	1.39
- 2	20	249.5	4.0	- 1.53	40.1	1.62
- 2	30	249.5	6.0	- 1.54	17.0	1.58
- 2	40	249.5	8.0	- 1.56	3.1	1.52
- 2	50	249.5	10.0	- 1.57	0.3	1.44
+ 9	60	237.5	12.2	- 1.51	26.8	1.67
+ 9	70	237.5	14.3	- 1.52	19.2	1.65
+ 9	80	237.5	16.3	- 1.53	1.2	1.54

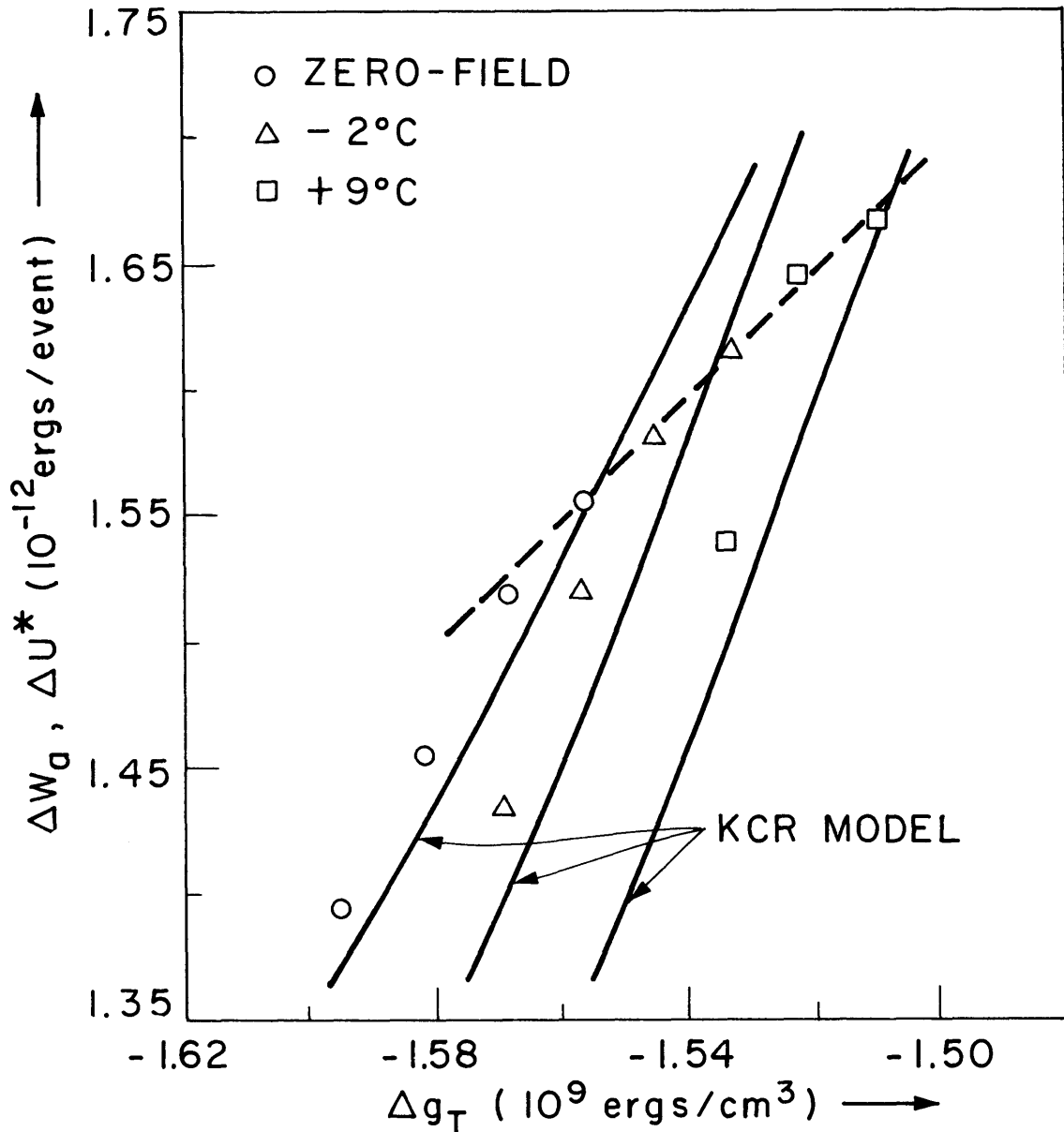


FIG. 16 ACTIVATION ENERGY VERSUS TOTAL GIBBS FREE-ENERGY CHANGE FOR Fe<sub>29.6</sub>Ni (THE DASHED LINE CONNECTS THE INITIAL LOWER DRIVING-FORCE POINTS OF EACH SERIES.)

One might not have expected that two identical specimens transforming with the same activation energy or driving force would have different kinetics and morphology. The reason behind this behavior is that the field not only accelerates the reaction by increasing the driving force, but it also enables it to occur at higher temperatures where the reaction reaps the additional benefit of higher thermal energy. The appropriate kinetic parameter is  $\Delta Wa/T$  which is plotted in Fig. 17. When comparisons are made between specimens with nearly the same  $\Delta Wa/T$  (and different  $\Delta g_T$ ), they have similar kinetics and morphology! The transition from lath-like to plate-like occurs at roughly  $\Delta Wa/T = 5.4 \times 10^{-15}$  ergs/event  $^\circ\text{K}$  in Fe 29.6 Ni. This is at a region that is barely measurable because of the small incubation times.

The preceding discussions are summarized graphically in Fig. 18; higher rates of transformation yield plate-like martensite, whereas slower rates yield a more lath-like structure. When this criterion is applied to the Fe 28.7 Ni alloy, the measured transformation curves have incubation times (or maximum transformation rates) that would fall in the lath-like region in Fig. 18 in agreement with the observed morphology illustrated in Fig. 8. The Fe 30.8 Ni alloy, to be discussed in the next section can show a large incubation time followed by a very rapid bursting region to plate martensite. Thus, the rate of transformation appears to be a better correlation parameter than the incubation time. The calculation of  $\Delta Wa/T$  from Eq. 26 using the measured incubation time is only a convenient approximation to the overall rate of transformation.

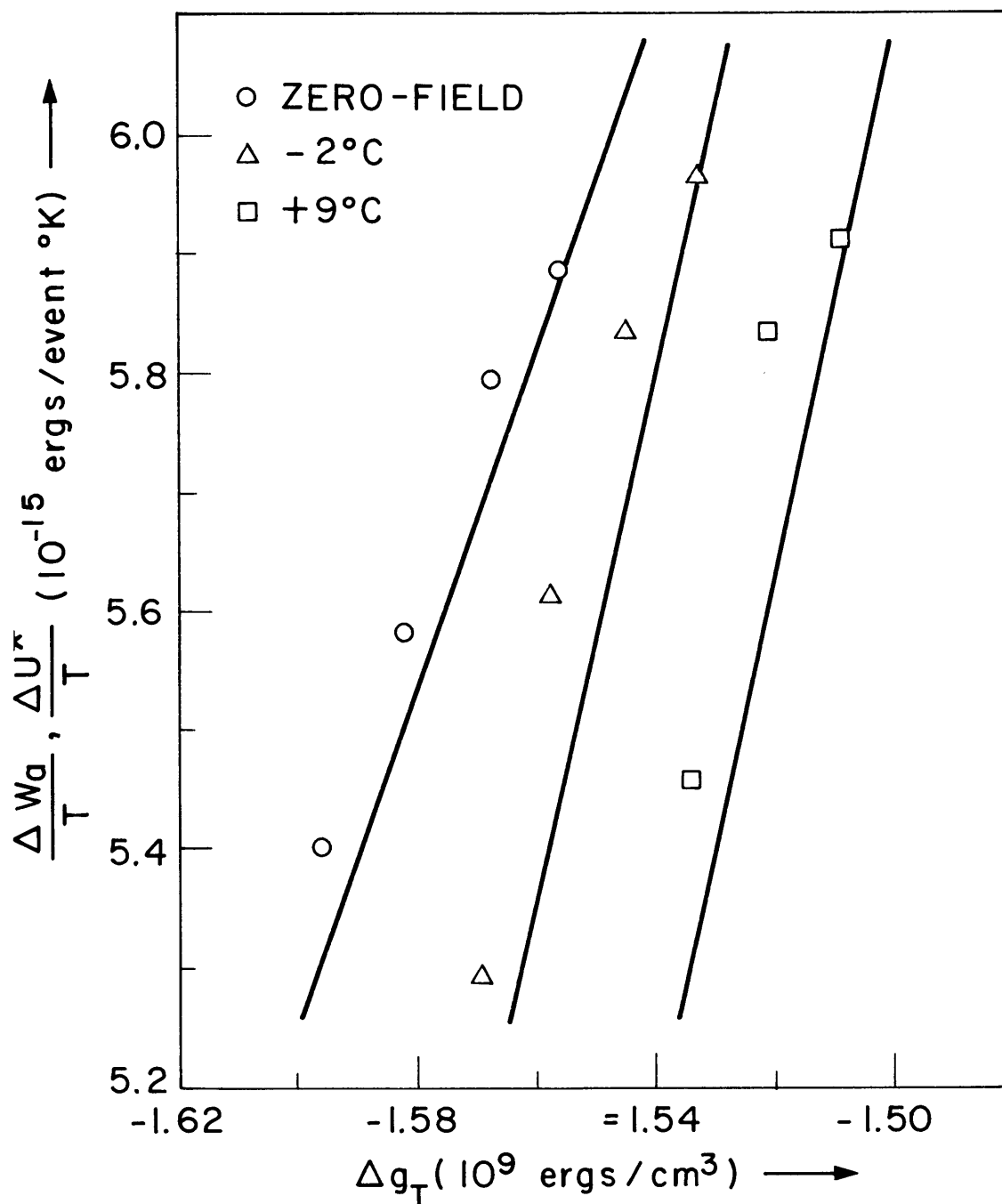


FIG. 17 ACTIVATION ENERGY DIVIDED BY THE TEMPERATURE VERSUS TOTAL GIBBS FREE-ENERGY CHANGE FOR Fe<sub>29.6</sub>Ni (THE SOLID LINES ILLUSTRATE THE FIT WITH THE KCR MODEL.)

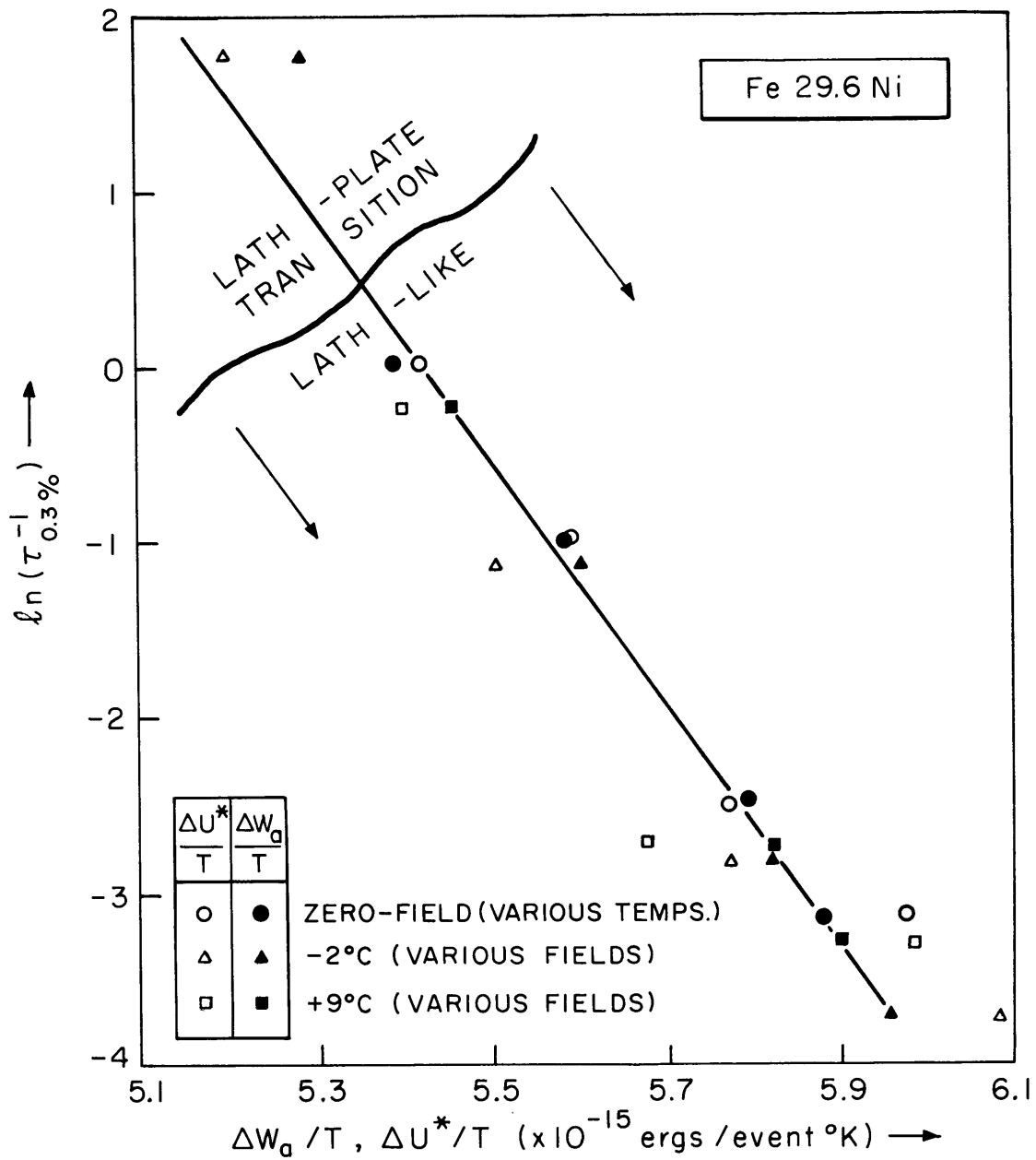


FIG. 18 LOGARITHM OF THE RATE OF TRANSFORMATION VERSUS EXPERIMENTAL  $\Delta W_a/T$  (CLOSED POINTS) AND CALCULATED  $\Delta U^*/T$  (OPEN POINTS), ILLUSTRATING THE MORPHOLOGICAL TRANSITIONS IN Fe 29.6 Ni (THE SOLID LINE IS FROM EQ. 26)

To hope to find a simple relationship between driving-force and temperature which will completely describe all the kinetic and morphological aspects of the martensitic transformation is a bit optimistic, to say the least. The KCR model employs these parameters and others, and still it requires one or two floating parameters. It is still true, however, that reactions with lower activation energy-to-temperature ratios tend to generate more plate-like products. This conclusion says that the commonly observed trend toward more plate-like structures at lower temperatures (e.g. Fig. 12) is actually due to the fact that the activation energy is very much lower at the lower temperatures because of the higher driving forces there. Therefore, it now appears that low temperature, at a given driving force, favors lath martensite and high temperature favors plate martensite. The magnetic fields have enabled us, for the first time, to separate the effects of driving force and temperature.

The quantitative kinetic comparisons have been limited to the incubation times. The overall kinetics of the transformation curves have not been analyzed using Eqs. 12 and 13 because it was felt that these equations do not give an adequate description of the transformation mode; therefore, the calculated parameter ( $\Delta W_a$  and  $p$ ) from curve-fitting would not have any real significance. The troublesome issues are (i) the use of a single activation energy to describe both initial and autocatalytic nucleation, (ii) the consideration of the autocatalytic embryo as a separate entity from the parent phase, and (iii) the assumption of an autocatalytic factor,  $p$ , per unit volume of transformed phase rather than per unit area of moving interface as the



discussions of Section V-4.2 imply. The development of the correct equations to describe these kinetics was outside the objectives of this thesis, but will be considered in the continuing program at MIT.

#### V-3.4 Fit with the KCR Model

The solid lines drawn in Figs. 16 and 17 illustrate the best possible fit with the KCR model. This fit looks very good in light of the assumptions made in calculating  $\Delta W_a$ ; however, the following section describing the procedures and assumptions necessary to arrive at these curves indicates that the model does not work as well as one might suppose from Figs. 16 and 17.

The fitting procedure is as follows: First, Eqs. 15 to 17 are used to fit a point (  $-9^\circ\text{C}$ ,  $H = 0$  ) on Fig. 16. This is done by adjusting the radius and semithickness of the most potent embryo. We assumed that the preexisting embryo is somewhere on the minimum energy fall-line off the saddle point along the free-energy surface, given by  $c^2/r = \sigma/A$ . It was not necessary to assume this relation to satisfy any conditions of the model; however, it provided a basis for the choices of  $r_e$  and  $c_e$ . The  $r_e$  and  $c_e$  values for an exact fit at the chosen point were found to be  $761\text{\AA}$  and  $27\text{\AA}$  respectively. In addition to substituting the density and shear-modulus values of Table 3 into Eqs. 15 to 17, we also assumed that  $A$  and  $\sigma$  are proportional to the modulus, as described previously. Using these procedures, the KCR model fell short of fitting the  $-2^\circ\text{C}$  and  $+9^\circ\text{C}$  field-induced points.

Since the KCR model is very sensitive to the shear modulus,  $\mu$ ,

it was necessary to examine the effect of magnetic fields on the modulus. Most reported modulus values increase with the application of a field on the order of 2 kOe. (An increase of  $\mu$  with H would worsen the fit) This, however, is not indicative of an intrinsic modulus change, but rather is a special case of the well-known modulus defect phenomenon. In short, when we measure the modulus of a demagnetized specimen, we are also including a magnetoelastic strain due to domain reorientation. When a field is applied, the domains become oriented with the field and do not move appreciably with the application of a stress. Thus, modulus measurements under applied magnetic fields give values of the moduli that are more characteristic of the elastic behavior of the lattice. We are interested in the variation of this intrinsic modulus with high fields. Alers, et al.<sup>(108)</sup> reported that  $\frac{1}{c_{44}} \frac{dc_{44}}{dH} = -3 \times 10^{-4}$  at 0°C for an Fe 31.0 Ni alloy under fields in the range of 4 to 10 kOe. This value shifted the KCR curves, matched to the -2°C and +9°C data, in the correct direction, but it overshot the points. The fit shown in Figs. 16 and 17 was obtained by assuming  $\frac{1}{\mu} \frac{d\mu}{dH} = -2 \times 10^{-4}$ . This is a reasonable number, but it still must be regarded as a floating parameter in the absence of a measured value. If the modulus were not a function of temperature and field, then the three lines of Fig. 16 would superimpose since  $\Delta W_a$  (i.e.  $\Delta U^*$ ) is primarily only a function of  $\mu$  and  $\Delta g_T$  in the KCR model. On the other hand, the lines of Fig. 17 would not superimpose under these conditions; consequently, this is a more revealing comparison with any model.

The values of the KCR critical loop radius,  $\rho^*$ , in the region of the isothermal transformations represented in Figs. 16 and 17 are near  $5\text{\AA}$ . Since this is less than twice the Burgers vector, core-overlap effects which are not taken into account in the KCR model could be significant.

Fitting Fig. 17 is a severe test for any model. The fit with the KCR model is fair in light of the discussions of the last paragraphs; however, it seems to fit best on the tailing-off points at higher driving forces. As pointed out earlier, these  $\Delta W_a$  values were probably influenced by autocatalysis which is not accounted for in Eq. 26. The initial, lower driving-force points of each series are the most representative of initial martensite nucleation. These are connected by a dashed line in Fig. 16. The KCR model does not match the slope of this line. Assuming that the size of the most potent embryo is a function of the magnetic field does not improve the situation.

## V-4 Fe 30.8 Ni -- (Bursting)

### V-4.1 Kinetics

Fig. 19 illustrates the zero-field behavior of the Fe 30.8 Ni alloy. The  $M_s$  temperature of  $-45.2^\circ\text{C}$  was an average of 8 specimens which showed a  $\pm 8^\circ\text{C}$  scatter. Within this scatter band, the final percent martensite was a linear function of  $M_s$ . The transformation curves are shown for three temperatures; however measurements were also made at  $4^\circ\text{K}$  in order to test the hypothesis<sup>(16)</sup> that the bursting alloys are isothermal and show a C-curve behavior (versus the KCR model prediction that a pure athermal behavior exists at temperatures below which  $\Delta U^* = 0$ ). The  $4^\circ\text{K}$  curve (not shown in Fig. 19) fell 0.5% below that at  $-196^\circ\text{C}$ . This may indicate that the overall transformation behavior of the alloy exhibits a C-curve behavior; but, 0.5% is a small difference and other complications could cloud the issue. In addition, the driving force versus temperature curves (shown in Fig. 5) demonstrate that, below about  $100^\circ\text{K}$ , there is little change of  $\Delta G_0^{\gamma \rightarrow \alpha}$  with temperature; therefore, even an athermal reaction would not benefit by a decrease in temperature. Even at  $4^\circ\text{K}$ , however, audible clicks could be heard for about  $1\frac{1}{2}$  minutes. Again, this implies that the reaction is isothermal even at these very low temperatures; unfortunately, the enthalpy change heating effects could cause significant temperature fluctuations after the initial burst. It appears that this issue cannot be clearly resolved with bulk specimens, but requires small-particle experiments with bursting alloys.

At higher temperatures, we found positive proof that the reaction

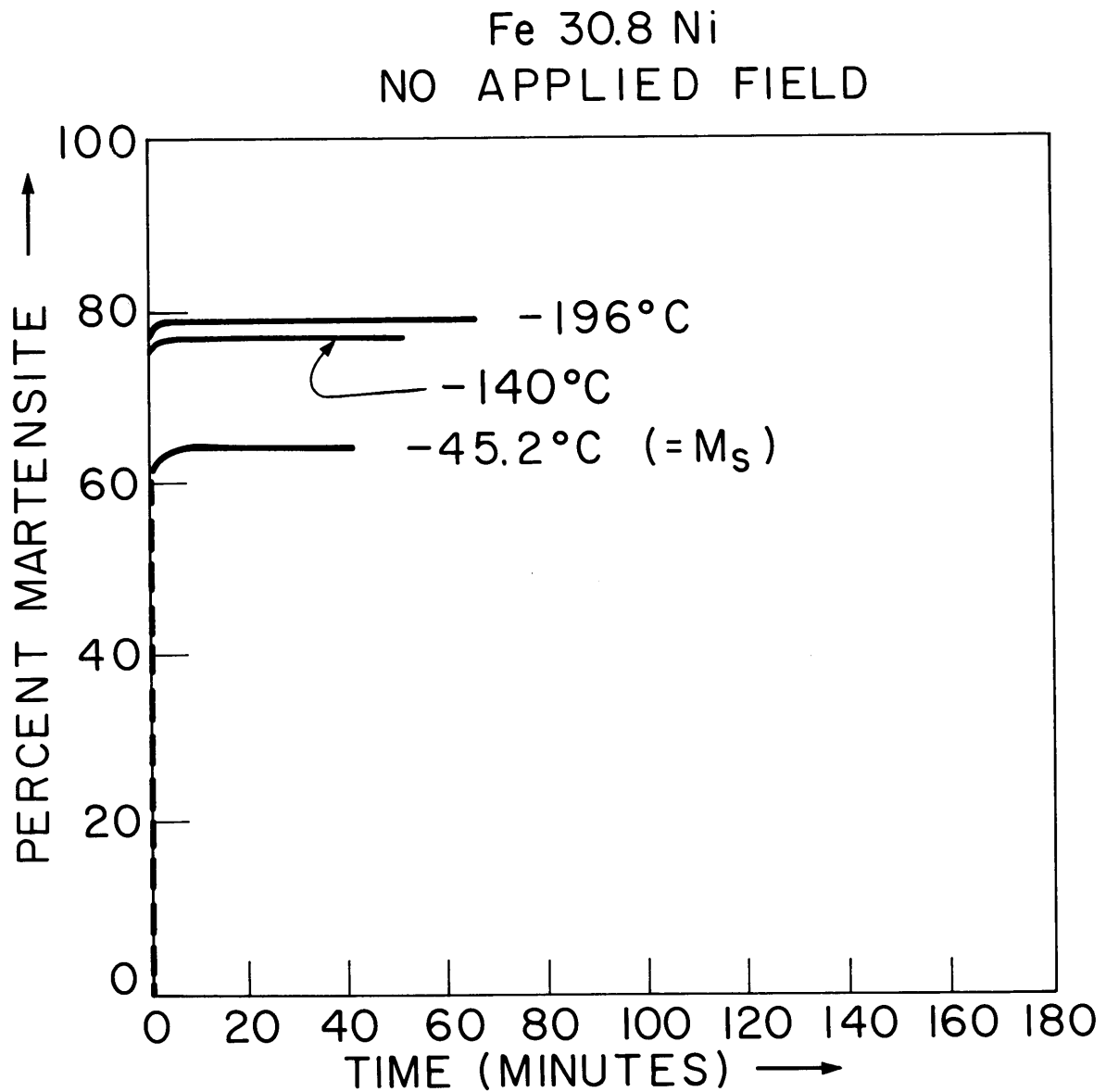


FIG. 19 TRANSFORMATION KINETICS OF Fe 30.8 Ni UNDER ZERO-FIELD CONDITIONS.

proceeds isothermally even though this is a bursting alloy. The specimens were doped to prevent surface nucleation, then slowly cooled and held for about 5 to 10 minutes at a series of decreasing temperatures just above  $M_S$ . Incubation times as long as 1.5 minutes were observed followed by a burst. This is definite proof that the reaction is isothermal near the  $M_S$  temperature.

Two specimens were impregnated with carbon by annealing  $\frac{1}{2}$  hour at  $800^\circ\text{C}$  in a vycor tube filled with CO. The  $M_S$  temperature was suppressed by  $9^\circ\text{C}$  and one specimen had a 6.8 minute incubation time prior to bursting. This illustrates that interstitial pinning has a strong influence on the initial nucleation event but not on the subsequent autocatalytic bursting mode.

When a magnetic field was applied at  $-20^\circ\text{C}$ , which is  $\sim 25^\circ\text{C}$  above  $M_S$ , the curves of Fig. 20 were obtained. The most obvious feature of these runs is that at 90 kOe a large ( $\sim 30$  minute) incubation time was observed. The application of the KCR model to this alloy (assuming that  $r_e = 761 \text{ \AA}$  as in the Fe 29.6 Ni alloy and that the shear modulus values of Table 3 can be extrapolated to lower temperatures) does predict that the  $-20^\circ\text{C}/90 \text{ kOe}$  specimen should have a longer incubation time than the  $-45^\circ\text{C}$  specimen at zero field, but the relative magnitudes are a factor of 10 off. This is not disturbing, however, in light of the approximations made. This exercise also predicts that the true zero-field  $M_S$  according to the KCR definition (i.e.  $\Delta W_a = 0$ ) is at  $\sim -140^\circ\text{C}$ .

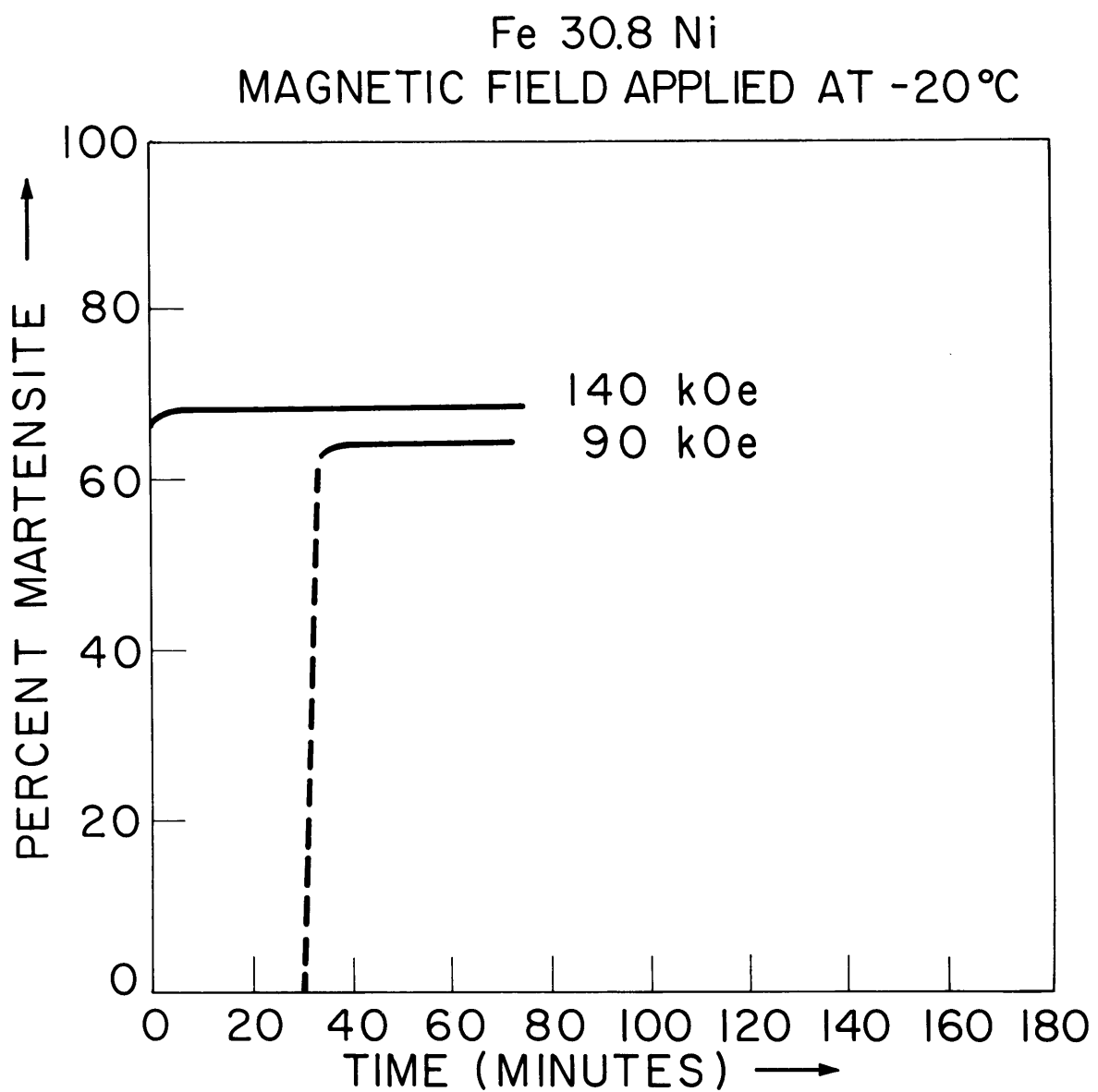


FIG. 20 FIELD-INDUCED TRANSFORMATION KINETICS OF Fe 30.8 Ni AT -20°C.

#### V-4.2 Morphology and Autocatalytic Nucleation

The zero-field structure of this alloy is shown in the micrographs of Fig. 21. This is definitely a typical  $\{259\}_{\gamma}$  bursting alloy. The zig-zag cooperative growth of these martensitic plates is very much in evidence, especially when quenched to liquid-nitrogen temperatures. When two plates impinge, they do not just meet at the point of impingement but rather they always meet at a common interface which can extend virtually the whole length of the plate. This illustrates the slow-growth stage of the plate-thickening step.

These Fe 30.8 Ni martensitic plates have a much smoother  $\alpha' - \gamma$  interface than those which were observed in the Fe 29.6 Ni alloys. From the discussion in Section V-3.3, it appears that the overriding factor governing the "degree-of-jaggedness" of the martensite-plate interface is its ability to overcome barriers. Under conditions of low  $\Delta W_a/T$ , the martensite interface breezes through obstacles very easily and grows at a fast rate; the atoms probably move in a long-range cooperative military fashion and are strongly influenced by such factors as mechanical constraints over long distances. Under conditions of high  $\Delta W_a/T$ , the interface can be more readily pinned at obstacles, thereby causing the lath-like effect at the advancing plate interface.

The field-induced structure at  $-20^{\circ}\text{C}$  shown in Fig. 22 is, once again, very similar to the zero-field structures at  $M_s$ . So far we have shown that the magnetic field can influence the morphology by changing the driving force or the temperature of transformation; however, there has not been any apparent intrinsic effect of the field itself. As



(a)

50  $\mu$ 

(b)



FIG. 21 ZERO - FIELD BURSTING MORPHOLOGY  
IN Fe 30.8 Ni

(a) - 46°C

(b) - 196°C

indicated in Section I-2, we might expect some orientation dependence of the plates with the field; however, it is not likely to find this effect in an alloy, such as this, in which the cooperative growth of neighboring plates is the overriding factor. This potential orientation effect will be examined on a more quantitative basis in connection with the next alloy.

The Fe 30.8 Ni structure illustrates three of the important autocatalytic nucleation sites for bursting alloys. The most obvious sites are at the impingement of midribs on growing plates. This is particularly evident at liquid-nitrogen temperatures, as shown in Fig. 21b. These autocatalytic sites must obviously be freshly created because it is highly unlikely that pre-existing embryos exist that are ready to fire off in the precise zig-zag array.

The second type of site, which must at least initially precede the midrib-impingement type, occurs when the lattice-invariant deformation mode during plate thickening changes from twinning to slip. Operation of this type of site probably generated the three plates shown in Fig. 23 which extend from the midrib. Both of the previously mentioned sites are always generated at an advancing martensite interface and are always associated with a prior midrib.

Christian<sup>(46)</sup> suggests that the interface determines the morphology, whereas Owen, et al.<sup>(45)</sup> say that the growth rate is the important factor. Both views are self-consistent with the  $\Delta W_a/T$  correlation, if the growth rate determines the interface (or vice versa); this, in turn, could determine the morphology and the nature of the autocatalytic nucleation sites.

One very important autocatalytic site has been ignored up to now.



FIG. 23 AN EXAMPLE OF AUTOCATALYTIC PLATES  
EMITTING FROM A MIDRIB IN Fe 30.8 Ni  
TRANSFORMED UNDER ZERO-FIELD  
CONDITIONS AT  $-46^{\circ}\text{C}$

The two sites just mentioned presumably operate mainly within a grain. Without a mechanism for spreading into other grains, we would depend on the initial nucleation sites to start up the transformation in the many grains. Estimates of  $10^7$  nuclei/cm<sup>3</sup> mean there is only about 1 nucleus for every 2 grains, with a grain size of 0.04 mm; but it is apparent that almost all the grains contain martensite. In addition, when an alloy such as Fe 30.8 Ni transforms, every grain fills up in a matter of seconds. The probability of every initial nuclei in every grain transforming at the same time is miniscule. Examination of specimens etched to reveal the austenitic grain boundaries show that many of the plates and even more of the midribs which hit a grain boundary are also touching a plate in the next grain. In addition, it was not uncommon to see midribs extending through a grain boundary and bent by a small angle. The effectiveness of the autocatalytic transfer from grain-to-grain is most likely a function of the relative orientations of adjacent grains. These observations indicate that plate growth or autocatalytic mechanisms can and do operate across incoherent grain boundaries. It is conceivable that a midrib moving at one-third the speed of sound in metal could shock-induce a new plate at the point of contact; however, since we do not know the exact nature of the incoherent grain boundary, we must speculate somewhat about the other possible mechanisms involved.

Since slower growing lath-like martensite can also spread to other grains, the midrib shock mode cannot be the only mechanism operating. Careful re-examination of the Fe 29.6 Ni specimens reveals that the lath-like martensite often grows right along one side of a grain boundary.

In many of these cases, martensite also grows on the other side of the grain boundary adjacent to the first martensite packet. This is most apparent in specimens which have just begun to transform and are not complicated by a large quantity of martensite. One possibility is that the grain boundary may have small regions coherent enough to let the slow-growing martensite pass through to the next grain. It was more common, however, to see the spreading through grain boundaries in the cases where the loose-packets hit a grain boundary head-on rather than in the packet-thickening direction. Thus, if the impinging shear is normal to the grain boundary, the spreading occurs more effectively. In any event, both of these lath-like spreading modes were less evident than the impinging-midrib mode, i.e. there were more examples in which grain boundaries confined the lath-like reaction. It follows that a bursting alloy has faster kinetics both because of the cooperative nature of its growth and because it has more efficient autocatalytic nucleation mechanisms.

## V-5 Fe 22.5 Ni 4.0 Mn -- (Isothermal C-Curve)

### V-5.1 Kinetics

The FeNiMn alloy studied here is at an exciting composition. It will not detectably transform by isothermal holding at any temperature. However, by applying magnetic fields in the range of 60 to 140 kOe, we were able to transform this alloy to up to 50% martensite. This illustrates quite clearly that applying a field is very different from lowering the temperature. Fig. 24 demonstrates the effect of applying higher and higher fields at constant temperature. Once again, as in the binary FeNi alloys, the field accelerates the reaction; however, with the Mn alloy there is no final plateau stage. This is reminiscent of their differences in the magnetization curves of Fig. 4. It is obvious that there is an intrinsic difference in the growth or autocatalytic spreading of these two types of alloys.

Fig. 25 illustrates the effect of varying the temperature at constant field. The transformation is definitely isothermal over the whole temperature range and exhibits a C-curve behavior, which is typical of FeNiMn alloys. The higher Mn content of the present alloy shifts the C-curves out of the experimentally detectable range, until they are "pulled back" by high magnetic fields. The variation of the average time for 0.3% martensite as a function of temperature and field is shown in Fig. 26. The mean values plotted in this figure indicate that the reaction is definitely C-curve in nature with a nose temperature near  $-120^{\circ}\text{C}$ . Attempts to further pinpoint the nose temperature, using interrupted

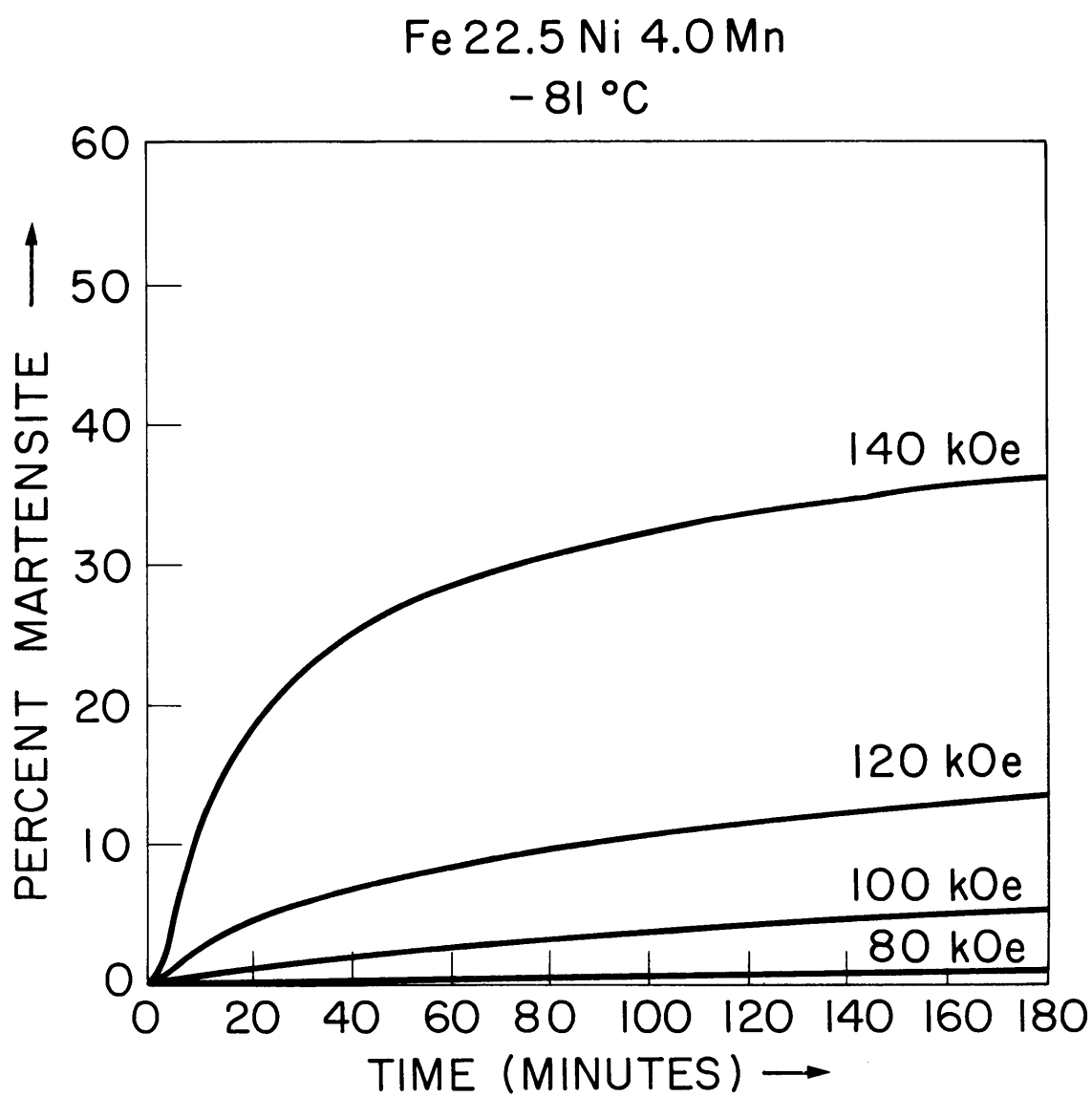


FIG. 24 FIELD-INDUCED TRANSFORMATION KINETICS OF Fe 22.5 Ni 4.0 Mn AT -81 °C.

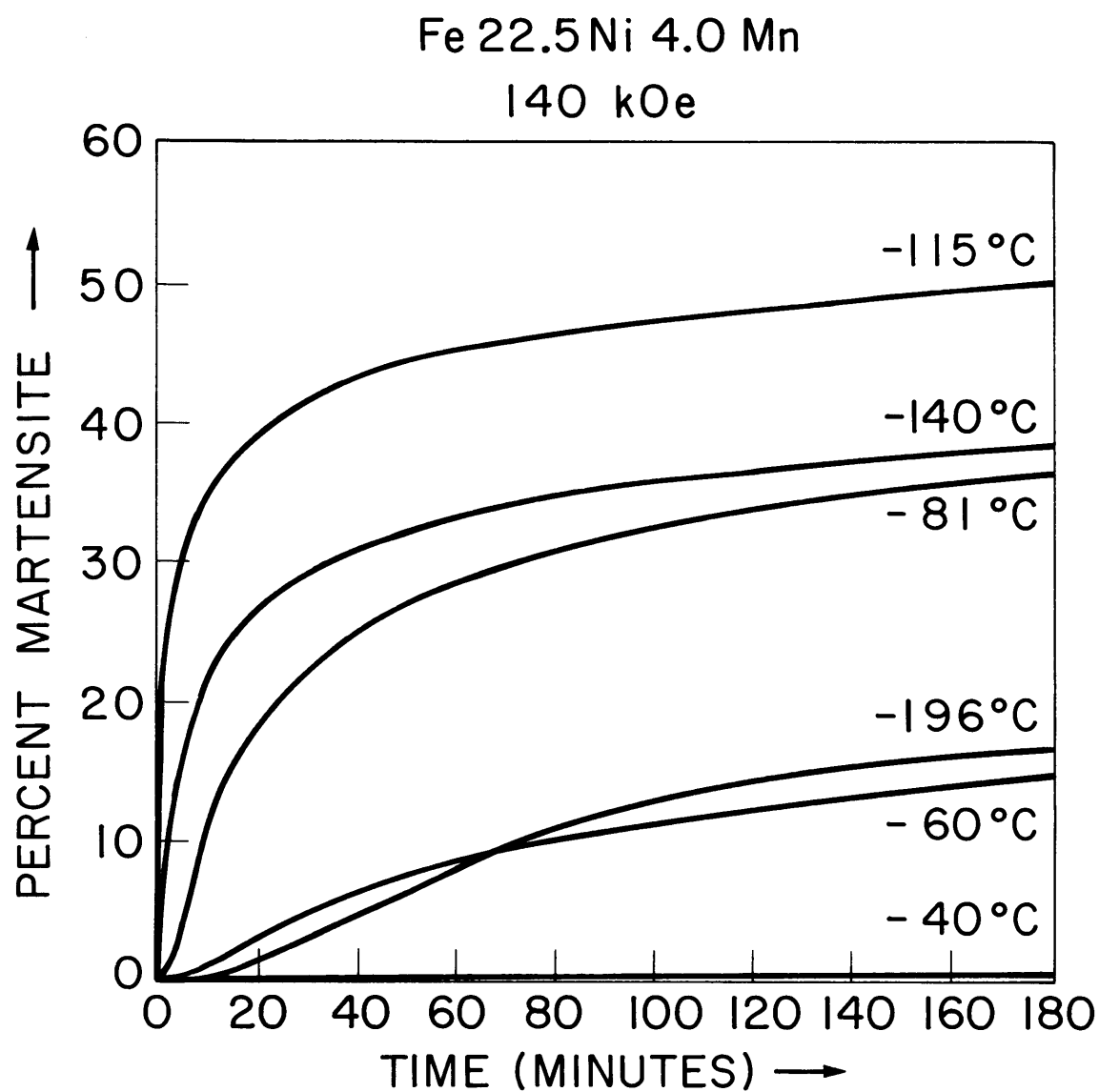


FIG.25 FIELD-INDUCED TRANSFORMATION KINETICS OF Fe<sub>22.5</sub>Ni<sub>4.0</sub>Mn AT 140 kOe AS FUNCTION OF VARIOUS TESTING TEMPERATURES.



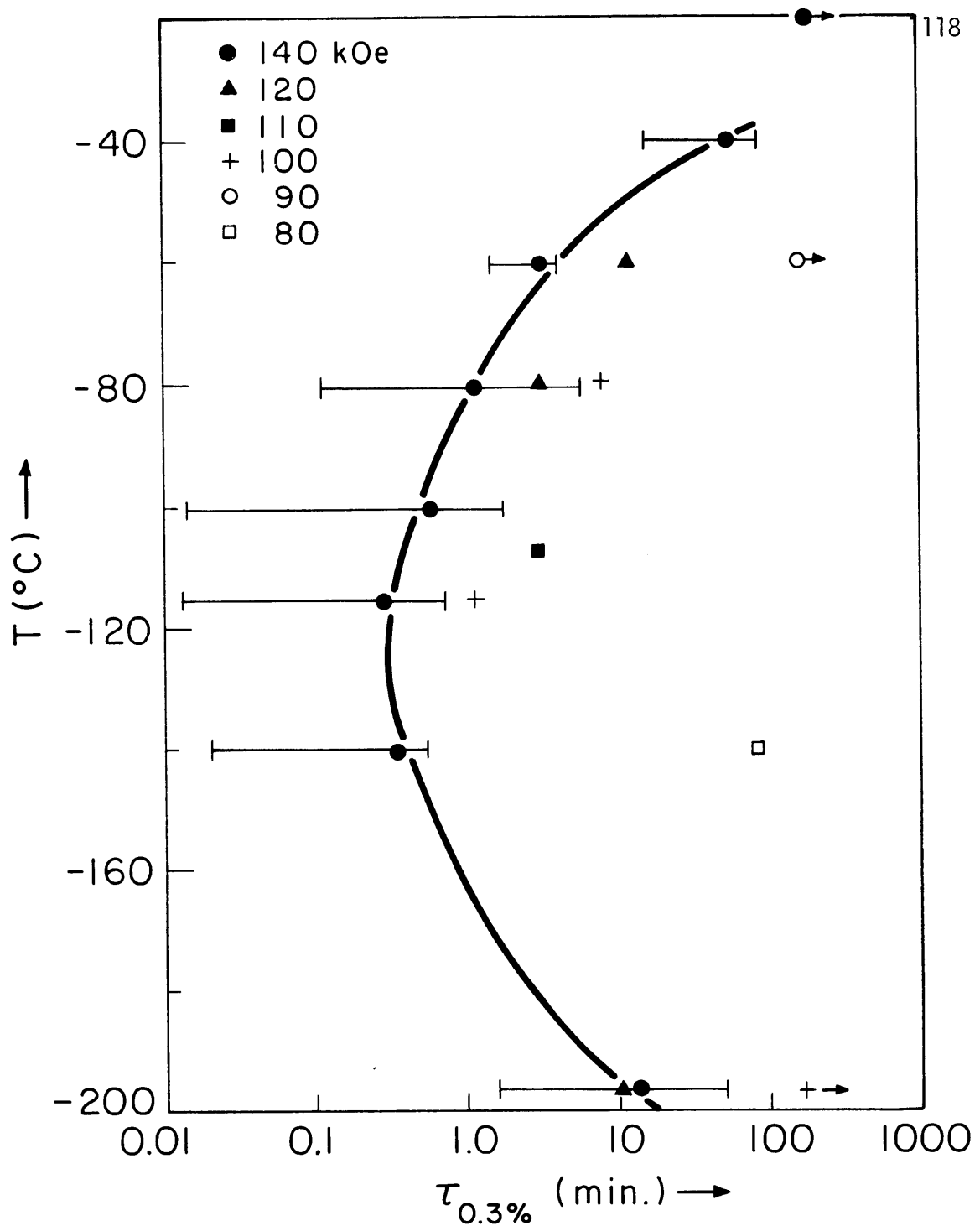


FIG.26 TIME TO TRANSFORM TO 0.3% MARTENSITE AS A FUNCTION OF MAGNETIC FIELD AND TEMPERATURE (THE SOLID LINE CONNECTS THE AVERAGE TIMES AT EACH TEMPERATURE AT 140 kOe)

upquenching and downquenching experiments, will be discussed in Section V-6.2.

The scatter involved in these experiments was met by repeating each condition as many as 15 times. Unfortunately, this used up so many specimens and so much magnet time that a complete C-curve at lower fields was not obtained. The question of whether the C-curve shifts to shorter times by moving horizontally along constant temperature lines or whether it also shifts up or down in temperature is one of fundamental significance. It is difficult to draw any conclusions from the sparse low-field data of Fig. 26. However, Shih, Averbach, and Cohen<sup>(109)</sup> empirically correlated the peak temperature versus % Mn. They normalized the available data to 23% Ni by assuming 1% Mn is twice as effective as 1% Ni. According to their correlation, the nose temperature of our composition should be less than -140°C, approximately 20°C lower than the 140 kOe field-induced peak temperature. Thus, apparently the magnetic field shifted the C-curve to shorter times and to higher temperatures. This behavior will be compared to that predicted by the KCR model in Section V-5.3.

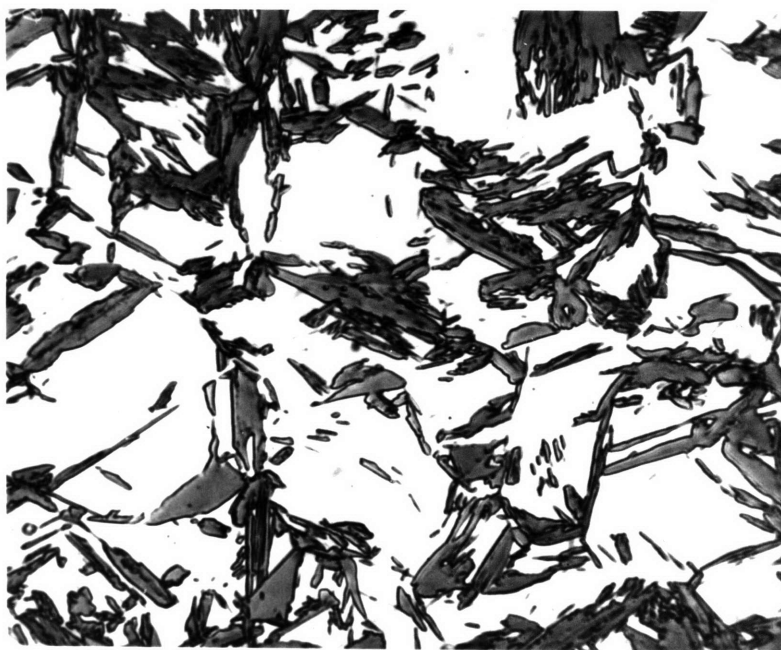
#### V-5.2 Morphology and Quantitative Metallography

The morphology of this alloy as a function of reaction temperature at constant field and approximately the same martensite content is shown in Figs. 27 a to d. This is similar to the structures observed by Pati<sup>(110)</sup> in his Fe 24.2 Ni 3.0 Mn alloy. The structure goes through a subtle transition as the temperature is decreased, i.e. the martensitic units become smoother and look more plate-like. The higher-temperature



(a) -60 °C

20  $\mu$



(b) -81 °C

FIG. 27 MORPHOLOGY OF THE Fe<sub>22.5</sub>Ni 4.0 Mn ALLOY TRANSFORMED WITH A 140 kOe FIELD AT VARIOUS TEMPERATURE

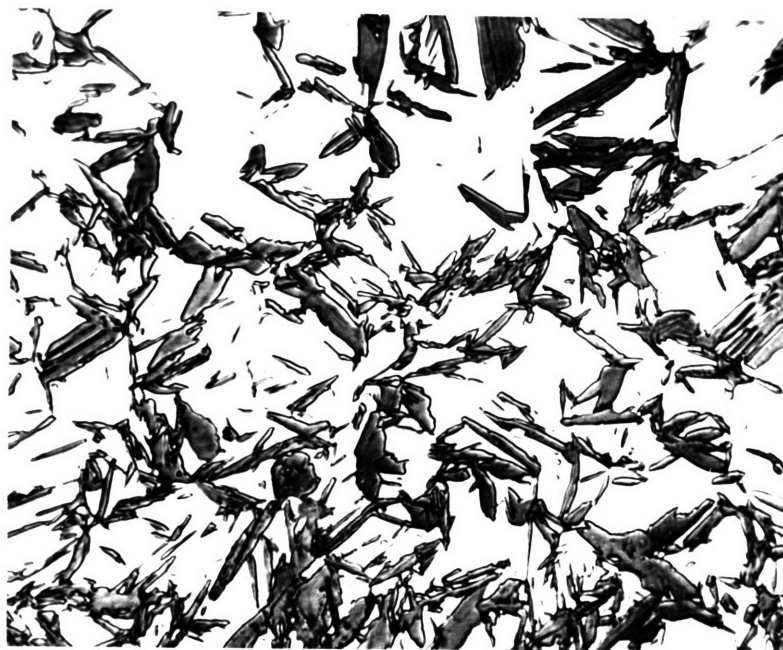
(c)  $-140^{\circ}\text{C}$  $20\mu$ (d)  $-196^{\circ}\text{C}$ 

FIG. 27 (CONTINUED)

structures look almost lath-like and are reminiscent of the Fe 28.7 Ni and Fe 29.6 Ni structures in Figs. 8 and 12. Pati<sup>(111)</sup> examined the electron microscopy of his alloy and found an internally twinned structure which is not characteristic of lath martensite. It appears therefore, that these are jagged plates. Comparisons of the structures obtained with various fields shows that the field has no noticeable effect on the morphology over the range of 100 to 140 kOe (other than the fact that there would not be any martensite at all without the field).

Pati<sup>(25)</sup> has investigated the effect of temperature and volume fraction martensite on  $\bar{V}$ , the average plate volume in his Fe 24 Ni 3 Mn alloy. He found that during the early stages of the transformation (i.e. < 1% martensite),  $\bar{V}$  was equal to  $4 \times 10^{-10} \text{ cm}^3$  near the nose of his C-curve and decreased to  $1 \times 10^{-10} \text{ cm}^3$  at 60°C above or below the nose temperature. At about 30% martensite,  $\bar{V}$  of specimens reacted at all temperatures was found to be equal to  $\sim 1 \times 10^{-10} \text{ cm}^3$ . Pati used linear extrapolations to connect his data because of the absence of the critical measurements between 2 and 33% martensite. Other workers<sup>(e.g. 27)</sup> have reported that  $\bar{V}$  remains constant over the range of 7 to 35% martensite. The latter results are consistent with our data, as illustrated in Fig. 28. We approximated the morphology as oblate spheroids and measured their volume using the procedures outlined in Section IV-6.3. We see at once that  $\bar{V}$  is initially a strong function of the martensite content, but after about 10% transformation it is approximately constant. (The least-square fit representing the initial behavior is  $\bar{V} = 1.150 \times 10^{-7} - 9.420 \times 10^{-9} \times \% \alpha'$ .)

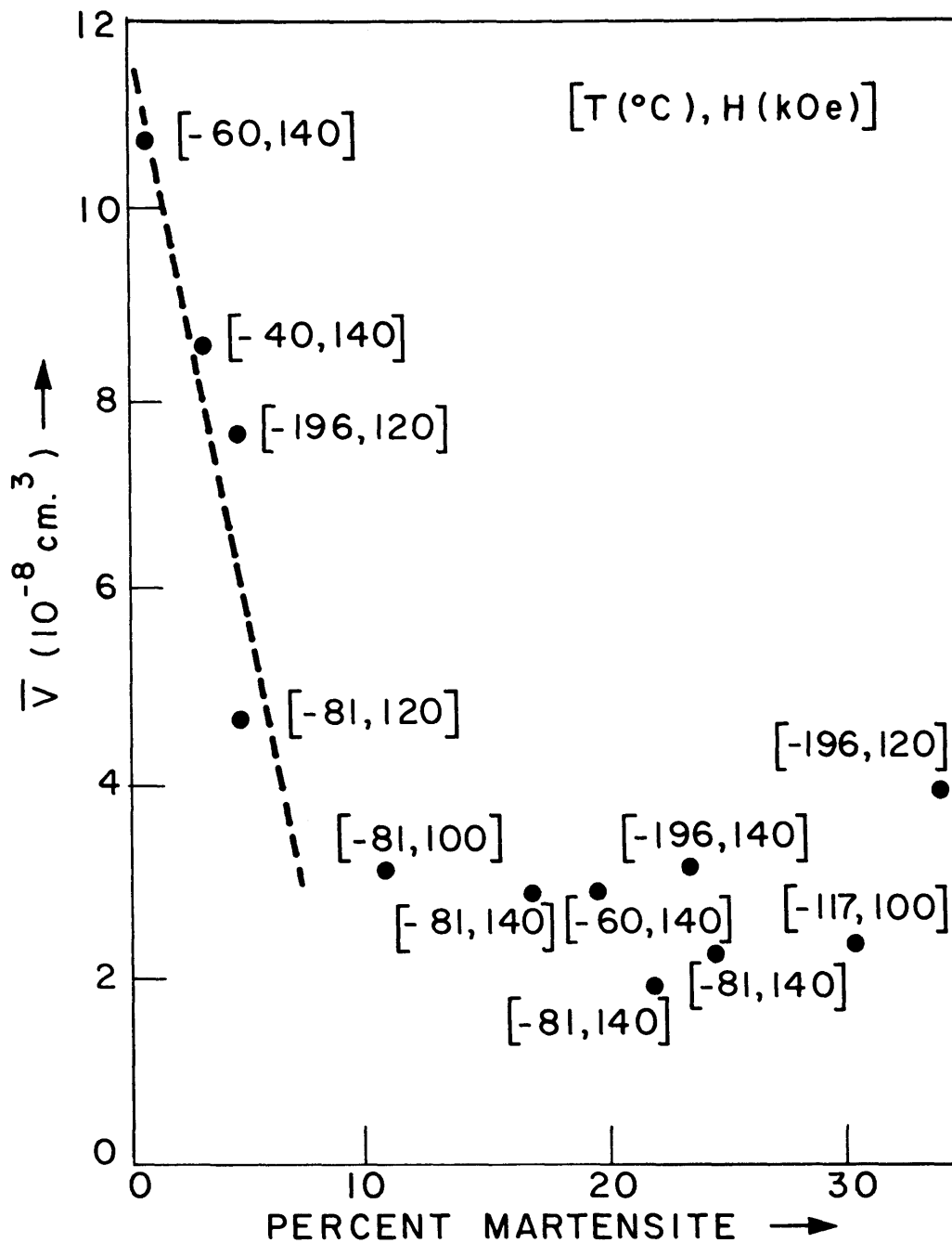


FIG. 28 AVERAGE PLATE VOLUME FOR Fe 22.5 Ni 4.0 Mn AS A FUNCTION OF PERCENT MARTENSITE, TEMPERATURE AND MAGNETIC-FIELD INTENSITY.

This behavior is consistent with the hypothesis that martensite can spread by autocatalysis from clusters of transformed plates. The initial plates of each cluster is the largest, thereby giving a large initial  $\bar{V}$ . The rapid initial drop-off of  $\bar{V}$  with percent martensite occurs as the smaller austenite pockets around the initial plates begin to transform. The relatively insensitive region after 10% martensite is apparently caused by the spreading of the cluster into untransformed austenite grains. It seems obvious that  $\bar{V}$  must eventually decrease after the clusters spread throughout the specimen, i.e. as the retained austenite pockets become smaller and smaller. If, however, the final transformation occurs by the thickening of existing plates rather than by the nucleation of new units,  $\bar{V}$  may even increase during the later stages of the reaction.

Except for the fact that the  $\bar{V}$  values at  $-196^{\circ}\text{C}$  are somewhat higher than the others, there does not appear to be any strong dependences on temperature or field. This disagrees with Pati's data which show a higher initial plate volume near the peak temperature. The reasons for this difference and for the large differences in the absolute value of our plate volumes compared to his are not known at this time.

The r/c ratios plotted in Fig. 29 are more scattered than the  $\bar{V}$  values; however, they do show a decreasing trend with increasing percent martensite. This could be due to plate thickening during the later stages of the transformation. In-situ transformation studies with the U. S. Steel Company high-voltage electron microscope of Pati's alloy did reveal evidence of plate thickening in discrete steps. These steps are on too fine a scale to be resolved with optical microscopy.

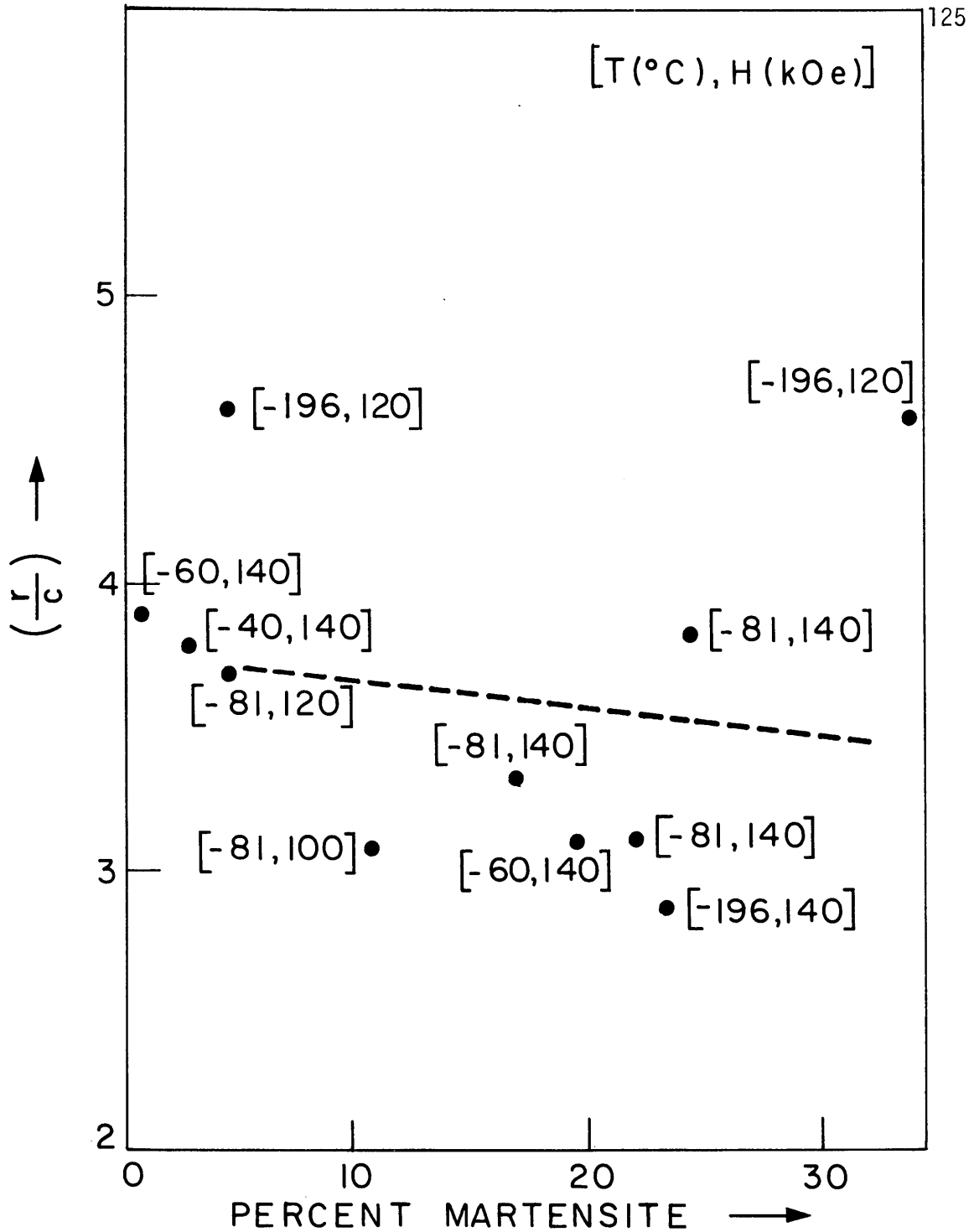


FIG. 29 RADIUS - TO - SEMITHICKNESS RATIO FOR Fe 22.5 Ni 4.0 Mn AS A FUNCTION OF PERCENT MARTENSITE, TEMPERATURE, AND MAGNETIC FIELD INTENSITY.



Finally, we decided to test the hypothesis discussed in Section I-2 that magnetostatic-energy effects might cause some morphological dependence on the field direction. In particular, the plates might tend to line up with the field and have a higher  $r/c$  ratio by being parallel to the field direction than by being normal to it. Two identical specimens were transformed simultaneously at  $-81^{\circ}\text{C}$  in a 140 kOe field to about 13% martensite. One was held parallel to the field direction and the other perpendicular to it. The transformation curves of these specimens were almost identical, indicating that polarization effects of the external field are negligible.

Visual examination of the structures of these two specimens (Fig. 30) does not reveal any tendency for the martensitic plates to align with the field. In order to test for subtle variations which might not be detectable by ordinary visual examination, a polar grid was superimposed on two 2000X blow-ups of each specimen. A line was drawn through each plate and its angle with the specimen axis was put into one of 18 difference angular sectors. In addition, the  $r/c$  ratios of these plates were measured as a function of this same angle. As Fig. 31 illustrates, there is no correlation with the field direction. Thus, kinetic autocatalytic effects seem to override any thermodynamically predicted orientation dependencies.

Fig. 31 does suggest a tendency for a greater number of plates (which have higher  $r/c$  ratios) to lie  $20$  to  $40^{\circ}$  from the specimen axis independent of the field direction. This behavior could be due to quenching stresses or it could be a consequence of the swaging operation used to produce the final specimen size. The specimens, however, were air cooled in a vycor encapsulating tube which is not a severe quench, and so if this effect

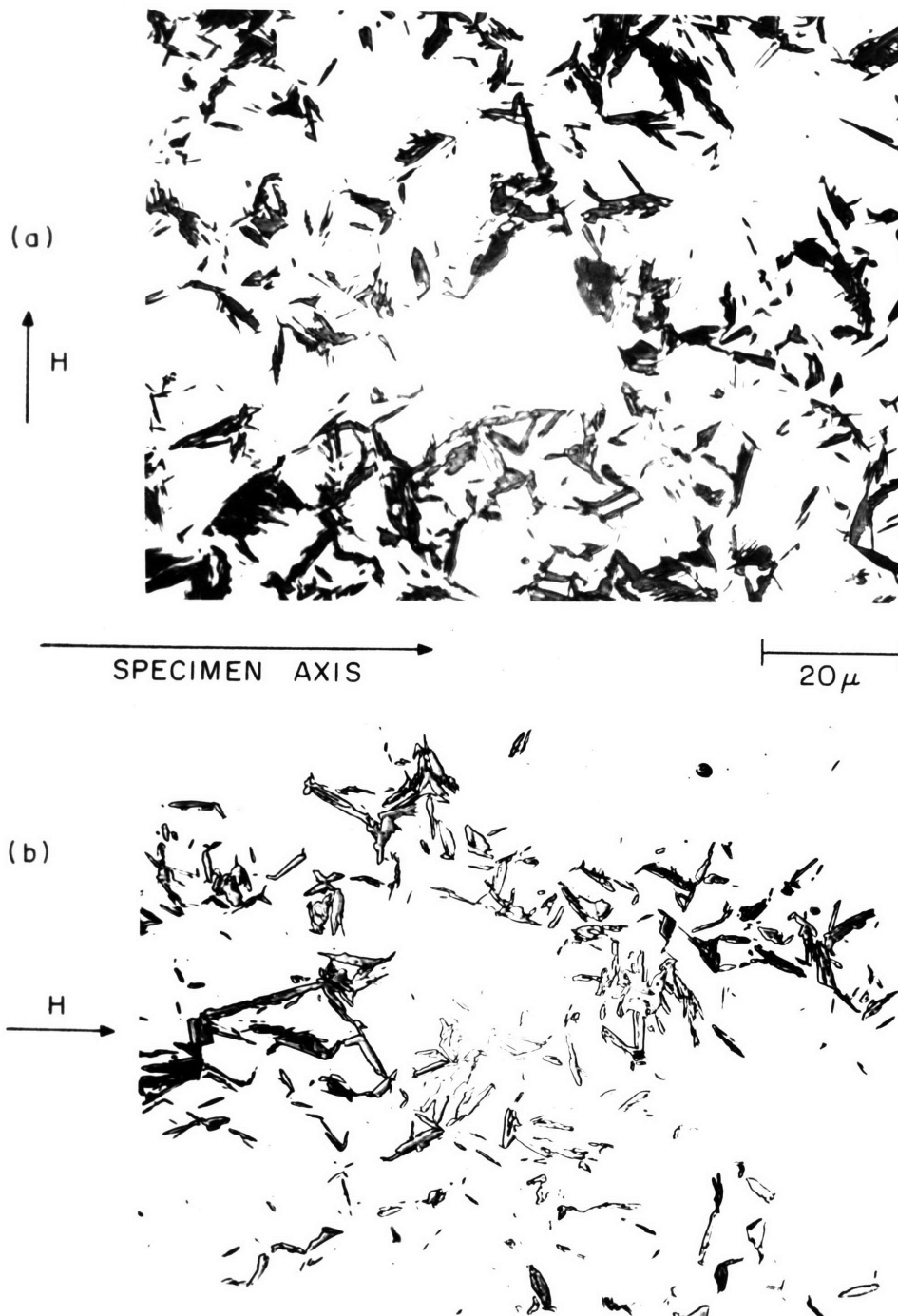


FIG. 30 ORIENTATION DEPENDENCE OF THE MORPHOLOGY OF Fe<sub>22.5</sub>Ni 4.0Mn AS A FUNCTION OF THE DIRECTION OF APPLIED FIELD (TESTED AT -81°C, 140 kOe).  
(a) FIELD PERPENDICULAR TO SPECIMEN AXIS.  
(b) FIELD PARALLEL TO SPECIMEN AXIS.

DIRECTION OF  
→  
SPECIMEN AXIS

—●— FIELD  $\parallel$  TO AXIS<sub>128</sub>  
- -▲- - FIELD  $\perp$  TO AXIS

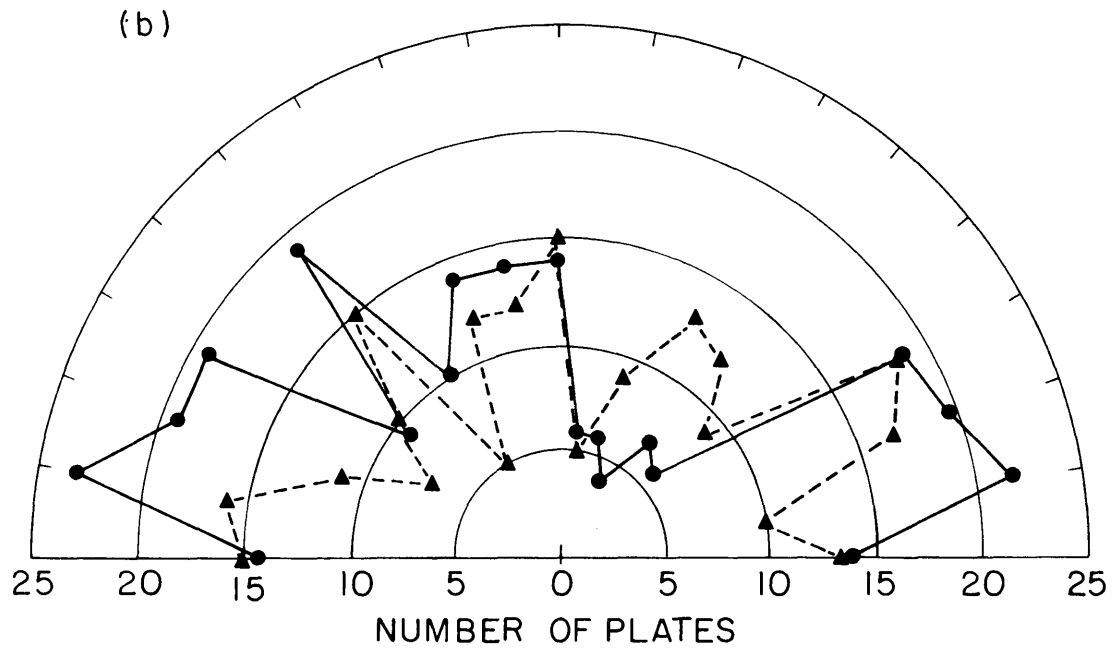
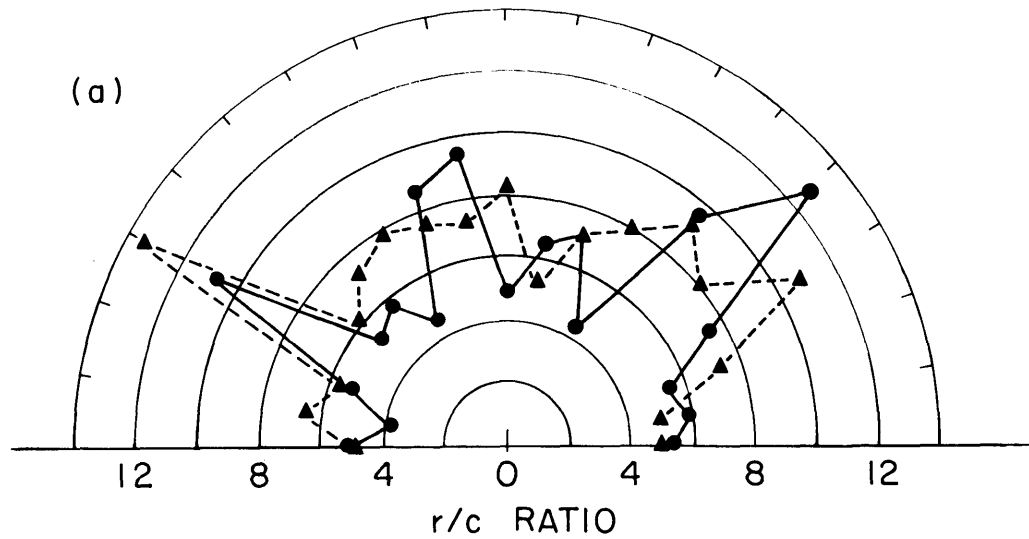


FIG. 31 DISTRIBUTION OF THE NUMBER OF PLATES ALIGNED IN A SPECIFIC DIRECTION AND THEIR RADIUS-TO-SEMI THICKNESS RATIOS AS A FUNCTION OF THE DIRECTION OF THE APPLIED MAGNETIC FIELD.

were due to some strain-induced artifact, it must have survived the recrystallization anneal. It is conceivable that the number and perfection of annealing twins (which have been suggested<sup>(28)</sup> as potent sites for martensite nucleation) could vary depending upon the local swaging conditions. Examination of our transformed specimens, however, did not reveal any pronounced tendency to nucleate at annealing twins. Still another possibility is that the swaging operation causes a fiber texture which could lead to some plate-orientation effects, since we have shown that autocatalytic spreading through grain boundaries is a function of the relative orientations of adjacent grains.

### V-5.3 Fit with the KCR Model

Eq. 26 was used to calculate the activation energy,  $\Delta W_a$ , from  $\tau_{0.3\%}$  assuming  $\bar{V}_i$  is constant and equal to  $9.3 \times 10^{-8} \text{ cm}^3$  i.e. as extrapolated from Fig. 28. The predictions of the KCR model were compared to these data using a procedure similar to that outlined in Section V-3.4. (The best fit was found for  $r_e = 534 \text{ \AA}$ .) The results of these calculations are presented in Table 5 and Fig. 32.

The  $\Delta W_a$  versus  $\Delta g_T$  plot of Fig. 32 is similar to that for Fe 29.6 Ni in Fig. 16, except that the slope of the curve is smaller for the FeNiMn alloy. The match with the KCR model appears fairly good over the whole range of driving forces; however, once again, the lower driving-force points do not fit too well.

Fig. 33, i.e.  $\Delta W_a/T$  versus  $\Delta g_T$ , is a more crucial test of the data. The KCR model does correctly predict a C-curve dependence, but the detailed fit with the data is not good. The predicted nose temperature is  $-138^\circ\text{C}$  while that observed is  $-120 \pm 5^\circ\text{C}$ . More seriously, the model predicts that as  $H$  increases from 0 to 140 kOe, the nose temperature should decrease from  $-127^\circ$  to  $-138^\circ\text{C}$ ; whereas as discussed in Section V-5.1, the empirical correlations of Shih et al.<sup>(109)</sup> indicate that it increases  $\sim 20^\circ\text{C}$ .

The KCR model is still our only prototype and it does afford some interesting predictions. At very high fields, in the range of 300 to 400 kOe, the predicted nose temperature drops rapidly with increasing field, as does  $\Delta U^*$ , the predicted activation energy for nucleation. At fields near 485 kOe, the nose of the C-curve becomes athermal as defined

TABLE 5  
Incubation Times, Activation Energies, and Driving Forces for Fe 22.5 Ni 4.0 Mn

<u>Temperature</u> (°C)	<u>Magnetic Field</u> (kOe)	<u>Chemical <math>\Delta g_0</math></u> (cal/mole)	<u>Magnetic <math>\Delta g_m</math></u> (cal/mole)	<u>Total <math>\Delta g_T</math></u> ( $10^9$ ergs/cm <sup>3</sup> )	<u>Median <math>\tau_{0.3\%}</math></u> (min)	<u><math>\frac{\Delta W_a}{a}</math></u> ( $10^{-12}$ ergs/event °K)
- 40	140	- 298	- 30.7	- 1.99	56.3	1.49
- 60	120	- 317	- 26.4	- 2.08	13.5	1.32
	140	- 317	- 30.8	- 2.10	2.6	0.76
- 81	100	- 334	- 22.1	- 2.16	5.0	1.15
	120	- 334	- 26.5	- 2.19	2.0	1.13
	140	- 334	- 30.9	- 2.21	0.7	0.76
- 100	140	- 349	- 31.1	- 2.30	0.3	0.96
- 110	110	- 355	- 24.5	- 2.30	1.9	0.83
- 115	100	- 358	- 22.3	- 2.30	0.9	0.92
	140	- 358	- 31.2	- 2.36	0.4	0.91
- 140	80	- 371	- 17.9	- 2.36	12.0	0.86
	140	- 371	- 31.3	- 2.44	0.4	0.76
- 196	120	- 385	- 26.2	- 2.50	3.7	0.40
	140	- 385	- 30.6	- 2.52	4.5	0.47

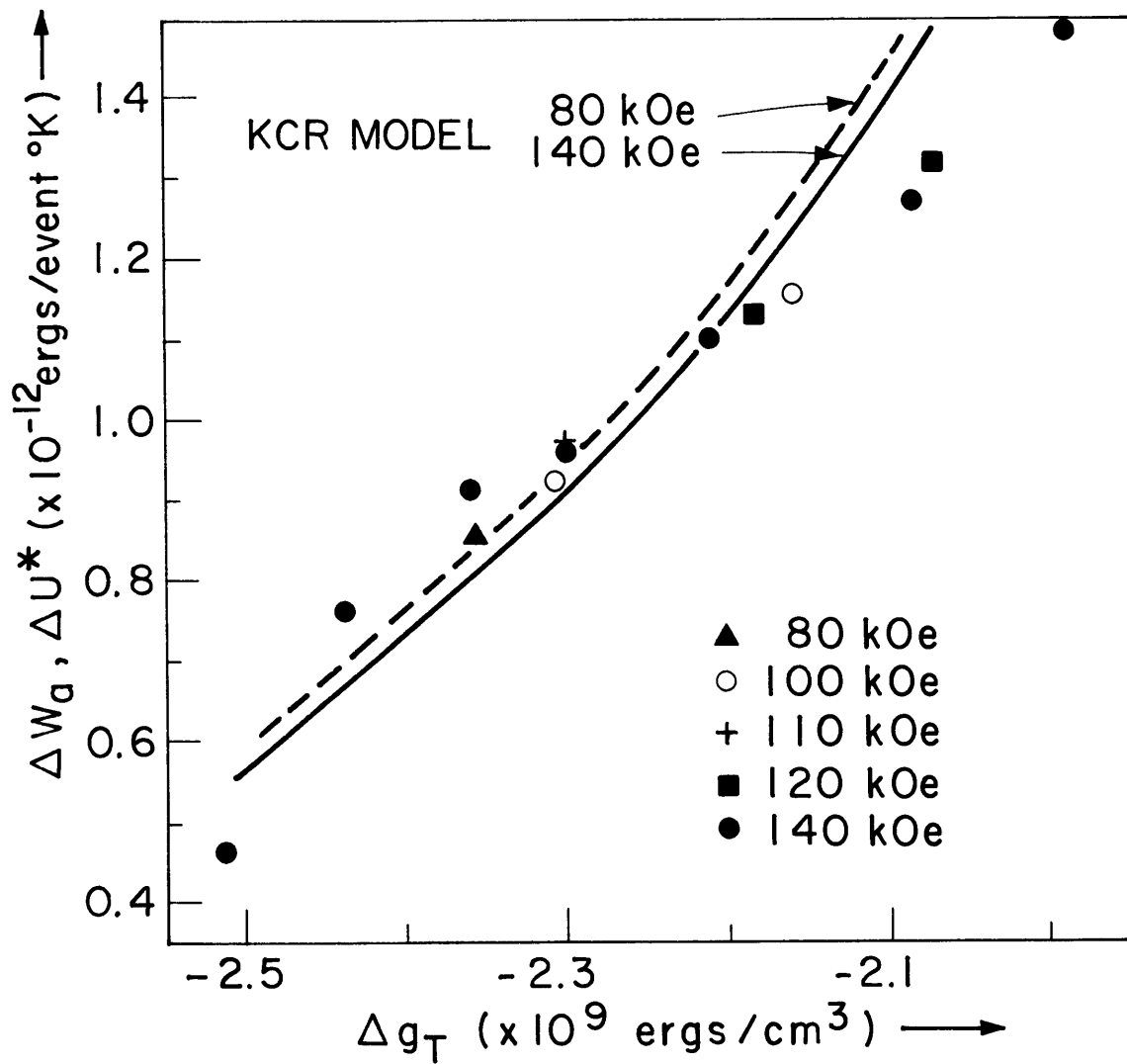


FIG. 32 COMPARISON OF THE RAGHAVAN-COHEN MODEL TO THE ACTIVATION ENERGY VERSUS DRIVING FORCE

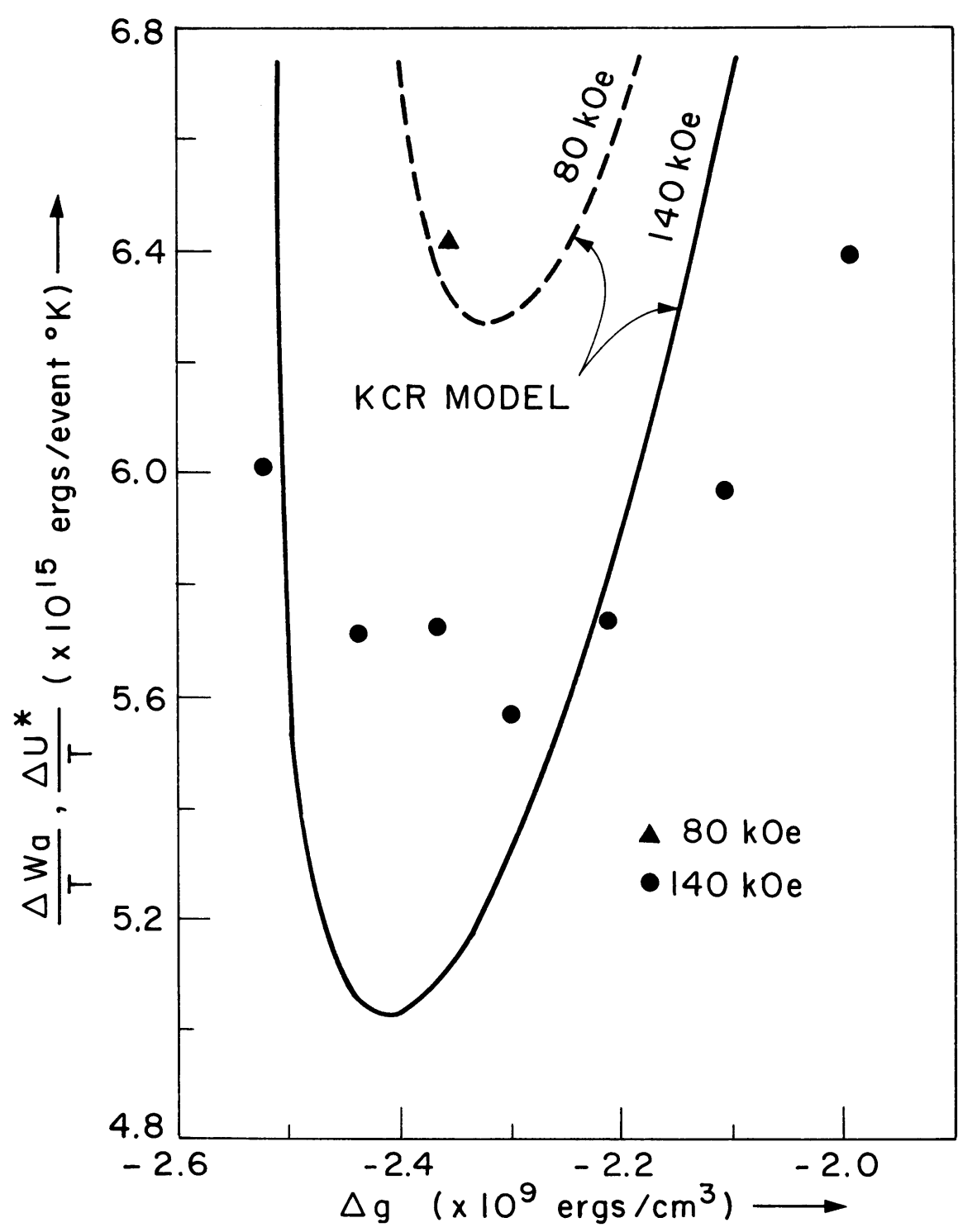


FIG. 33 COMPARISON OF THE KCR MODEL TO  $\Delta W_q/T$  VERSUS DRIVING FORCE



by  $\Delta U^* = 0$ . With fields as high as 595 kOe, there is a predicted isothermal mode below the athermal nose of the C-curve. At higher fields still, the reaction is athermal to 0.2°K. These predictions can explain the results of Malinen, et al.<sup>(86)</sup> who applied a pulsed field of 360 to 400 kOe to Fe 23.6 Ni (3.3 and 3.6) Mn alloys which had zero-field isothermal nose temperatures of - 100° and - 140°C respectively. They did not find a field-induced C-curve but rather an athermal-like behavior, i.e. the extent of transformation in both alloys rose monotonically with decreasing temperature (as depicted in Fig. 2d in Section II-2.1). Thus, although the detailed predictions of the model leave something to be desired, the overall predictions can explain many of the experimental observations.

## V-6 Embryo Experiments

### V-6.1 High-Temperature Magnetic Annealing

The classical high-pressure embryo experiments of Kaufman et al.<sup>(58)</sup> lend credibility to the K-C version of the martensite embryo, i.e. a mini-plate of martensite in the parent phase. Unfortunately, these experiments have never been repeated, while other high-pressure work<sup>(59)</sup>, not specifically designed to examine the embryo effects, have been able to explain the suppression of  $M_s$  while cooling under pressure by pure thermodynamic arguments without any recourse to second-order effects from changes in embryo potency.

A portion of our investigation involved experiments similar to those of Kaufman et al. using a magnetic field instead of pressure to vary the driving force during austenitizing. The simple reasoning behind these experiments was that, if the embryos exist at high temperatures and if they are mini-plates as envisioned by the KCR model, then they may be ferromagnetic, and a magnetic field could increase their size just as the high-pressure should decrease it.

The thermal-magnetic history of a typical experiment is illustrated in Fig. 34. The encapsulated specimens were heated in a magnetic field to temperatures ranging from 400 to 700°C, held for 15 minutes to 1 hour in a high magnetic field, and then air-blast cooled to 100 to 200°C. They were then removed from their encapsulating tubes and transformed under zero-field conditions at subzero temperatures. The results of these runs were compared with control runs made without any magnetic field during the

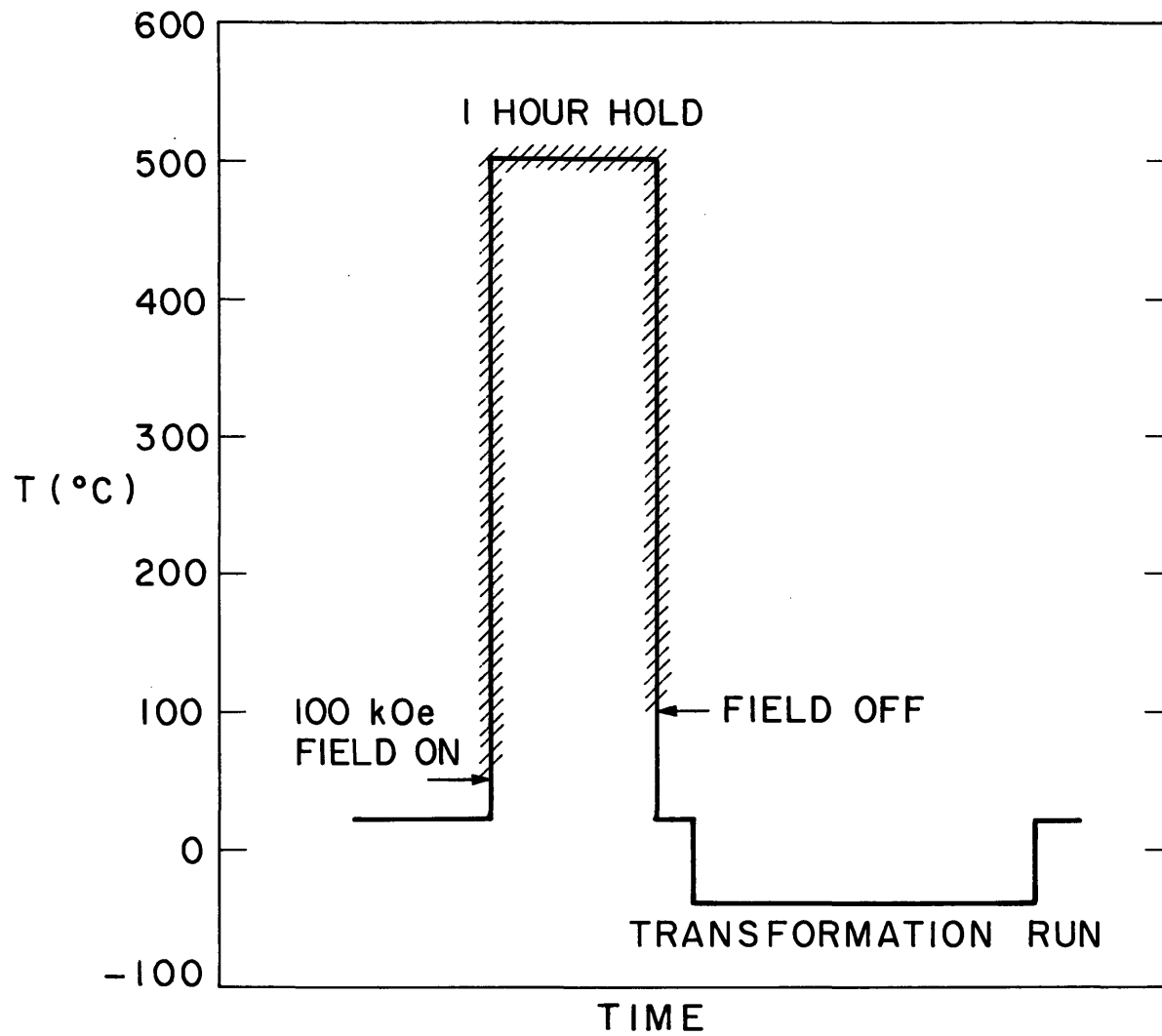


FIG. 34 THERMAL -MAGNETIC HISTORY OF A TYPICAL EMBRYO EXPERIMENT

high-temperature cycle.

The temperature of the thermal-magnetic hold is critical. (Refer to Fig. 35.) First of all, we would like to be above the equilibrium  $\alpha + \gamma \rightarrow \gamma$  solvus line in order to avoid any complication from equilibrium ferrite. (Magee<sup>(28)</sup> has shown that prior equilibrium ferrite suppresses the subsequent martensitic transformation.) In addition, we must be above the "freeze-in temperature" which Kaufman and Cohen<sup>(19)</sup> envisioned to be near 537°C. E. Owen and Y. Liu<sup>(111)</sup> while studying FeNi equilibrium diagrams showed that at temperatures below 500°C the bulk samples would not come to equilibrium within feasible annealing times (e.g. 1 day to 500°C, 1 year at 365°C); of course, for an embryo we would not require equilibrium of a bulk specimen, but rather of a very small volume aided by dislocation motion. Finally, other magnetic annealing experiments<sup>(e.g. 112)</sup> designed to induce short-range alignment of Ni atoms with the field have shown a freeze-in temperature of 400°C.

We must also be at least 50°C below the ferrite Curie temperature,  $\theta_{C\alpha}$ , of the alloy under study in order to have a significant degree of ferromagnetism in the embryo. Determination of the Curie temperature of a non-equilibrium phase is a tricky problem. Bozorth<sup>(1)</sup> published a plot of  $\theta_{C\alpha}$  versus nickel content, but the data were taken at a time when martensitic phase transformations were not well understood; therefore, the  $\alpha' \rightarrow \gamma$  reverse reaction casts a shadow of doubt on their results. Colling<sup>(113)</sup>, however, determined  $\theta_{C\alpha}$  for a series of FeNiCo alloys and a linear extrapolation of his data to 33% Ni falls right onto an extrapolation of Bozorth's data. The Weiss-Tauer<sup>(114)</sup>  $\theta_{C\alpha}$  values (also shown in Fig. 35),

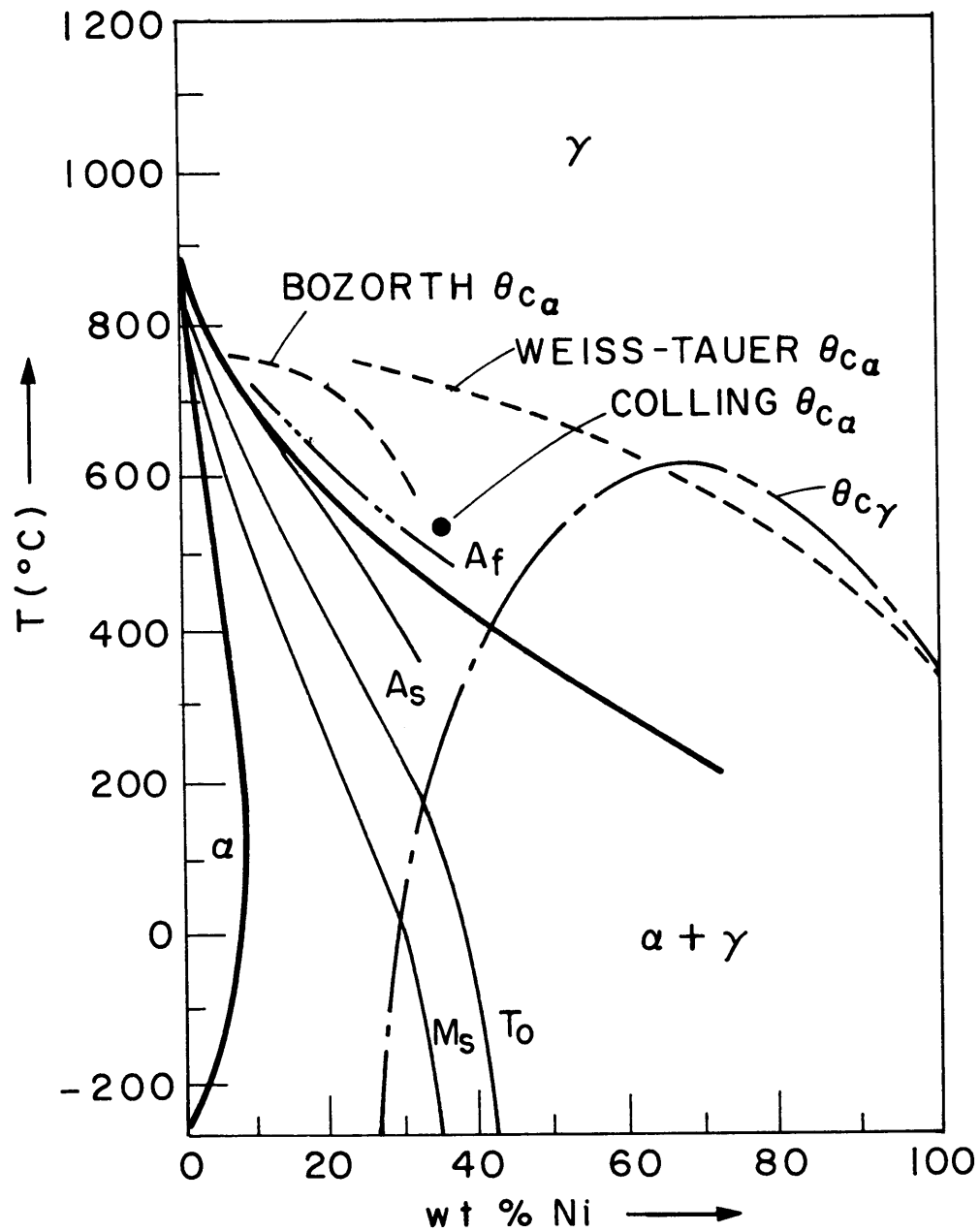


FIG. 35 EQUILIBRIUM DIAGRAM ILLUSTRATING THE CURIE TEMPERATURES AND MARTENSITIC-TRANSFORMATION RANGE OF Fe Ni ALLOYS (FROM REFERENCES 113-116)

calculated from the average Bohr magneton number of the alloy by averaging the nearest-neighbor interactions, are higher than the Bozorth data over the whole alloy range.

It is apparent that there is only a small "window" in which a magnetic anneal could affect a pre-existing embryo. The bulk of the magnetic annealing experiments were done with the Fe 28.7 Ni alloy which has the highest  $\theta_{C\alpha}$ . The annealing temperatures were varied from 400 to 700°C in order to be sure to hit the "window".

The results of these experiments can be summarized as negative. If anything, there was a 1 or 2°C depression of the reaction by the magnetic austenitizing. We also found that the subzero transformation rate was a weak function of the severity of the air-blast cooling quench, i.e. slower cooling in the range of  $\sim 1^\circ\text{C}/\text{sec}$  depressed the transformation by about 2°C. This effect will be discussed shortly.

To circumvent any complications of interstitial pinning of prior embryos (which did not seem to interfere with the Kaufman pressure experiments even though they used higher C contents), we decided to recrystallize the parent phase in a magnetic field to produce "virgin embryos". To accomplish this, the Fe 29.6 Ni specimens were first quenched into liquid nitrogen producing about 90% martensite. They were then heated to 700°C under a 100 kOe field, held for 15 minutes, and quenched to room temperature ( $\sim 1^\circ\text{C}/\text{sec}$ ). The subsequent transformation did not show any enhancement of the magnetically annealed specimens over those used for control purposes. Once again, however, the magnetically annealed specimens were somewhat (1 to 2°C) depressed. This could be due to small differences in

in quenching rates as will be discussed shortly.

These experiments are not watertight, but they do not offer any support for the hypothesis that the martensitic embryo is ferromagnetic in nature. Experiments are currently under way to test FeNiCo alloys which have higher  $\theta_{C\alpha}$  temperatures and to test bursting alloys and small particles; the latter should reflect the effects of initial embryos without undue autocatalytic complications.

One interesting result of the recrystallization study was that these specimens (with or without the magnetic field) were much more sensitive to cooling rate (particularly in the temperature range below 300°C) than the specimens which were not freshly recrystallized. This suggests that embryos are created during recrystallization or during the subsequent cooling and can be stabilized by slow cooling or by annealing at room temperature. We also found that only a factor of 2 decrease in cooling rate ( $\sim 1^\circ\text{C}/\text{sec}$ ) can depress the observable transformation from  $-7^\circ\text{C}$  to  $-35^\circ\text{C}$ ! This depression could be due to interstitial pinning of virgin embryos in the sensitive temperature range below 300°C, or it is also possible that embryos are actually created in the temperature range below  $T_0$  from existing heterogeneities or through quenching stresses. Additional experiments are needed to sort out these issues.

## V-6.2 Low-Temperature Magnetic Annealing and Cycling Experiments

Working on the presumption that the autocatalytic embryos exist as separate entities from the martensitic plates (which we have shown to be unlikely), we decided to apply the magnetic fields to influence these embryos in a series of upquenching experiments. Examination of Fig. 9 reveals that the zero-field transformation of Fe 29.6 Ni at  $-11^{\circ}\text{C}$  has a fairly linear region from 40 to 100 minutes. We up- and downquenched from this curve to various temperatures and fields and then returned to  $-11^{\circ}\text{C}$ , in order to study the effect on the subsequent transformation. The resistivity change during a typical run is shown in Fig. 36. In this experiment, the transformation was first interrupted by an upquench to  $20^{\circ}\text{C}$  and a magnetic field of 80 kOe, during which the transformation progressed isothermally by an additional 1% martensite. The transformation on the subsequent downquench to  $-11^{\circ}\text{C}$  exhibited a 15-minute incubation time.

In order to eliminate interstitial pinning or other stabilization effects as a viable explanation of this behavior, the specimen was upquenched once again for 15 minutes at  $+20^{\circ}\text{C}$ , but without an applied field. Upon returning to  $-11^{\circ}\text{C}$ , there was only a very small incubation time; later experiments showed that this was probably due to a small amount of transformation which occurs during the up- and downquenching operations. This effect is not intrinsically related to the application of the magnetic field\*, because we can also induce an incubation time by upquenching

---

\*The magnetic field simply provides a greater driving force for the transformation.



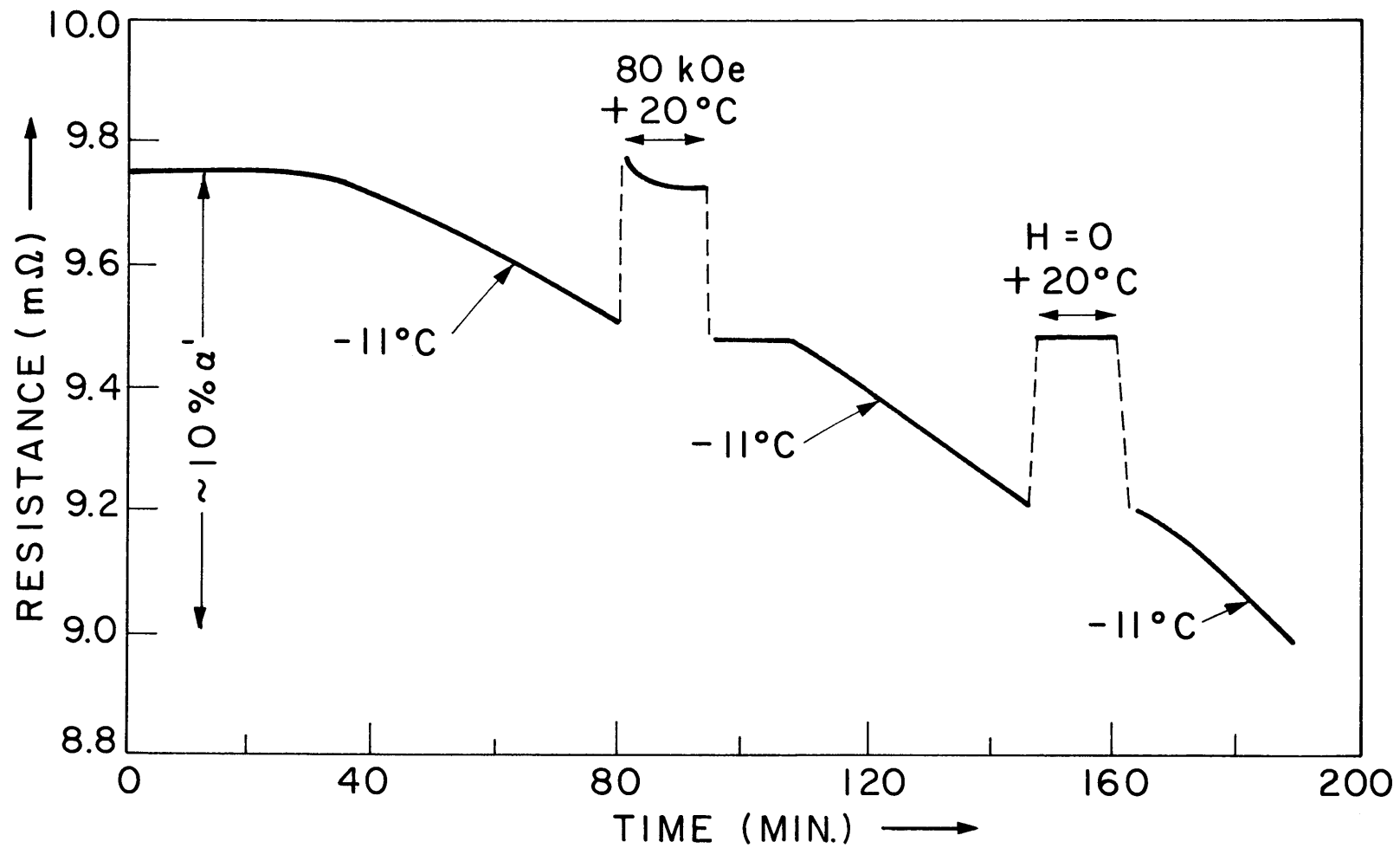


FIG. 36 LOW TEMPERATURE TRANSFORMATION IN Fe<sub>29.6</sub>Ni INTERRUPTED BY UPQUENCHING, WITH AND WITHOUT A MAGNETIC FIELD

from  $-11^{\circ}\text{C}$  to temperatures as low as  $+2^{\circ}\text{C}$  without a magnetic field. The subsequent  $-11^{\circ}\text{C}$  transformation is also delayed by the small amount of additional transformation at the higher temperatures.

We have shown that this behavior is not due to any stabilization effect; however, it is consistent with our interpretation presented earlier in Section V-4.2 that autocatalytic nucleation occurs directly from a moving interface. The small amount of martensite that is produced at the upquenching temperature appears to be due to the thickening of existing martensitic units. Since it is growing under conditions of higher  $\Delta W_a/T$ , this could inhibit the degree of autocatalytic nucleation. If we had taken the more classical approach and hypothesized that the small transformation during the upquenching hold was due to the triggering off of the most potent existing embryos, we would have to further hypothesize that the new martensite did not produce any equally potent new embryos. This alternative does not seem to be in accord with the optical metallography described in Sections V-3.2 and V-4.2.

Attempts were also made to pinpoint the nose of the C-curve in the Fe 22.5 Ni 4.0 Mn alloy by altering the temperature of the transformation during the course of the reaction. These runs were not successful because small amounts of martensite formed during the up- and downquenching and inhibited the subsequent transformation, as in the Fe 29.6 Ni case. The correlations that could be made, however, indicated that the nose of the C-curve determined in this manner ( $> -110^{\circ}\text{C}$ ) was higher than that indicated from the incubation times ( $-120 \pm 5^{\circ}\text{C}$ ). This illustrates that the partitioned and stressed austenite behaves differently from virgin

austenite.

Finally, we attempted to discover if the nose temperature of the FeNiMn alloy changed with the field by increasing the field during the course of the reaction from 110 to 140 kOe. By repeating this type of experiment at a series of temperatures, the ratios of the relative transformation rates before and after the field-increase should indicate whether the C-curve is shifting with field. These experiments were abandoned when it was noticed that the effect is not reversible, i.e. the ratio of rates on decreasing the field is much greater than the inverse of this ratio on increasing the field. This irreversibility casts some uncertainty on the Peters, Bolton, and Miodownik<sup>(96)</sup> experiments which were based on the interpretation of the increase of the transformation rate on the application of a magnetic field.

## VI. CONCLUSIONS

1. Magnetic fields accelerate the martensitic transformation in FeNi alloys both by increasing the Gibbs free-energy difference between the product and parent phases and by allowing the reaction to occur at higher temperatures.
2. The orientation of martensite plates and their radius-to-semithickness ratios are not metallographically correlative with the direction of the applied field.
3. Plate and lath martensites in FeNi alloys are two extremes of a continuous spectrum of morphologies. The transition structures contain a mixture of lath-like and plate-like martensite, each of which, in themselves, are intermediate transition morphologies. The jagged, lath-like interface of the transition plates is relatively slow-growing slipped martensite which propagates in antiparallel directions 25 to 30° on either side of the midrib.
4. The initial nucleation of bursting alloys near their  $M_s$  temperatures is thermally activated as evidenced by an observable nucleation time which is increased by carbon additions.
5. The lath-to-plate morphological transition in FeNi alloys is not a simple function of the temperature, Gibbs free-energy change, nickel content,  $\theta_{c\gamma} - M_s$ , or the activation energy,  $\Delta W_a$ . The best correlation parameter is the rate of transformation which can be approximated by the incubation time; the latter correlates with  $\Delta W_a/T$ . As  $\Delta W_a/T$

decreases, the morphology changes from lath to a lath-plate transition and then to plate. Lower temperature favors lath martensite which, before the use of magnetic fields, has always been overshadowed by the large increases in the chemical driving force with decreasing temperature. An increase in driving force favors the plate morphology.

6. Autocatalytic nucleation sites in Fe-Ni alloys appear to be an integral part of the moving austenite-martensite interface. Three important sites are pointed out and discussed: midrib impingement on a growing martensitic plate, the transition region in which the lattice-invariant mode changes from twinning to slip, and grain-boundary impingement.
7. The Fe 22.5 Ni 4.0 Mn alloy does not transform detectably at any temperature until fields in the range of 60 to 140 kOe are applied. The transformation is then characterized by isothermal C-curve kinetics which shifts to shorter times as the field is increased.
8. The effects of magnetic fields on the martensitic kinetic behavior imposes a severe test on the current nucleation theories. The Cohen-Raghavan model can be fitted to much of the data; however, it does not adequately explain the detailed kinetic behavior under high fields.
9. The average plate volume of the Fe 22.5 Ni 4.0 Mn alloy is insensitive to temperature and magnetic field; however, it decreases rapidly with the extent of transformation to 7% martensite and, thereafter, becomes

insensitive to the amount of martensite. This behavior is correlated with the autocatalytic spreading of clusters of martensitic plates.

10. High-temperature magnetic-annealing experiments do not support the hypothesis that the pre-existing martensitic embryos are ferromagnetic in nature.
11. The Fullman quantitative metallography equations are extended to the case of oblate spheroids.

VII SUGGESTIONS FOR FUTURE WORK

1. Use electron microscopy to study the lath-to-plate transition on a finer scale and to examine the details of the proposed autocatalytic mechanisms.
2. Use FeNiCo alloys, bursting alloys, and small particles to extend the magnetic annealing experiments.
3. Produce embryos by prior plastic deformation and use the magnetic field to effect their potency.
4. Devise magnetic mechanical-deformation experiments to show whether this can be a viable commercial process for the fabrication of sheet metal auto-body parts.
5. Measure the incubation times of the Fe 30.8 Ni bursting alloy as a function of temperature, magnetic field, and carbon content.
6. Use magnetic fields to induce martensite in Fe > 34 wt% Ni to test the hypothesis that the transformation should be C-curve in nature.
7. Use single crystals for precision orientation effects of the magnetic field.
8. Extend the quantitative metallography to determine the nucleation rate versus percent martensite in magnetic fields.
9. Develop kinetic equations to fit the full transformation curves, thereby determining  $\Delta W_a$  and the effect of the magnetic field on the autocatalytic factor.

## APPENDIX I

MAGNETIC CLAUSIUS--CLAPEYRON EQUATION

$T_0$  is the temperature at which the free energies of the austenite and martensite are equal as expressed by

$$g_{\alpha'} = g_{\gamma}$$

In order to maintain this equality for incremental temperature and magnetic-field changes (at constant pressure and composition), the following relations must hold:

$$dg_{\alpha'} = dg_{\gamma}$$

$$\left(\frac{\partial g_{\alpha'}}{\partial T}\right)_{x,p} dT + \left(\frac{\partial g_{\alpha'}}{\partial H}\right)_{x,p} dH = \left(\frac{\partial g_{\gamma}}{\partial T}\right)_{x,p} dT + \left(\frac{\partial g_{\gamma}}{\partial H}\right)_{x,p} dH$$

$$- S_{\alpha'} dT + I_{\alpha'} dH = - S_{\gamma} dT + I_{\gamma} dH$$

$$\frac{dT}{dH} = \frac{I_{\gamma} - I_{\alpha'}}{S_{\gamma} - S_{\alpha'}} \quad (A-1)$$

$$\int \Delta S dT = \int \Delta I dH \quad (A-2)$$

If we assume that the heat-capacity difference at constant pressure is not a function of temperature, (i.e. the slope of the free-energy curve versus temperature is constant) and that the difference in magnetization of the phases is not a function of the field, then Eq. A-2 can be



integrated:

$$\Delta S = \int_{T_0}^T dT = \Delta I \int_0^H dH$$

$$(T_0 - T) = \Delta T = \frac{H\Delta I}{\Delta S} \quad (\text{A-3})$$

in which  $T_0$  is the equilibrium temperature corresponding to zero applied field. (This is the equation first derived by Meyer and Taglang<sup>(71)</sup> by assuming that one can just equate the expressions for  $g_\alpha$ , and  $g_\gamma$  and later by Satyanarayan, Elias, and Miodownik<sup>(92)</sup> using similar triangles on a linear  $\Delta g$  versus  $T$  curve.) For reversible equilibrium:

$$\Delta S = \frac{L}{T_0}$$

where  $L$  is the latent heat of the reaction or the enthalpy difference between the two phases. Eq. A-3 can now be written as:

$$\Delta T = \frac{T_0 H \Delta I}{L} \quad (\text{A-4})$$

When applying this equation to the "athermal" martensitic transformation, it is a useful approximation to set  $T_0 = M_S$  (rather than the true  $T_0$  in which  $g_\alpha = g_\gamma$ ) and to assume that surface and strain energies are integral parts of the  $\alpha'$  phase.

APPENDIX 2

QUANTITATIVE METALLOGRAPHY OF THIN OBLATE SPHEROIDS

Fullman<sup>(117)</sup> has developed appropriate equations for the quantitative metallography of multi-sized thin disks in a matrix. In this appendix, the analysis is extended to include thin oblate spheroids as a closer approximation to the martensite morphology than the previously-assumed thin disks. Most of Fullman's thin-disk equations are actually better approximations for thin oblate spheroids because of the rounded nature of the spheroidal rim.

Rather than duplicate the Fullman treatment, the reader is referred to that paper<sup>(117)</sup> for all definitions and for the details of much of the following development. The equations for the thin oblate spheroid will simply be listed unless they are significantly different from the Fullman thin-disk analysis.

A.1 Particles of Uniform Size

Consider a sample containing particles of a phase  $\alpha$  in the form of thin oblate spheroids of radius  $r$  and semithickness  $c$ , where  $r \gg c$ . ( $c = t/2$  in the Fullman notation.)

$$f = N_V V = N_V \left( \frac{4}{3} \pi r^2 c \right) = N_S \bar{s} = \frac{\pi}{2} r N_V \bar{s}$$

$$\bar{s} = \frac{8}{3} rc$$

where  $\bar{s}$  = average area of particles intersected by a random cross-section

$$f = N_V V = N_V \left( \frac{4}{3} \pi r^2 c \right) = N_L \bar{\ell} = N_V \frac{\pi}{2} r^2 \bar{\ell}$$

$$\bar{\ell} = \frac{8}{3} c$$

where  $\bar{\ell}$  = mean traverse length for plates of uniform size.

## A.2 Particles of Nonuniform Size

When the particles under consideration are in the form of thin oblate spheroids with a distribution of radius  $r$  and semithickness  $c$ , the distribution may be divided into a number of arbitrarily small ranges of particles of radius  $r_i$ , and within each such range the plates may be further subdivided into arbitrarily small ranges of semithickness  $c_j$ .

$$N_{sij} = \frac{\pi}{2} r_i N_{vij}$$

$$s_{ij} = \frac{8}{3} r_i c_j$$

$$N_{Lij} = \frac{\pi}{2} r_i^2 N_{vij}$$

$$\ell_{ij} = \frac{8}{3} c_j$$

$$\bar{s} = \frac{2\bar{V}}{\pi \bar{r}}$$

$$\bar{\ell} = \frac{4V}{\bar{A}}$$

The expression for  $\bar{E}$  (average of the reciprocal lengths of particle intersections with a random sectioning plane) is identical to the thin-disk case:

$$\bar{E} = \frac{\pi}{4\bar{r}}$$

However,  $\bar{F}$  for the oblate spheroids (average of the reciprocal thickness of particle intersections with a random sectioning plane) is now a function of both  $\phi$  and  $X$ , as shown below:

$$\begin{aligned} F_{ij} &= \frac{\sin \phi}{2c_j \sqrt{1 - X^2/r_i^2}} \\ \bar{F}_{ij} &= \int_0^{\pi/2} \int_0^{r_i} F_{ij} P_\phi P_X dX d\phi \\ &= \int_0^{\pi/2} \int_0^{r_i} \frac{\sin \phi}{2c_j \sqrt{1 - X^2/r_i^2}} \frac{4}{\pi} \sin^2 \phi d\phi dX \\ &= \frac{2}{3c_j} \\ \bar{F} &= \frac{\sum_i \sum_j N_{sij} \bar{F}_{ij}}{\sum_i \sum_j N_{sij}} \\ &= \frac{\sum_i \sum_j \frac{\pi}{2} N_{vij} r_i \frac{2}{3c_j}}{\sum_i \sum_j \frac{\pi}{2} N_{vij} r_i} \\ &= \frac{2(\bar{r}/c)}{3\bar{r}} \end{aligned}$$

$\bar{G}$  (average thickness-to-length ratios of the particle intersections with a random sectioning plane) is derived as follows:

$$G_{ij} = \frac{c_j}{r_i \sin \phi}$$

$$\begin{aligned} \bar{G}_{ij} &= \int_0^{\pi/2} \frac{c_j}{r_i \sin \phi} p_\phi d\phi \\ &= \int_0^{\pi/2} \frac{c_j}{r_i \sin \phi} \frac{4}{\pi} \sin^2 \phi d\phi \\ &= \frac{4c_j}{\pi r_i} \end{aligned}$$

$$\begin{aligned} \bar{G} &= \frac{\sum_i \sum_j N_{sij} \bar{G}_{ij}}{\sum_i \sum_j N_{sij}} \\ &= \frac{\sum_i \sum_j \frac{\pi}{2} N_{vij} r_i \frac{4}{\pi} \frac{c_j}{r_i}}{\sum_i \sum_j \frac{\pi}{2} N_{vij} r_i} \\ &= \frac{4}{\pi} \frac{\bar{c}}{\bar{r}} \end{aligned}$$

These equations may be combined to yield the following useful relations:

$$\bar{r} = \frac{\pi}{4\bar{E}}$$

$$\bar{c} = \frac{\pi^2}{16} \frac{\bar{G}}{\bar{E}}$$

$$\bar{V} = \frac{\pi}{2} \bar{s} \bar{r} = \frac{\pi}{8} \frac{\bar{s}^2}{\bar{E}} = \frac{\pi f^2}{8 \bar{E} N_s}$$

$$\bar{A} = \frac{\pi N_L^2}{2 \bar{E} N_s}$$

$$N_V = \frac{f}{\bar{V}} = \frac{8 f \bar{E}}{\pi \bar{s}^2} = \frac{8 \bar{E} N_s}{\pi \bar{c}^2}$$

$$\overline{\left(\frac{r}{c}\right)} = \frac{3\pi}{8} \frac{\bar{F}}{\bar{E}}$$

BIBLIOGRAPHY

1. Richard M. Bozorth, Ferromagnetism. New York: Van Nostrand 1951.
2. Herbert B. Callen, Thermodynamics. New York: John Wiley and Sons, Inc., 1960.
3. E. A. Guggenheim, Thermodynamics. New York: John Wiley and Sons, Inc., 1967.
4. E. A. Guggenheim, "On Magnetic and Electrostatic Energy", Proc. Royal Soc. Series A 155 49(1936); "The Thermodynamics of Magnetization." 70.
5. S. Chikazumi, Physics of Magnetism. N.Y.: John Wiley and Sons, Inc., 1964.
6. D. J. Craik, Structure and Properties of Magnetic Materials. London: J. W. Arrowsmith Limited, 1971.
7. B. D. Cullity, Introduction to Magnetic Materials. Reading, Mass.: Addison-Wesley, 1972.
8. C. Killel and J. K. Galt, "Ferromagnetic Domain Theory", Solid State Physics 3 437 (1956).
9. J. Goddard and J. G. Wright, "The Effect of Solution pH and Applied Magnetic Field on the Electrodeposition of Thin Single-Crystal Films of Cobalt", Brit. J. Appl. Phys. 15 807(1964).
10. M. L. Bernshteyn, G. I. Gronik, and P. R. Dolzhanskiy, "Effect of a Magnetic Field on the Phase Transformations in Nickel Steels", Physics Metals Metallogr. 19 (6) 77(1965).
11. A. S. Yermolayev, A. Z. Men'shikov, and P. A. Malinen, "Development of Uniaxial Magnetic Anisotropy on the Martensitic Transformation in a Magnetic Field", Physics Metals Metallogr. 26 (1) 73(1968).
12. E. C. Stoner, "The Demagnetizing Factors for Ellipsoids", Phil. Mag. 36 (7) 803(1945).
13. "Symposium on the Formation of Martensite in Iron Alloys", Met. Trans. 2 2327-2462 (1971).
14. Phase Transformations. Metals Park, Ohio: American Society for Metals, pp. 1-180 (1970).

15. V. Raghavan and A. R. Entwisle, "Isothermal Martensite Kinetics in Iron Alloys", Iron and Steel Institute Special Report No. 93, p. 30 (1965)
16. C. L. Magee, Transformation Kinetics, Microplasticity, and Aging of Martensite, Ph.D. Thesis, Carnegie Institute of Technology, (1966).
17. V. Raghavan and M. Cohen, "Measurement and Interpretation of Isothermal-Martensitic Kinetics", Met. Trans. 2 2409 (1971).
18. J. Philibert and C. Cussard, "Kinetics of the Martensite Transformation in a Hyper-Eutectoid Steel", J. Iron and Steel Inst. 180 34 (1955).
19. M. Cohen, "Nucleation of Solid-State Transformations", Trans. AIME 212 171 (1958).
20. V. Raghavan and M. Cohen, "A Nucleation Model for Martensitic Transformations in Iron-Base Alloys", Acta Met. 20 333 (1972).
21. E. S. Machlin and M. Cohen, "Isothermal Mode of the Martensitic Transformation", Trans. TMS-AIME 194 489 (1952).
22. C. Magee, "The Kinetics of Martensite Formation in Small Particles", Met. Trans. 2 2419 (1971).
23. S. R. Pati and M. Cohen, "Nucleation of the Isothermal Martensitic Transformation", Acta Met. 17 189 (1969).
24. J. C. Fisher, J. H. Hollomon, and D. Turnbull, "Kinetics of the Austenite-Martensite Transformation", Trans. AIME 185 691 (1949).
25. S. R. Pati and M. Cohen, "Kinetics of Isothermal Martensitic Transformations in an Iron-Nickel-Manganese Alloy", Acta Met. 19 1327 (1971).
26. V. Raghavan, "Formation Sequence of Plates in Isothermal Martensite Transformation", Acta Met. 17 1299 (1969).
27. D. G. McMurtrie and C. L. Magee, "The Average Volume of Martensite Plates During Transformation", Met. Trans. 1 3185 (1970).
28. C. L. Magee, "The Nucleation of Martensite," Phase Transformations. Metals Park, Ohio: American Society for Metals, p.115 (1970).
29. J. F. Breedis and W. D. Robertson, "Martensitic Transformation and Plastic Deformation in Iron Alloy Single Crystals", Acta Met. 11 547 (1963).
30. J. F. Breedis, "Martensitic Transformations in Iron-Chromium-Nickel Alloys", Trans. AIME 230 1583 (1964).



31. G. R. Speich, "Tempering of Low-Carbon Martensite", Trans. AIME 245 2553 (1969).
32. A. R. Marder and G. Krauss, "The Formation of Low-Carbon Martensite in Fe-C Alloys", Trans. ASM 62 957 (1969).
33. G. Krauss and A. R. Marder, "The Morphology of Martensite in Iron Alloys", Met. Trans. 2 2343 (1971).
34. T. Bell and R. G. Bryans, "The Effects of Prior Transformation and Prestrain on the Habit Planes of Acicular Iron-Nickel Martensite", J. Met. Sci. 5 135 (1971).
35. J. S. Bowles and D. P. Dunne, "The Role of Plastic Accomodation in the (225) Martensite Transformation", Acta Met. 17 677 (1969).
36. J. C. Bokros and E. R. Parker, "The Mechanism of the Martensite Burst Transformation in Fe-Ni Single Crystals", Acta Met. 11 1291 (1963).
37. G. Krauss and W. Pitsch, "The Fine Structure and Habit Planes of Martensite in an Fe-33 Wt Pct Ni Single Crystal", Trans. AIME 233 919 (1965).
38. R. L. Patterson and C. M. Wayman, "The Crystallography and Growth of Partially-Twinned Martensite Plates in Fe-Ni Alloys," Acta Met. 14 347 (1966).
39. R. P. Reed, "The Plate-Like Martensite Transformation in Fe-Ni Alloys", Acta Met. 15 1287 (1967).
40. R. Huizing and J. A. Klostermann, "The Martensite Transformation in Small (0.1-0.3mm) Iron-Nickel Single Crystals", Acta Met. 14 1693 (1966).
41. W. S. Owen, E. A. Wilson, and T. Bell, High Strength Materials, ed. V. F. Zackay, New York: John Wiley and Sons, p.167 (1965).
42. R. G. Davies and C. L. Magee, "Austenite Ferromagnetism and Martensite Morphology", Met. Trans. 1 2927 (1970).
43. H. Schumann, Arch Eisenhuettenw. 8 647 (1967).
44. G. Thomas "Electron Microscopy Investigations of Ferrous Martensites", Met. Trans. 2 2373 (1971).
45. W. S. Owen, F. J. Schoen, and G. R. Srinivasan, "The Growth of a Plate of Martensite", Phase Transformations. Metals Park, Ohio: American Society for Metals, p. 157 (1970).

46. J. W. Christian, "Military Transformations: An Introductory Survey", Iron and Steel Institute Special Report No. 93, p.3 (1965).
47. T. Bell and W. S. Owen, "The Thermodynamics of the Martensite Transformation in Iron-Carbon and Iron-Nitrogen", Trans. AIME 239 1940 (1967).
48. J. S. Pascover and S. V. Radcliffe, "Athermal Transformations in the Iron-Chromium System", Trans. TMS-AIME 242 673 (1968).
49. G. Olson, private communications.
50. V. Raghavan and M. Cohen, "Growth Path of a Martensite Particle", Acta Met. 20 779 (1972).
51. H. Knapp and U. Dehlinger, "Mechanism and Kinetics of the Austenite-Martensite Transformation", Acta Met. 4 289 (1956).
52. F. C. Frank, "Martensite", Acta Met. 1 15 (1953).
53. J. W. Christian, "Martensitic Transformations: A Current Assessment", Iron and Steel Institute Special Report No. 33, p. 129 (1969).
54. J. W. Christian, private communications.
55. J. A. Venables, "The Martensite Transformation in Stainless Steel", Phil. Mag. 7 32 (1962).
56. G. B. Olson and M. Cohen, "A Mechanism for the Strain-Induced Nucleation of Martensitic Transformations", J. Less-Common Metals 28 107 (1972).
57. R. E. Cech and D. Turnbull, "Heterogeneous Nucleation of the Martensite Transformation", Trans. TMS-AIME 206 124 (1956).
58. L. Kaufman, A. Leyenaar, and J. S. Harvey, Progress in Very High Pressure Research, Eds. F. P. Bundy, W. R. Hibbard, and H. Strong, New York: John Wiley and Sons, Inc. p.90 (1960).
59. S. V. Radcliffe and M. Schatz, "The Effect of High Pressure on the Martensitic Reaction in Iron-Carbon Alloys", Acta Met. 10 201 (1962).
60. M. Takahashi and T. Kōno, J. Phys. Soc. Japan 15 936 (1960).
61. C. D. Graham, Jr., J. Phys. Soc. Japan 16 1481 (1961); Suppl. B-I 17 321 (1962).
62. T. Sambongi and T. Mitui, J. Phys. Soc. Japan 16 1478 (1961); 18 1253 (1963).

63. R. Smoluchowski and R. W. Turner, J. Appl. Phys. 20 745 (1949); Physics 16 397 (1950).
64. B. Sawyer and R. Smoluchowski, J. Appl. Phys. 28 1069 (1957).
65. A. H. Geisler, J. P. Martin, E. Both, and J. H. Crede, Trans. AIME 203 985 (1955).
66. V. S. Bhandary and B. D. Cullity, Trans. TMS-AIME 224 1194 (1962).
67. O. L. Boothby, D. H. Wenny, and E. E. Thomas, J. Appl. Phys. 29 353 (1958).
68. S. Chikazumi and C. D. Graham, Jr. "Directional Order", Magnetism and Metallurgy. 2 Eds. A. E. Berkowitz and E. Kneller, N. Y.: Academic Press, p.577 (1969).
69. L. Neel, J. Pauleve, R. Pauthenet, J. Laughier, and D. Dautreppe, "Magnetic Properties of an Iron-Nickel Single Crystal Ordered by Neutron Bombardment," J. Appl. Phys. 35 873 (1964).
70. C. Kittel, E. A. Nesbitt, and W. Shockley, "Theory of Magnetic Properties and Nucleation in Alnico V", Phys. Rev. Series 2 77 839 (1950).
71. A. P. J. Meyer and P. Taglang, "Influence of the Magnetic Field on a Polymorphic Transformation of a Ferromagnetic Material", J. Phys. Radium 14 82 (1953).
72. H. Jahn, " The Influence of Heat Treatment in a Magnetic Field on the Structure and Mechanical Properties of Steel", Stahl u. Eisen 78 (3) 178 (1958).
73. J. W. Cahn, "Magnetic Aging of Spinodal Alloys", J. Appl. Phys. 34 (12) 3581 (1963).
74. E. G. Herbert, Iron and Steel Inst. 120 239 (1929).
75. V. D. Sadovskiy, N. M. Rudigin, L. V. Smirnov, G. M. Filonchik, and I. G. Fakidov, "The Question of the Influence of Magnetic Fields on Martensitic Transformation in Steel", Physics Metals Metallogr. 12 (2) 131 (1961).
76. E. A. Zavadskii and Fukidov, "Magnetization of the Intermetallic Compound MnAu<sub>2</sub> in Superstrong Pulsating Magnetic Fields ", Physics Metals Metallogr. 12 (6) 47 (1961).
77. Ye. A. Fokina and E. A. Zavadskiy, "Effect of a Magnetic Field on the Martensitic Transformation in Steel", Physics Metals Metallogr. 16 (2) 128 (1963).

78. M. A. Krivoglaz and V. D. Sadovskiy, "Effect of Strong Magnetic Fields on Phase Transformations", *Physics Metals Metallogr.* 18 (4) 23 (1964).
79. Ye. A. Fokina, L. V. Smirnov, and V. D. Sadovskiy, "Effect of a Pulsating Magnetic Field on the Position of the Martensitic Transformation Range in Steel", *Physics Metals Metallogr.* 19 (4) 101 (1965).
80. I. G. Fukidov, L. D. Voronchikhin, E. A. Zavadskiy, and A. M. Burkhanov, "The Variation in the Magnetic Intensity of Austenitic Steel Exposed to a Strong Pulsating Magnetic Field", *Physics Metals Metallogr.* 19 (6) 49 (1965).
81. Ye. A. Fokina, L. V. Smirnov, and V. D. Sadovskiy, "Destabilization of Austenite By a Strong Pulsating Magnetic Field", *Physics Metals Metallogr.* 19 (5) 73 (1965).
82. E. I. Estrin, "Effect of a Magnetic Field on the Martensitic Transformation", *Physics Metals Metallogr.* 19 (6) 117 (1965).
83. Ye. A. Fokina, L. V. Smirnov, V. D. Sadovskiy, and A. F. Peikul, "Effect of a Permanent Magnetic Field on the Martensitic Transformation in Steel", *Physics Metals Metallogr.* 19 (6) 121 (1965).
84. L. V. Voronshikhin and I. G. Fakidov, "Determining the Latent Heat of the Martensitic Transformation Induced by a Magnetic Field in Steel", *Physics Metals Metallogr.* 21 (3) 119 (1966).
85. P. A. Malinen and V. D. Sadovskiy, "Effect of a Magnetic Field on the  $\alpha \rightarrow \gamma$  Transformation in Iron-Nickel Alloys". *Physics Metals Metallogr.* 21 (5) 139 (1966).
86. P. A. Malinen, V. D. Sadovskiy, and I. P. Sorokin, "Effect of Magnetic Field on the Martensite Transformation in Alloys of the 24 Ni 4Mn Type", *Physics Metals Metallogr.* 24 (2) 101 (1967).
87. P. A. Malinen, V. D. Sadovskiy, L. V. Smirnov, and Ye. A. Fokina, "Reasons for the Influence of a Pulsating Magnetic Field on Martensitic Transformations in Steels and Alloys", *Physics Metals Metallogr.* 23 (3) 138 (1967).
88. V. D. Sadovskiy, L. V. Smirnov, Ye. A. Fokina, P. A. Malinen, and I. P. Sorokin, "Quenching Steel in a Magnetic Field", *Physics Metals Metallogr.* 24 (5) 144 (1967).
89. G. I. Granik, M. L. Bernshteyn, and O. D. Dolgunovskaya, "Influence of Magnetic Field on Certain Phase Transformations in Nickel Systems", *Physics Metals Metallogr.* 24 (6) 151 (1967).

90. L. D. Voronchikhin, L. N. Romashev, and I. G. Fakidov, "Influence of the Initial State of Austenitic Steel on the Martensitic Transformation in a Strong Magnetic Field", Physics Metals Metallogr. 26 (5) 183 (1968).
91. L. N. Romashev, I. G. Fakodov, and L. D. Voronchikhin, "Influence of a Strong Magnetic Field on the Martensitic Transformation of an Iron-Nickel Alloy", Physics Metals Metallogr. 25 (6) (1968).
92. K. R. Satyanarayan, W. Eliaz, and A. P. Miodownik, "The Effect of a Magnetic Field on the Martensite Transformation in Steels", Acta Met. 16 877 (1968).
93. Ye. A. Fokina, L. V. Smirnov, and V. D. Sadovskiy, "Effect of Magnetic Field on the Position of the Martensitic Transformation Point in Carbon Steels", Physics Metals Metallogr. 27 (4) 190 (1969).
94. P. A. Malinen and V. D. Sadovskiy, "Effect of Magnetic Field on the  $\epsilon \rightarrow \alpha$  Transformation in Fe Mn Alloys", Physics Metals Metallogr. 28 (6) 54 (1969).
95. K. R. Satyanarayan and A. P. Miodownik, "The Effect of Magnetic Fields on Transformations in Steels", Institute of Metals, Monograph and Report Series No. 33, 162 (1969).
96. C. T. Peters, P. Bolton, and A. P. Miodownik, "The Effect of Magnetic Fields on Isothermal Martensitic Transformations", Acta Met. 20 881 (1972).
97. F. D. Miroshnichenko, A. I. Stolyarenko, V. G. Kanibolotsky, V. L. Snezhnoy, and A. M. Brynza, "The Effect of Pulsed Magnetic Field on Phase Transformations in Steel kh15N5D2T at 400-650°C", Met. Sci. Heat Treat. 13 (13) 326 (1971).
98. M. I. Prudnikov and A. P. Feygin, Kuznets. no-shtamp. proizvod. 5 6 (1964).
99. Ye. A. Popov, Yu. A. Bochvar, S. M. Polyak, A. S. Stolbunov, and D. V. Raykh, Kuznechno-shtampov. proizvod. 5 1 (1966).
100. A. P. J. Meyer and P. Taglang, "Influence of the Magnetic Field on a Polymorphic Transformation of a Ferromagnetic Material", J. Phys. Radium 14 82 (1953).
101. B. S. Lement, B. L. Averbach and M. Cohen, "Microstructural Changes on Tempering Iron-Carbon Alloys", Trans. ASM 46 851 (1954).

102. C. H. Shih, B. L. Averbach and M. Cohen, "Some Characteristics of the Isothermal Martensitic Transformation", *Trans. AIME* 203 183 (1955).
103. J. W. Christian, "Accommodation Strains in Martensite Formation and the Use of a Dilatation Parameter", *Acta Met.*, 6 377 (1958).
104. A. J. Goldman and W. D. Robertson, "Elastic Properties of Austenite and Martensite in Iron-Nickel Alloys", *Acta Met.* 12 1265 (1964).
105. L. H. Bennett and L. J. Swartzendruber, "On the Interpretation of Mossbauer Effect Spectra as Related to the Constitution of Cu-Ni-Fe Alloys", *Acta Met.* 18 485 (1970).
106. A. P. Miodownik, "The Effect of Two Gamma States on the Magnetic Properties of Fcc Iron-Cobalt Alloys", *Scripta Met.* 3 931 (1969).
107. L. Kaufman, "Calculations of Binary Phase Diagrams", *Proc. Intl. Conf. on Metallurgical Thermochemistry Fundamentals*, Brunel Univ. and NPL, London (1971).
108. G. A. Alers, J. R. Neighbours, and H. Sata, "Temperature Dependent Magnetic Contributions to the High Field Elastic Constants of Nickel and an Fe-Ni Alloy", *J. Phys. Chem. Solids* 13 40 (1960).
109. C. H. Shih, B. L. Averbach, and M. Cohen, "Some Characteristics of the Isothermal Martensitic Transformation", *Trans. AIME.* 202 183 (1955).
110. S. R. Pati, Nucleation of the Isothermal Martensitic Transformation in Iron-Nickel-Manganese Alloys, Sc.D. Thesis, M.I.T. (1967).
111. E. Owen and Y. Liu, "Further X-Ray Study of the Equilibrium Diagram of the Iron-Nickel System", *J. Iron and Steel Inst.* 163 132 (1949).
112. C. D. Graham, Jr., "Magnetic Annealing", Magnetic Properties of Metals and Alloys, Metals Park, Ohio: American Society for Metals, p. 288 (1958).
113. D. A. Colling, "Magnetic Investigation of Martensite~~→~~Austenite Transformations in Fe-Ni-Co Alloys," *Met. Trans.* 2 2889 (1971).
114. R. J. Weiss and K. J. Tauer, "A Metallurgical Slide Rule for Determining Magnetic Properties of 3D Transition Alloys", *Theory of Alloy Phases*, Metals Park, Ohio: American Society for Metals, p. 290 (1955).

115. M. Hanson, Constitution of Binary Alloys. N.Y.: McGraw-Hill Book Company, Inc., (1958).
116. G. F. Bolling, A. Arrott, and R. H. Richman, "A Study of Curie Temperatures and the Effect of Carbon in Face-Centered Cubic Iron-Nickel Alloys", phys. stat. sol. 26 743 (1968).
117. R. L. Fullman, "Measurement of Particle Sizes in Opaque Bodies", Trans. AIME 197 447 (1953).

BIOGRAPHICAL NOTE

The author was born on June 21, 1945 in Cleveland, Ohio. He graduated from Garfield Heights High School in June, 1962 and received his B. S. degree from Case Institute of Technology in June, 1966. His M. S. thesis at the newly federated Case-Western Reserve University involved studying the Bordoni internal friction peaks in plastically deformed molybdenum single crystals. In July, 1968, he was married to his wife, Elaine and moved to the Boston/Cambridge area. In September of that year, he entered graduate school at the Massachusetts Institute of Technology and has remained there to the present time. His formal education has been supplemented with summer jobs in the construction industry and, later at General Electric, N.A.S.A. Lewis Research Center, and the U. S. Steel Laboratory for Fundamental Research.

After completing his Sc.D. requirements, he plans to extend his work with a short postdoctoral appointment at M.I.T. followed by a N.A.T.O. Postdoctoral Fellowship at Oxford University under Professor J. W. Christian.

His extracurricular activities include fishing, skiing, and scuba diving, while his immediate professional objective is university teaching and research in materials science.